



Republic of Iraq

Ministry of Higher Education & Scientific Research

University of Kerbala

College of Engineering

Department of Civil Engineering

Numerical Investigation to Estimate Flow Rate through Regulators

**A Thesis Submitted to the Council of the Faculty of the College of the
Engineering/University of Kerbala in Partial Fulfillment of the Requirements
for Master's Degree in Infrastructure Engineering**

Written By:

B.Sc. Hamid Ahmed Mahdi

Supervised By:

Prof. Dr. Husam Hadi Alwan

May 2023

Dhul Qi'da 1444

بِسْمِ اللَّهِ الرَّحْمَنِ الرَّحِيمِ
يَرْفَعِ اللَّهُ الَّذِينَ آمَنُوا مِنْكُمْ وَالَّذِينَ
أُوتُوا الْعِلْمَ دَرَجَاتٍ

صدق الله العلي العظيم

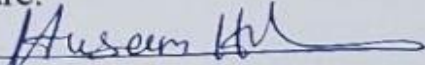
(المجادلة: من الآية 11)

Examination committee certification

We certify that we have read the thesis entitled "Numerical Investigation to Estimate Flow Rate through Regulators" and as an examining committee, we examined the student "Hamid Ahmed Mahdi" in its content and in what is connected with it, and that in our opinion it is adequate as a thesis for the degree of master of science in infrastructure engineering.

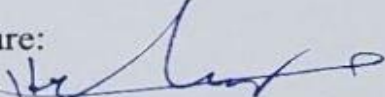
Supervisor

Signature:


Name : Prof. Dr. Husam Hadi Alwan
Date: 10 / 9 / 2023

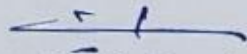
Member

Signature:


Name : Asst. Prof. Dr. Hayder
Hussein Alwan Algretawee
Date: 10 / 9 / 2023

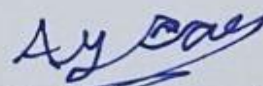
Member

Signature:



Name : Asst. Prof. Dr. Ameen
Mohammed Salih Ameen
Date: 10 / 9 / 2023

Chairman


Signature:


Name : Asst. Prof. Dr. Aysar T. Joudah
Date: 10 / 9 / 2023

Signature:

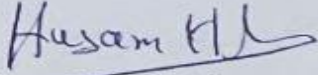

Name : Dr. Awad Ali Sagheer
Head of the Department of Civil Engineering
Date: 10 / 9 / 2023

Signature:


Name : Prof. Dr. Laith Shakir
Rasheed
Dean of the Engineering College
Date: 10 / 9 / 2023

Supervisor certificate

I certify that the thesis entitled “**Numerical Investigation to Estimate Flow Rate through Regulators**” was prepared by **Hamid Ahmed Mahdi** under our supervision at the department of civil engineering, faculty of Engineering, University of Kerbala as a partial of the fulfillment of the requirements for the degree of master of science in infrastructure engineering.

Signature: 

Prof. Dr. Husam Hadi Alwan

Date: / / 2023

اقرار المقوم اللغوي

أشهد أنني قد اطلعت على رسالة طالب الماجستير (حامد احمد مهدي) الموسومة ب

**Calibration of flow equations through regulators
using computational fluid dynamics CFD modelling**

وقد قومتها من الناحية اللغوية والاسلوبية وبذلك تكون صالحة لأغراض المناقشة مع
توصيتنا بالأخذ بنظر الاعتبار تصحيح بعض الملاحظات اللغوية المؤشر عليها
مع التقدير....



التوقيع:

أسم المقوم ولقبه العلمي : أ.د. عيسى كاظم

التخصص العام : E

التخصص الدقيق : Linguistics

محل العمل : جامعة كربلاء - كلية التربية / الشايع

رقم الهاتف النقال : 07718484676

التاريخ : 9 - 7 - 2023

Abstract

In this study, the two cases of flow at the total opening and partial opening of the regulator gate were examined. The simulation was conducted using three-dimensional flow software, and the results were compared with the general and empirical equations for calculating the discharge through the water facilities that were get at in Labeed's 1987 research.

The objectives of this research is to knowing the effect of gate opening and width and Froude number on volume of flow rate, studying the dimensional and nondimensional factors most affecting the discharge, calibrate the discharge from laboratory experiments with the discharge extracted from a software CFD in FLOW-3D software and extracting an equation to calculate the discharge based on the available data in the water resources departments.

Based on the modeling outcomes from calibration, it may be said that the CFD approach is a useful tool for modelling the flow pattern in regulators, the main equation was extracted, which showed good aggrement with a value of $R^2=0.756$ and $RMSE=0.004872$ with $MAE=0.00412$ without the need for softwares, field works, or models, only the initial measurements that can be obtained from state departments and it was concluded that (H/Y) has the most effect on the flow rate by 45.8%, followed by (B/Y) with a rate of 29.4%, and finally (Fr) with a rate of 24.8%. Six models of regulators with a single opening or with multiple opening were used in laboratory water experiments. These models were calibrated by using data from Labeed 1987 by calculating the discharge based on the results of laboratory measurements.

Undertaking

I certify that research work titled “**Numerical Investigation to Estimate Flow Rate through Regulators**” is my own work. The work has not been presented elsewhere for assessment. Where material has been used from other sources it has been properly referred.

Signature:

Hamid Ahmed Mahdi

Date: / / 2023

Dedication

I dedicate this humble work

To my father and mother, who gave me affection and love; I say to them: you gave me life, hope, and the emergence of a passion for learning and knowledge;

To my family, my close friends, and especially to my Supervisor and guidance Prof. Dr. Husam Hadi Alwan.

I would like to dedicate this modest effort as a token of gratitude to all those who have provided me with advice, guidance, and support.

Signature:

Hamid Ahmed Mahdi

Date: / / 2023

Acknowledgments

In the name of Allah, the most merciful the most compassionate. praise be to Allah and pray and peace be on his prophet Mohammad and kinsfolk in his home.

With the guidance of Almighty God to finish this study, it honors and pleases me to show my sincere thanks and gratitude to Prof. Dr. Husam Hadi Alwan (University of Kerbala), the supervisor on this study, for his guidance, help, and encouragement.

Acknowledgment to the dean of the faculty of engineering and his collaborators and all staff of the civil engineering department, university of Kerbala for their cooperation and assistance.

Table of Contents

Abstract.....	iv
Undertaking	v
Dedication.....	vi
Acknowledgments	vii
List of Tables	xi
List of Figures.....	xii
List of Abbreviations	xiv
List of Symbols.....	xv
Chapter One	1
1.1 General Background	1
1.2 Problem Statement	3
1.3 Aim of the study.....	3
1.4 Flow Chart (methology).....	4
1.5 Limitation.....	5
Chapter Two	7
2.1 Theoretical background.....	7
2.2 Gates, piers, and abutments	8
2.3 Spss software.....	9
2.3.1 Artificial Neural Network (ANN)	9
2.3.2 Structure of an Artificial Neural Network.....	11
2.3.3 Modeling and Preprocessing for Data Division	12
2.3.4 Artificial Neural Network Model (ANN).....	13
2.4 Previous Studies.....	14
2.5 Summary of the results of previous studies	26

Chapter Three	31
3.1 Introduction	31
3.2 Definition of CFD	32
3.3 Flow 3D Approach.....	33
3.4 Steps of working on the software can be summarize:	33
3.5 Turbulence Models	35
3.6 The Complexity of the Turbulence Model	35
3.7 Mathematical Model and Numerical Solution Technique.....	36
3.7.1 Governing Equations	36
3.7.1.1 VOF Turbulence Model.....	36
3.7.1.2 Mixture turbulence model.....	38
3.8 CFD Sumlation	39
3.9 Geometry of Regulator.....	40
3.10 Mesh, Numerical Modeling and Analysis	41
3.11 Boundary and Initial Conditions.....	44
3.12 Solver Option	45
3.13 The method of work.....	46
3.14 Dimensional Analysis	47
3.15 The standard performance measures.....	51
Chapter Four	54
4.1 Introduction	54
4.2 Results and their evaluation.....	54
4.3 Nonlinear multiple regression analysis.....	58
4.4 Validation of the formulation.....	59

4.5 Artificial Neural Network (ANN) Model by parameters of dimensional analysis	65
4.5.1 Network Information and Results.....	65
4.6 Discussion	70
Chapter Five.....	72
5.1 introduction	72
5.2 Conclusion	72
5.3 Recommendations	73
Appendices	82

List of Tables

Table 3-1: The classification of parameters that affect on the discharge.....	48
Table 3-2: parameter influence of flow rate	50
Table 4-1:Data to validation the estimated value and measured.....	60
Table 4-2:parameters of the ANN model's statistics	62
Table 4-3 : The factors most affecting the discharge	63
Table 4-4:MLP-ANN model synopsis.....	65
Table 4-5: Case processing summary	66
Table 4-6: The relative errors for the ANN model.....	67
Table 4-7: The outcome of independent variables on the estimate of the discharge	69

List of Figures

Figure 1.1 : Transition and type of regulators	2
Figure 2.1 : Sluice gate installed in the laboratory flume (Silva & Rijo, 2017)	8
<i>Figure.2.2: operation of ANN (Shahin et al., 2009).....</i>	10
Figure 2.3: Structure of an Artificial Neural Network (Marugán et al., 2018)	10
Figure 2.4: Hydraulics Laboratory at the University of Baghdad.....	15
<i>Figure 2.5 : Sluice Gate 1 of the experimental irrigation canal</i>	16
Figure 2.6 : The main flow direction is from left to right	19
Figure 2.7 : Surface discharge of the Al-Ghubrah desalination plant, the largest such facility in Oman	21
Figure 2.8 : Photographs of the experimental flume with the equipment installed on it and some of the models	22
Figure 2.9 : Free (a) and submerged (b) flow in oblique/inclined sluice gate.	25
Figure 3.1 : working on the software.....	34
Figure 3.2: Geometric model conFigured by the FLOW 3D software software with one gate.....	40
Figure 3.3: Geometric model conFigured by the FLOW 3D software software with three gate.....	41
Figure 3.4: Favor option with different cell sizes (Mohammed et al., 2015).....	42
Figure 3.5: Total mesch in model.....	43
Figure 3.6: Boundary conditions	44
Figure 4.1: Software calibration with Labeed’s study	55
Figure 4.2: Equations of 15 cm width and 16 cm open of the gate.....	56

Figure 4.3: Equations of 15 cm width and full opening of the gate.....	56
Figure 4.4 : Equations of 25 cm width and 12 cm open of the gate.....	57
Figure 4.5 : Equations of 25 cm width and full opening of the gate.....	57
Figure 4.6: correlation coefficient between discharge software and discharge measured	60
Figure 4.7:Activation layers	67
Figure 4.8: Scatter comparison.....	68
Figure 4.9:The outcome of independent variables on the estimate of the discharge	69

List of Abbreviations

ANN	Artificial Neural Network
ARC	Agricultural Research Council
CFD	Computational fluid dynamics
CNN	Canfis network
CSIR	The Council for Scientific and Industrial Research
GMRES	Generalized minimal residual method
ICSM	Irrigation Canal Simulation Model
LES	large eddy simulation
MLP	Inear multilayer perceptron
MNN	Modular neural network
PDE	Partial differential equation
RANS	Reynolds-averaged navier-stokes equation
RNG	Renormalization Normalization Group
RNN	Recurrent network
SPSS	Statistical Package For Social Sciences
STL	File format
TKE	Turbulence kinetic energy
VOF	Volume of fluid
3D	Three-dimensional

List of Symbols

Symbol	Definition	Dimensions
B	width of the gate	m
b	Width of the channel	m
Fr	Froude number	-
GK	the production rate of the turbulent kinetic	-
g	Gravitational acceleration	m/s^2
H	Height of the open gate	m
h	Depths of water in the gate	m
k	the turbulent kinetic energy	J/kg
L	Length of model	m
N	Number of gates	-
p	the fluid pressure	Pa
Q_e	The estimated discharge	m^3/s
Q_m	The measured discharge	m^3/s
Q_p	The software discharge	m^3/s
S	model bed slop	-
t	time	s
V1	The velocity of the water in the upstream flow	m/s
W	width of model	m
Y1	Depths of the water in the upstream flow	m
ρ	mass density	Kg/m^3
ε	turbulent dissipation	m^2/s^3
μ	dynamic viscosity of the fluid	$N.s/m^3$

Chapter One

Introduction

Chapter One

Introduction

1.1 General Background

Water was not always existing or available everywhere, and if it was got from many abundant sources when it reaches the farmers it becomes little, and urge that farmers dispute and problems appear around it.

Controlling the flow developet step by step coupling with the nations developments, so some ancient peoples relied on the area of the canal cross-section in comparing the flow of water without looking at its slope, and it is a valid method for comparison if the charge of height is proven, and with the progress of time. The irrigation developed and computational sciences entered into its applications as facilities began to be built to regulator the level of water.

In the modern period when the volume in the unit of time considered the measurement and the means of time measurement were available, the empirical equations were used to calculate the amount of water and then developed into mathematical derivations. Engineering softwares are used to simulate reality and show the results, as will be done in this research in the coming chapters.

Concerning irrigation regulators, there was no agreement on a single formula for the flow equations, but the agreement is almost done on measuring variables and coefficients, either in the field or in the laboratory, on models from which the final equations are derived, which is called the regulator's calibration equation.

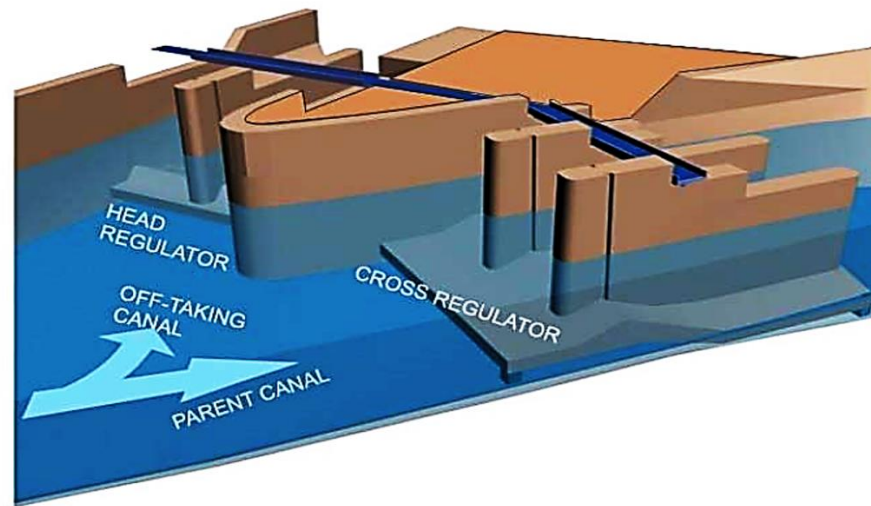


Figure 0.1: Transition and type of regulators

Control of water flow in irrigation canals is carried out utilizing regulators, weirs, or other water-measuring devices. Regulators are used in lands with little slope, the process of controlling the flow includes controlling the water level or its quantity or calculating this quantity or the three cases together.

Regulators are built of concrete, brick, or stone, and the regulator channel is usually of a rectangular cross-section with an area less than the cross-sectional area of the channel upstream and downstream, also consists of piers and abutments that support it as well as inlet and outlet transitions that link it to the Table section. The regulator also has a floor that supports the entire structure and is lined with concrete walls or other waterproofing materials.

The inlet or outlet transition is a change of location in the cross-section that causes a change in the flow from a certain regular state to another and the aim of transition is to reduce the loss of charge when the velocity increases and then restore part of loss charge when the velocity decreases and thus it

works on reducing energy loss and reduce the disturbances and waves, thus providing safety for the structure.

In this research, the results depended on the Computational fluid dynamics (FLOW 3D) simulation software, in addition to labeled measurements to estimate the parameters and elements included in the software's calculations, which can be used in calculating the discharge of regulators based on simple field measurements.

1.2 Problem Statement

Because of the large number of empirical equations for measurement and the difficulty of dealing with them, and because it consumes a lot of time when dealing with them and because of the difficulty of taking some of the measurements in the field, this research was achieved to shorten the time when calculating the discharge using a software CFD flow 3D.

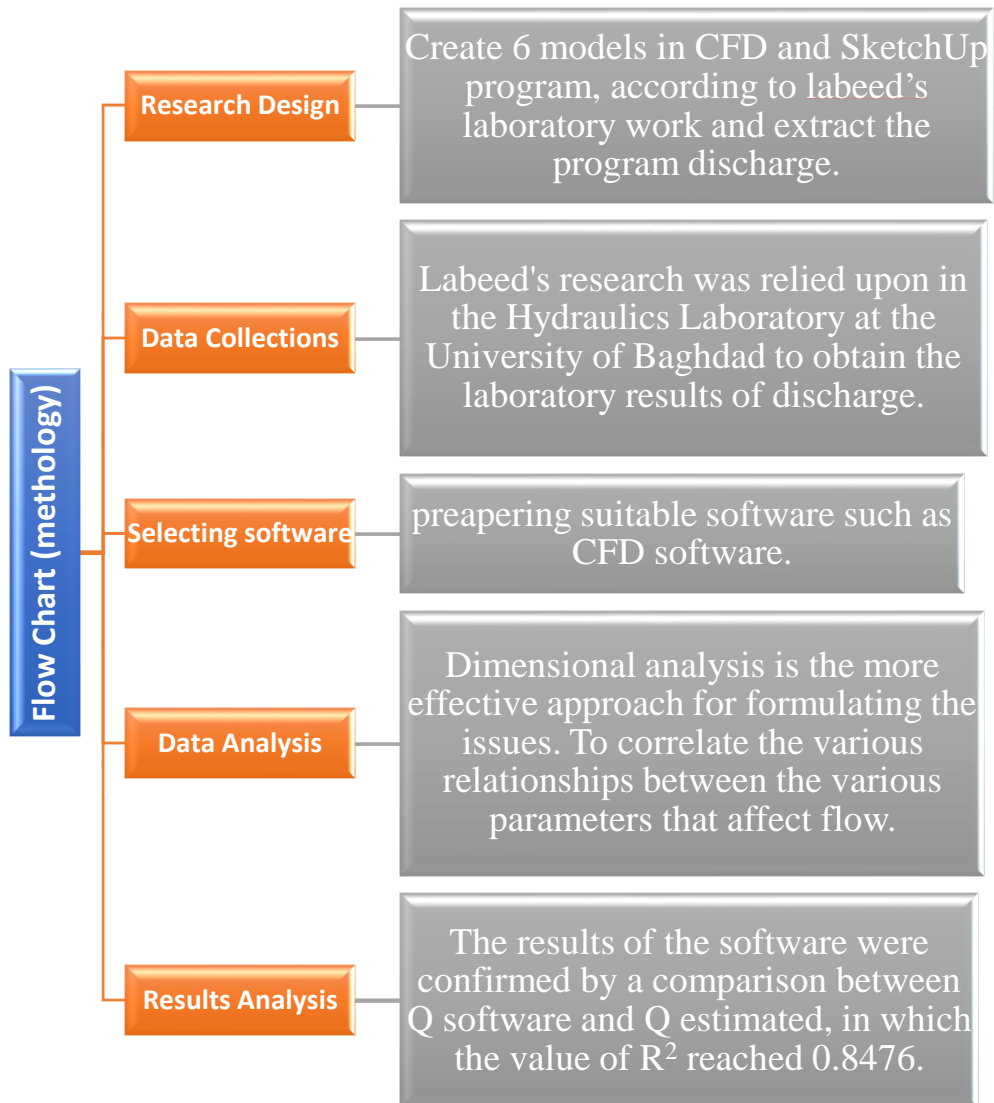
1.3 Aim of the study

It is important to perform water calculations to find the discharge passing through regulators using the recorded measurement data and the gate opening, and because of the different methods and equations at different times and their adoption wholly or partly based on the information. The following points represent a summary of the objectives of this research:

1. Knowing the effect of gates opening and width and Froude number on volume of flow rate.
2. Studying the dimensional and nondimensional factors most affecting the discharge.
3. Calibrate the discharge from labeled experiments with the discharge extracted from a program CFD in FLOW-3D software.

4. Extracting a formula to calculate the discharge based on the available data in the water resources departments.

1.4 Flow Chart (methology)



1.5 Limitation

The present study was carried out within the following limitations:

1. The first group includes four different types of models are used with a scale from 1/20 of a level regulator with a single opening of different widths (15, 25, 35, 50) cm, the second group includes tow models in a scale of 1/50 of 24 cm fixed length multi-slot regulators, contain two struts and three openings (10, 20) cm wide for the opening.
2. The regulator is connected to the conduit with a 45-degree inlet transition with the center line and a 12.5-degree outlet transition with the center line.
3. The gate is located at a distance of 5 cm from the beginning of the regulator channel and its lower edge is straight with a thickness of 12 mm.
4. The gate in this group of models is located at a distance of 2 cm from the beginning of the regulator channel.
5. Six models were made 12 mm thick and 30 cm high with smooth faces - a characteristic consistent with the assumption that the effect of friction is neglected.
6. The models are designed in the form of a bottom-level regulator with a vertical sliding gate and a straight connection.
7. The expected accuracy of the hydraulic analysis of the model is within 5% and the error rate exceeds 5% when using hydraulic analysis in estimating the water behavior of the prototype.

Chapter Two
Literature Review of Study

Chapter Two

Literature Review of Study

2.1 Theoretical background

The knowledge of flow through regulators is based on experiment, as it relies on the shape and dimensions of the regulator, that includes such as the roughness of the regulator the canal and their inclination etc, and the factors affecting the flow.

The majority of the passed study group on the employ of computational fluid dynamics (CFD) to flow of water modeling came from studies carried out utilizing a range of simulation tools.

These include details on how CFD and Fluent software can be used effectively, as well as comparisons of these softwares. Flow 3D and Fluent were regarded as useful applications for complex problems in prior studies dealing with hydraulic concerns.

This chapter gives a brief introduction to the regulator, and factors affecting their design and use numerical studies to predict discharge. Also, it includes the effects of the gate opening and the importance of piers. Finally, the focus is made on previous studies on the major approaches used to study the discharge, the result of increasing the quantity of flow on the gates, division of pressure on the spillway, management and diagnostic for open canal irrigation projects and calculate flow rate coefficient in the mutual weir-gate structure. (Akoz et al., 2009)

2.2 Gates, piers, and abutments

In irrigation channels, gates are frequently used to control upstream and downstream water levels. These gates are normally sluice gates, which can be raised and lowered vertically to change the opening. The regulation of the water level upstream of the gate and the accuracy of the flow measurements depend on the degree of gate opening. The hydraulic and geometrical parameters of sluice gates were determined through several analytical and experimental research until now. Estimating the discharge coefficient and, thus, arriving at the flow rate under gates, is a fundamental problem in hydraulic engineering. When the design gate opening surpasses a certain threshold, double or triple gates are used, however their usage is financially expensive. (Daneshfaraz, et al., 2022). Gates obstruct the flow and produce irregular flow conditions upstream and downstream of the gate. Depending on the tailwater depth, the outflow from these gates is categorized as either free or submerged. (Rajaratnam, 1978)(Supercritical & Gate, 1994)(Alhamid, 1999)

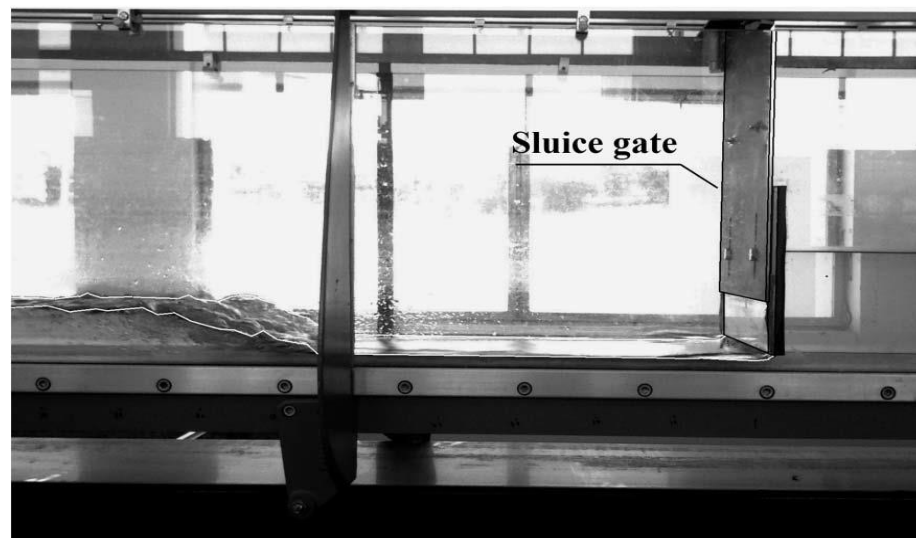


Figure 2.1 : Sluice gate installed in the laboratory flume (Silva & Rijo, 2017)

Unusual velocity patterns or (velocity distributions) are caused by the multi-opining, which in turn causes unexpected flow patterns. Because piers and abutments are components of these structures, when some or all of their gates are operating together, the flow that emerges from their gates behaves as flow in suddenly expanding stilling basins. Most of the time, symmetric flow downstream of suddenly increasing stilling basins led to symmetric scour.(Negm & Saleh, 2014)

2.3 Spss software

Most data-driven professions, including academics, are aware that collecting and organizing data takes much more work than creating models or generating reports. So statistical package for social sciences (SPSS) is available with a wide range of tools for conducting those data administration tasks. This software provides a variety of tools that may be used to import data from virtually any source, clean it, modify it, combine it with other data, and get it into the kind of shape needed to create accurate models and accurate reports. (Levesque, 2005)

2.3.1 Artificial Neural Network (ANN)

Applications of ANN have become more common across a wide range of human needs. Several companies are investing in neural networks to address problems in a number of sectors and the economy that often come within the purview of operations research (Boyacioglu et al., 2009). Complex input-output interactions can be described and captured using the data modeling technique known as ANN. Compared to tasks produced by the human brain, this approach is capable of doing more clever activities (Salmasi et al., 2013). Artificial intelligence is unique in that it is regularly

recommended for data analysis by academics in the fields of social science and engineering, in addition to its use in science and engineering (Abiodun et al., 2018). Figures (3-6) and (3-7) demonstrate the ANN's usual structure and processing.

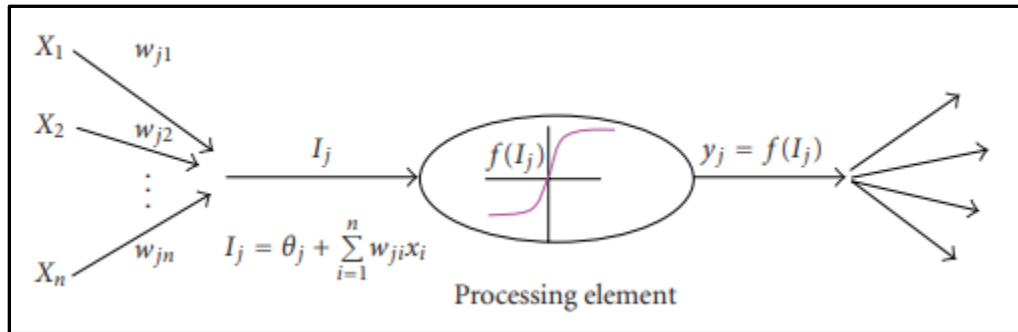


Figure.2.2: operation of ANN (Shahin et al., 2009)

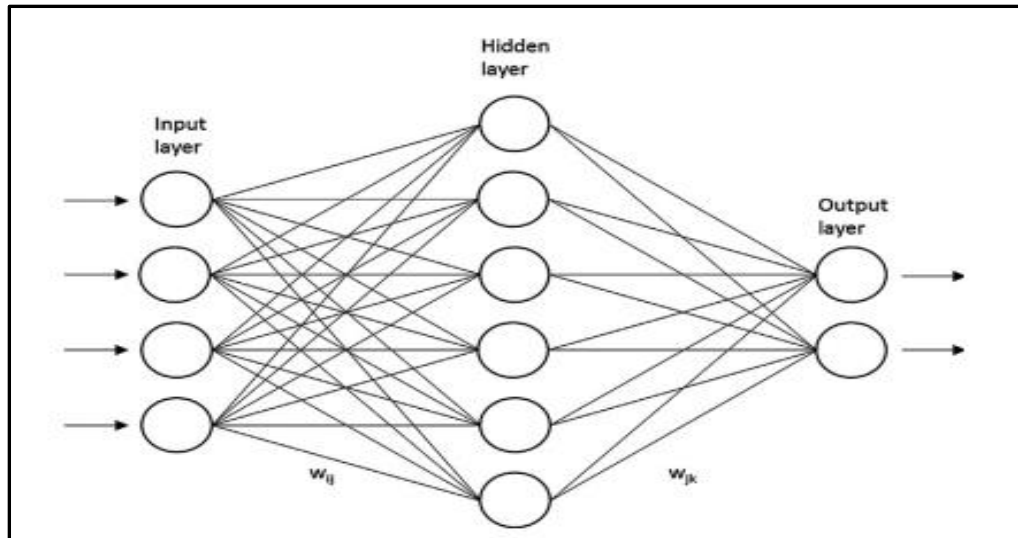


Figure 2.3: Structure of an Artificial Neural Network (Marugán et al., 2018)

2.3.2 Structure of an Artificial Neural Network

The three main components of an artificial neural network are the hidden layer, output layer, and input layer. A further unit is known as the bias unit (β), nodes or neurons are present in each of the input and hidden layers. By interconnecting ANN components, a parallel distributed processing system may be built. (Saleh, 2018)(Mahmoudi et al., 2016)

When it comes to layered neural network architectures, network size is influenced by the amount of nodes in every layer as well as the connections that connect these nodes. There may be a large number of network architectures that apply to understanding the properties of a given data set. Unfortunately, the solution to this issue is not straightforward. The best neural network design for a specific job can only be discovered through testing. How successfully a neural network solves a problem is significantly influenced by the size of the network it uses. Network size affects network complexity, learning time, and most notably, the network's generalization capabilities. The volume of a neural network to extrapolate and interpolate data that it has never seen before is known as generalization. (Kavzoglu, 1999)

Input information is sent into the input layer of the multilayer perceptron (MLP), and connection weights enhance the process as they pass from the input layer to the hidden layer. Weighted inputs are combined with a bias (β) value in the buried layer and managed by a non-linear role, frequently the hyperbolic tangent. ANN is repeatedly shown the input information in the back-propagation method. With each performance, the output of the neural network is compared to the desired output to determine the error. The weights are then adjusted using this fault, it is then transmitted back to the neural network. The process is repeated as necessary to get the

lowest possible error between the input and the output. This activity is referred to as training or learning. (Das, 2013)

2.3.3 Modeling and Preprocessing for Data Division

A neural network typically uses continuous or discrete variables as its input or output. (Das, 2013) The available data are typically divided into three main categories:

1. Through simulation, the training dataset is applied to continually change the linking weights of the ANN. The fundamental objective of training is to reduce mistakes by developing a set of connection strengths and biases that enables the ANN to create outputs that are equivalent to or substantially identical to the real outcomes. (Hamed et al., 2004)
2. To assess the network's performance at various learning phases and avoid overtraining, the testing data set is used. (Z. Zacharis, 2016)
3. The holdout data set is applied to validate the ANN model's functionality after successful training. (Al-zwainy, 2016)

It is crucial to preprocess the data before utilizing it in the ANN to obtain the suitable data type and guarantee that all variables are taken into account equally during the training process. Preprocessing frequently velocities up the training process, too. Data scaling, normalization, and transformation are three methods of preprocessing. Because it needs to work with the transfer (activation) functions used in the output layer, output data must be scaled. To assess how well an ANN model predicts the future, researchers usually use the coefficient of determination (R^2) and the root-mean-square error (RMSE).

2.3.4 Artificial Neural Network Model (ANN)

The goal of ANN model's design is to identify the optimum purpose that explains the connection between the input and output variables. A simulation model for forecasting the flow rate of six various kinds of regulators was built in this study utilizing artificial neural networks (ANN). Using the most popular backpropagation approach for engineering issues, the multilayer perceptron ANN was used. Feedforward architecture is the foundation of ANN models. A feed-forward planning is one in which neural connections flow from the input layer to the hidden layer, then to the output layer.

The ANN models for this investigation were created using the ANN and SPSS version 26 software. The discharge (Q) was selected as the output parameter, while the gate opening (H), gate width (B), and water level in the inlet (Y) functioned as the input parameters. The dataset used in this study was divided into three groups: holdout, testing (validation), and training, each with a random member. For covariates, the standardized rescaling approach was utilized. The mean is subtracted from the data in this rescaling procedure, and the result is divided by the standard deviation. Additional rescaling techniques include normalized, adjusted normalized, and none. These ANN models employed the default approach. The gradient descent approach was combined with a batch training technique to train the network. On that, the SPSS software's default settings were applied. ANN that has been correctly trained may predict how a process will behave. Given that ANN has a remarkable ability to generalize, they can produce reliable results even in scenarios that they have never encountered after being properly trained. (Alsaadi, 2022)

2.4 Previous Studies

This section covers an analysis and review of prior research to help readers better comprehend the research in various regions' techniques of analysis on the experiment's issue.

Calculating the discharge through regulators based on the software requires calculating the transactions and elements in these transactions, which cannot be achieved without knowing the discharge passing through the regulator. The objective of conducting experiments is to take measurements that can be available in the field to find the equation of flow, and those measurements are the water level upstream and its level downstream. The natural depth of flow and the opening of the gate are observed, followed by the calculation of the flow passing through the regulator opening after performing the calibration. The same thing applies to laboratory measurements, then calculating the flow passing through the regulator opening after performing the calibration. The same applies to laboratory measurements. The depth of the upstream flow was measured at a distance of 1 m from the model, and the depth of the natural flow downstream and at a distance of 1 m from the model, was calculated from the natural flow equation, assuming neglect of slop.

The flow was measured by the triangular submersible dam. In addition to these measurements, the depth of the water through the regulator, as well as the distribution of its velocity charge in the front, was recorded. The appendix G includes the results of Labeed study for comparison with the resultss of this research. This research was used since it had many gate types with various dimensions and numbers, which did not existing in other research, thus, this gap was closed by making a formula that includes all these variables together (Labeed A. Jawad Al-Taher, 1987).

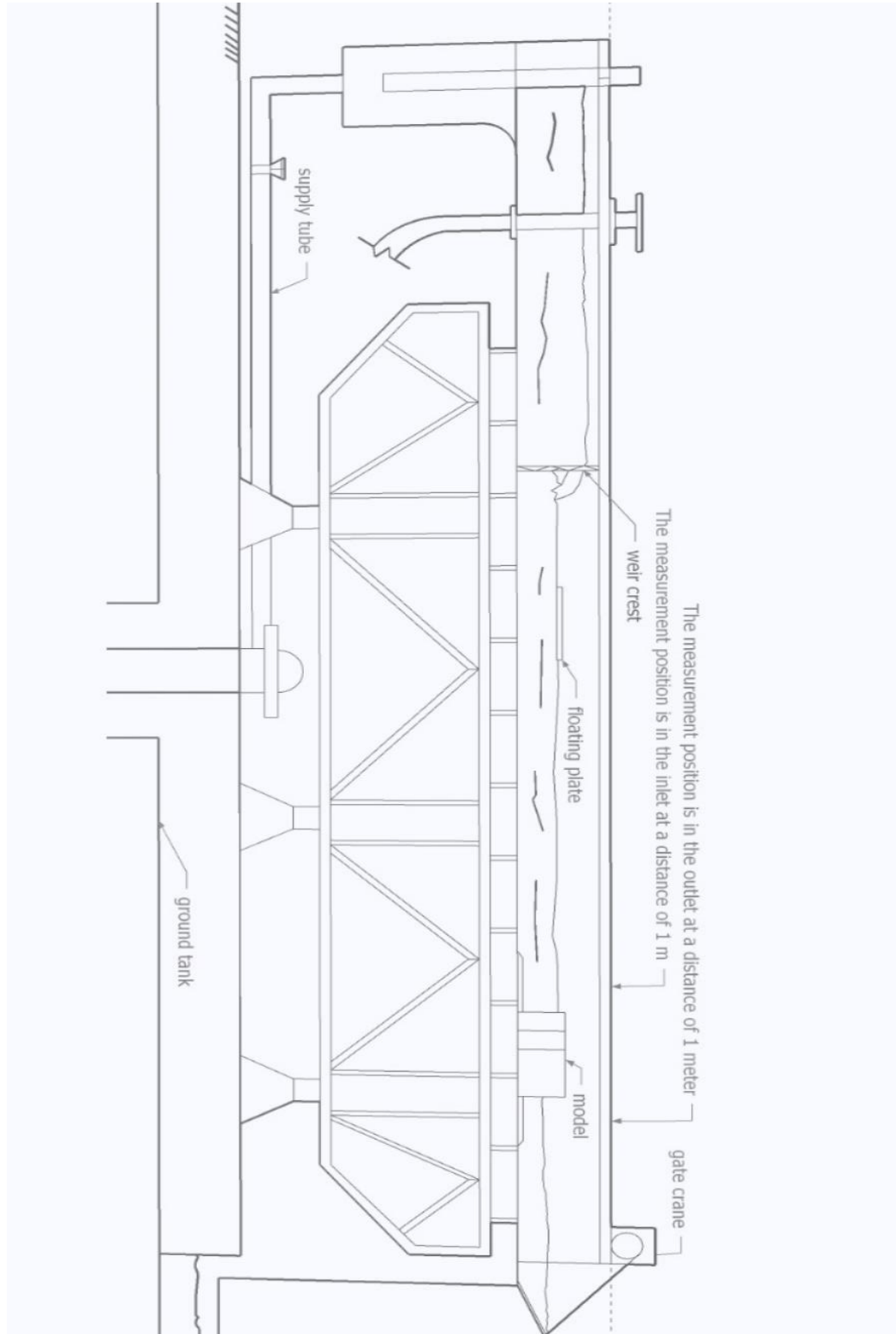


Figure 2.4: Hydraulics Laboratory at the University of Baghdad

Used a physical model, a numerical model, and data from multiple design publications to test the discharge characteristics and pressure distribution for flows passing over an unsubmerged ogee spillway. The relative error shows that the numerical model agrees within 1% with the physical model for $H_e/H_d > 0.7$ (Savage & Johnson, 2001).

SuiTable contraction coefficient (C_c) for the gate may be used to more accurately predict the flow conditions for sluice gates. This will enhance the functionality and design of sluice gates. Sluice gate hydraulic properties are significantly influenced by the contraction coefficient.

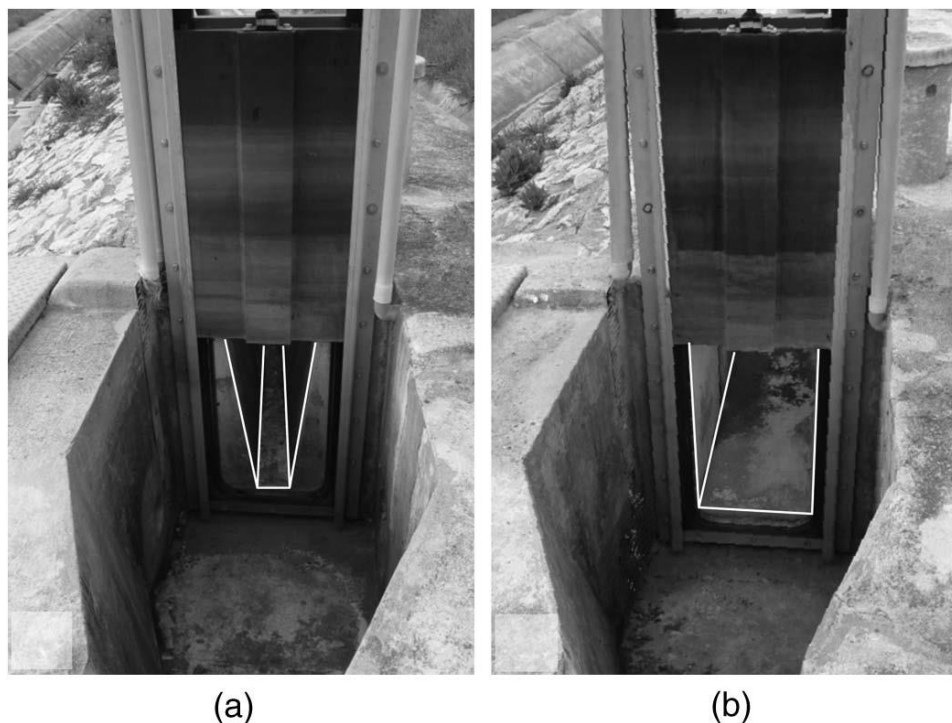


Figure 2.5 : Sluice Gate 1 of the experimental irrigation canal: (a) before cross section changes; (b) after cross section changes

Contrasted the results of numerical simulation predictions with other researchers' experimental experiments. Results indicated that the current approach for estimating discharge coefficient was highly accurate (Yen et al., 2001).

The results of system identification trials are used to create models of the water level in irrigation channels. They outline the whole system identification process, from experiment design through model validation, while accounting for previous physical knowledge and noting that the models' intended applications are prediction and control. First and second-order models are demonstrated to capture the data's major patterns accurately. Additionally, it is demonstrated that predictions made using a third-order nonlinear model that can simulate wave dynamics are astonishingly accurate. It was found that a third order nonlinear model gave very accurate predictions. It was even able to predict waves. While the first and second order models were not able to capture waves (Weyer, 2001).

In combined sewer systems, it might be difficult to regulate flows and in-line storage in real time optimally. The dynamic optimum control module generates optimal policies that are used to train a recurrent Jordan neural network architecture that serves as the foundation for the neural-optimal control module. In a simulated real-time control experiment for the King County combined sewer system in Seattle, Washington, USA, the neural-optimal control method is exhibited. The method demonstrates an efficient capacity for adaptive learning, leading to near-optimal performance of the control system while addressing the demands of real-time implementation (Darsono & Labadie, 2007).

A two-dimensional hybrid numerical model for free surface flows is proposed in this study. The numerical studies show that the turbulence plays an important role in the evolution of free surface when the reflected wave propagates upstream during the fluid flow passing the submerged obstacle (Lin et al., 2008)

Experimental fluid dynamics, theoretical fluid dynamics, and numerically computational fluid dynamics are the three main approaches used to study fluid flow. By employing a numerical approach to solve the mathematical equations governing fluid flow and related events, these phenomena can be anticipated. Combining experimental and numerical methods, to validate a mathematical model that may be utilized to conduct parametric investigations under simulated physical settings, experimental studies that have the benefit of physical realism are used. Irrigation efficacy and safety are greatly impacted by irrigation needle tip design, which also affects flow pattern, flow velocity, and apical wall pressure. A useful method for analyzing the effects of needle tip design on various parameters is computational fluid dynamics (Shen et al., 2010).

Using both computational and experimental methods, attainment flow is shown to pass over a trapezoidal crest with sharp edges. The outcomes demonstrated that the ratio of the crest length over the upstream depth, weir sidewall slope, and weir height over the upstream depth of the side weir, known as the Froude number, is related to the discharge coefficient in subcritical flow (Rahimpour et al., 2011).

The main problems with simulating water flow in irrigation canals and the environmental factors that make it possible to study and quantify these problems were examined and related to the needs and actual applications of ICSMs. The usefulness of such a technology to the irrigation plans in south africa was also evaluated. It was suggested that to start the process of developing a friendly ICSM, specialists can be recruited from research institutions such universities, the Council for Scientific and Industrial Research (CSIR), the Agricultural Research Council (ARC), and the

department of water and environment. Given the enormous financial investments made in the softwares, this will help manage them. It's cost-effectiveness in terms of time, energy, human, and material resource savings is one advantage of its adoption (Upport et al., 2011).

Using field measurements in the Al-Tawfiki, Al-Menoufi, and Abasi canals, they assessed the dimensionless calibration techniques for radial gates. The mean absolute percentage errors for these approaches ranged from 3.88% to 20%. The dimensional analysis approach using the imperfect self-likeness notion produced the best results. The ISS theory and the π -theorem were then used to create an equation for submerged PRGs.

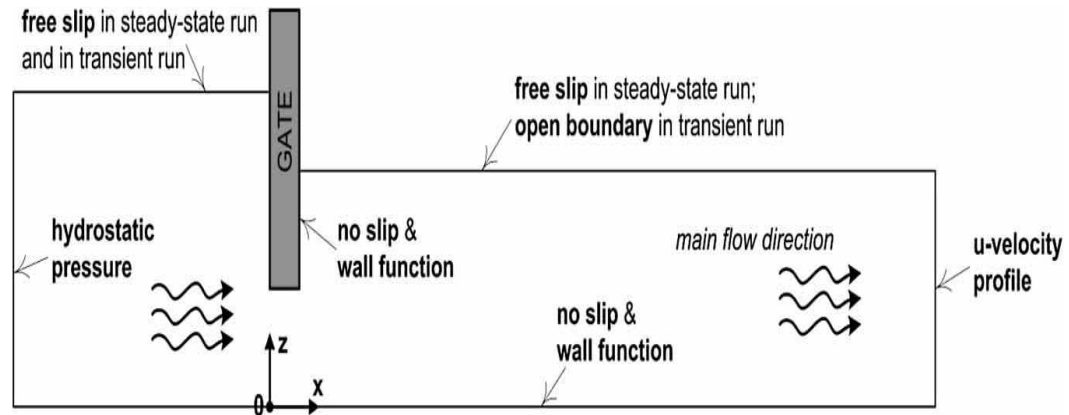


Figure 2.6 : The main flow direction is from left to right

The suggested formula was tested using field data and shown to be accurate, producing consistent results with less than 5% of error (Erdbrink et al., 2014).

The energy-momentum technique (EM), orifice flow rate formula, and application of the π -theorem of dimensional analysis may all be used to calculate the discharge beneath sluice gates. Experimental results were compared to the various discharge techniques that were available for free and submerged hydraulic jumps, including the transition between flows. Analysis was achieved on the effectiveness of the various calibrating techniques. The

test software demonstrates that the approaches based on the EM produced better results for the evaluation of the discharge beneath sluice gates for free and submerged flows as well as for the transition between the two flows. The results also demonstrate that the approaches that take into account the segmentation of the submerged flow partly and completely submerged did not improve the discharge results (Silva & Rijo, 2017).

Average discrepancy of around 4%, numerical and experimental models produced accurate predictions of discharge coefficients (Bilhan et al., 2018).

Artificial intelligence models were more accurate in estimating coefficient of discharge C_d . The multilayer perceptron (MLP) network model demonstrated a much-improved accuracy, with R and RMSE of 0.985 and 0.043, respectively (Norouzi et al., 2019).

A broad channel with the same flow conditions takes less time to evolve to the equilibrium state than the original, incised straight channel. After 8–12 hours, the equilibrium condition was reached the trials with the initial incised channel, whereas the initial broad channel was at equilibrium with the same flow parameters after 4-6 hours (Al-waeli, 2019).

Additionally, it is used in many fields, such as jet mixing, where improvements in computational power and resources have increased the use of CFD modeling for jet mixing and dispersion during the past 20 years. Due to a variety of factors, certain jet designs have drawn more attention than others. These justifications include, but are not limited to, simpler mesh generating geometries, simpler boundary conditions, easier compilation in numerical models, and the availability of data.



Figure 2.7 : Surface discharge of the Al-Ghubrah desalination plant, the largest such facility in Oman

However, more realistic CFD modeling in jet studies is now possible because to recent improvements in experimental configurations for jet studies and the accessibility of open-source CFD software. Using a thorough assessment of the literature on CFD modeling of effluent releases in the near-field region (Mohammadian et al., 2020).

An evaluation using numbers to show how free and submerged flows affect the coefficient of discharge (C_d) at labyrinth weirs. It has a characteristic shape and is made up of various parts, including the intake, the twisted weir, and the side entrance, which are often made of stainless steel or concrete. The upstream and downstream portions of the labyrinth weir's free surface flow profiles were also examined. The results showed that CFD models can properly forecast the coefficient of discharge on submerged and free flow through labyrinth weirs for a considerable sidewall angle (Carrillo et al., 2020).

The maximum sluice gate discharge coefficients for rectangular and semicircular sills are 2 and 0.5, respectively, in this case. As a result, the sluice gate's coefficient rises by 8.3% and 23%, respectively. For both sill types, the maximum sluice gate discharge coefficients are 2 and 0.5 in P/w , respectively. The sill height to gate opening (P/w) ratio is known as the discharge coefficient. The placement of the gate in respect to the start of the sill has an impact on the discharge coefficient of a sluice gate with a rectangular sill.



Figure 2.8 : Photographs of the experimental flume with the equipment installed on it and some of the models

The discharge coefficient starts to decrease when there is more space between the gate and the start of the sill. In other words, the sill causes a drop in the discharge coefficient. The Flow-3D model was used in this work to provide equations for figuring out the discharge coefficient of a sluice gate with rectangular sills. The models' results show that these equations can have an error of no more than 3% (Karami et al., 2020).

In rivers and canals, side weirs are used to manage water surface, discharge, and water elevation. According to the results by (Ghaderi et al., 2020) the depth of flow along the channel and weir reduces as the crest length grows with constant P/B (P = weir height, B = main channel width). Additionally, the discharge coefficient increases for long crest lengths and reduces for short crest lengths with an increasing P/y_1 ratio (P : weir height, y_1 : upstream flow depth). The results demonstrate that increasing the length, height, and sidewall slope of a side weir will enhance the discharge coefficient for a fixed T/L ratio (T : passing flow width, L : side weir crest length). When employing the dimensionless parameters of P/y_1 , T/L , and Fr_1 , certain relationships with high correlation factors are finally provided for getting discharge coefficients. It is demonstrated that T/L and P/y_1 are the most effective parameters for lowering the discharge coefficient based on hypothesized relations and sensitivity analysis (Ghaderi et al., 2020).

To calculate the flow discharge coefficient (C_d) for the combined rectangular broad crested weir-gate structure, add the discharge coefficients from each individual structure. To make this, the impact of the subsequent dimensionless parameters on the C_d was investigated: the central weir's width to the width of the whole structure (B/B_o), the central weir's height to the height of the central weir floor (Z/P), and the gate's width to the width of the

entire structure (b/B_o), The C_d was calculated using a recurrent network (RNN), a modular neural network (MNN), and a regression equation in order to estimate the ratio of the gate opening height to the height of the central weir floor (d/P), canfis network, and artificial intelligence models like the linear multilayer perceptron. The resultss demonstrated that when the d/P and b/B_o ratios increased, this coefficient declined. When the B/B_o ratio was increased for $h_1/H < 0.4$, the turbulence intensity and C_d decreased, but for $h_1/H > 0.4$, there was no clear difference. Furthermore, raising the Z/P ratio raised the flow's resistance, which caused C_d to decrease. Additionally, the results of the regression equation and artificial intelligence models demonstrated that the MNN model could provide a reliable estimate of the C_d values with an RMSE and R^2 of 0.03 and 0.97, respectively (Nouri & Hemmati, 2020).

Investigates the impact of sill form beneath a vertical sluice gate on C_d is examined. The impact of height is also included in the study.

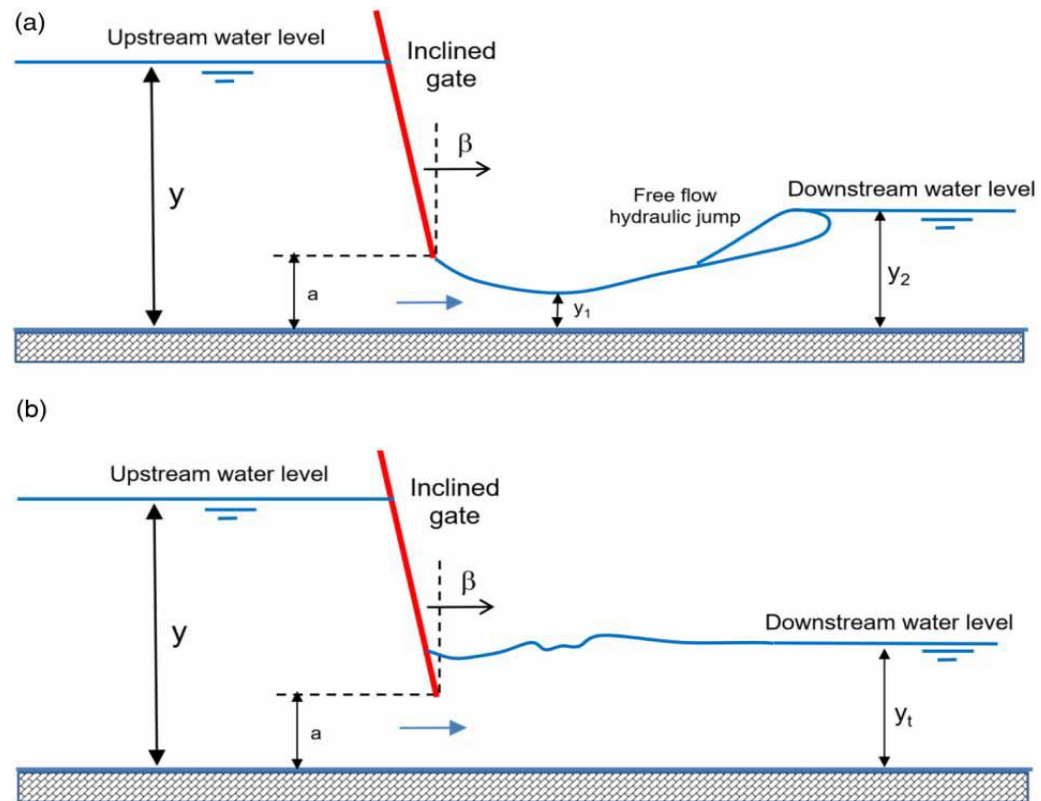


Figure 2.9 : Free (a) and submerged (b) flow in oblique/inclined sluice gate.

Polyhedral and non-polyhedral sills are present in both of the examined forms. C_d levels are predicted using multiple nonlinear regression (MNL), and the results suggest that circular sills beneath gates can raise C_d by 23–31%. The maximum C_d is found in a circular sill with a 3 cm diameter, while the lowest C_d is found in a trapezoidal sill (Salmasi & Abraham, 2021).

A collection of parallel groynes that were positioned vertically was the subject of numerical modeling and hydro-morphological research. In coastal engineering, parallel groynes are placed perpendicular to the coastline to stabilize beaches and stop coastal erosion. Typically, they are built by lining the coastline with rows of wooden or concrete pilings and filling the spaces between them with pebbles or other materials. The authors discovered that the

approach Froude number and the critical velocity ratio (V_{avg}/V_{cr}) affected the accuracy of the FLOW-3D model's simulation (Pourshahbaz, 2022).

Investigating the discharge coefficients of inclined sluice gates in both free-flow and submerged-flow scenarios was the major goal of their work. In the beginning, an inclined gate was built at a hydraulics lab at the Iranian University of Tabriz. The inclined gate was an inclined weir. At various openings, it was examined how the gate behaves as a supercritical flow generator in terms of contraction coefficient, discharge coefficient, and relative energy dissipation. Concerning gates, the one with the least amount of opening has the highest contraction coefficient value. Inversely correlated with the discharge coefficient is the gate opening amount. The hydrodynamic force acting on the gate and the upstream water depth are both inversely linked to the amount of opening (Daneshfaraz, et al 2022).

Five models were used to examine the effects of stepped mound breakwaters on breaking wave behavior with varying main sea levels above the breakwater crest. The results demonstrate that Flow 3D software is progressing since it can now generate waves of a variety of lengths and heights. Additionally, a larger wave transmission coefficient and energy dissipation are produced by the more stages (Hasan Ibrahim Al Shaikhli & Prof. Dr. Saleh Issa Khassaf, 2022).

2.5 Summary of the results of previous studies

- Calibration of flow equations on a physical model (Labeed A. Jawad Al-Taher, 1987).
- Used a physical model to test the discharge characteristics and pressure distribution for flows passing over an unsubmerged ogee spillway, The

relative error shows that the numerical model agrees within 1% with the physical model for $He/Hd > 0.7$ (Savage & Johnson, 2001).

- Sluice gate hydraulic properties are significantly influenced by the contraction coefficient. (Yen et al., 2001).
- Third order nonlinear model gave very accurate predictions. It was even able to predict waves. While the first and second order models were not able to capture waves (Weyer, 2001).
- The method demonstrates an efficient capacity for adaptive learning, leading to near-optimal performance of the control system while addressing the demands of real-time implementation (Darsono & Labadie, 2007).
- The numerical studies show that the turbulence plays an important role in the evolution of free surface when the reflected wave propagates upstream during the fluid flow passing the submerged obstacle (Lin et al., 2008)
- A useful method for analyzing the effects of needle tip design on various parameters is computational fluid dynamics (Shen et al., 2010).
- The outcomes demonstrated that the ratio of the crest length over the upstream depth, weir sidewall slope, and weir height over the upstream depth of the side weir, known as the Froude number, is related to the discharge coefficient in subcritical flow (Rahimpour et al., 2011).
- The introduction of the ICSMs to South African irrigation schemes may help in addressing operation and maintenance problems (Upport et al., 2011).

-
- The mean absolute percentage errors for these approaches ranged from 3.88% to 20%. The dimensional analysis approach using the imperfect self-likeness notion produced the best results (Erdbrink et al., 2014).
 - The test software demonstrates that the approaches based on the EM produced better results for the evaluation of the discharge beneath sluice gates for free and submerged flows as well as for the transition between the two flows (Silva & Rijo, 2017).
 - Average discrepancy of around 4%, numerical and experimental models produced accurate predictions of discharge coefficients (Bilhan et al., 2018).
 - Artificial intelligence models were more accurate in estimating coefficient of discharge C_d (Norouzi et al., 2019).
 - A broad channel with the same flow conditions takes less time to evolve to the equilibrium state than the original (Al-waeli, 2019).
 - An evaluation using numbers to show how free and submerged flows affect the coefficient of discharge (C_d) (Carrillo et al., 2020).
 - The Flow-3D model was used in this work to provide equations for figuring out the discharge coefficient of a sluice gate with rectangular sills. The models' results show that these equations can have an error of no more than 3% (Karami et al., 2020).
 - The results demonstrate that increasing the length, height, and sidewall slope of a side weir will enhance the discharge coefficient for a fixed T/L ratio (T: passing flow width, L: side weir crest length) (Ghaderi et al., 2020).
 - The results demonstrated that when the d/P and b/B_0 ratios increased, this coefficient declined. When the B/B_0 ratio was increased for h_1/H

0.4, the turbulence intensity and C_d decreased, but for $h_1/H > 0.4$, there was no clear difference (Nouri & Hemmati, 2020).

- the results suggest that circular sills beneath gates can raise C_d by 23–31%. The maximum C_d is found in a circular sill with a 3 cm diameter, while the lowest C_d is found in a trapezoidal sill (Salmasi & Abraham, 2021).
- The authors discovered that the approach Froude number and the critical velocity ratio (V_{avg}/V_{cr}) affected the accuracy of the FLOW-3D model's simulation (Pourshahbaz, 2022).
- At various openings, it was examined how the gate behaves as a supercritical flow generator in terms of contraction coefficient, discharge coefficient, and relative energy dissipation (Daneshfaraz, et al 2022).
- The results demonstrate that Flow 3D software is progressing since it can now generate waves of a variety of lengths and heights (Hasan Ibrahim Al Shaikhli & Prof. Dr. Saleh Issa Khassaf, 2022).

Chapter Three
CFD Modeling Creation and
Evaluation Methodology

Chapter Three

CFD Modeling Creation and Evaluation Methodology

3.1 Introduction

Physical modeling is commonly used to study the flow through hydraulic systems. The fundamental equations of fluid mechanics serve as the foundation for physical modeling. To physically represent hydraulic structures, a scaled laboratory model based on the prototype should be built. Researchers have attempted to use numerical simulation in conjunction with physical modeling due to the expensive expense of laboratory tests. In the area of numerical simulation, the governing equations of the flow, which are often Navier-Stokes equations, as well as turbulence models are solved using robust numerical techniques like finite volume method and finite elements method. To solve the turbulent flow, several turbulence models were presented (Dehdar-Behbahani & Parsaie, 2016).

The majority of the present corpus of research on the use of CFD to flow water modeling has come from studies conducted utilizing a variety of simulation tools. These experiments, which employed Flow 3D to model several different hydraulic structures, suggested that the experimental data and conventional design standards were in reasonable agreement, however, there are a variety of alternative software tools that can be used to model and examine the flow of water in the regulator. These include advice on how to use CFD effectively, as well as hydraulic concerns were the subject of previous studies.(Ibrahim Al Shaikhli et al., 2022)

Verified that CFD can be a useful alternative to solve and analyze an issue rather than producing a final suTable solution, in large part because of the number of assumptions utilized in the numerical methods to obtain

outcomes in CFD. The modeling technique is more difficult when the flow is three-dimensional 3D. (Ghare et al., 2008)

The results of running a series of numerical simulations in this study with the sole objective of confirming the experimental data is to be able to undertake the majority of the analysis with numerical simulations during the design stage. This would leave only the most basic scenarios for costly experimental analysis.(Muk-Pavic et al., 2006)

3.2 Definition of CFD

(CFD) is an abbreviation for computational fluid dynamics. It is a large area of numerical analysis on the subject of fluid flow. The advancement of computer-related techniques, as well as our understanding and solution of ordinary and partial differential equations, is critical to the advancement of CFD simulation. The direct numerical solution of complicated flows in real-world settings, on the other hand, necessitates a high degree of computing success in dealing with these problems; thus, CFD is much more than just "computer science" and numerical science. CFD software is used in several similar ways to prepare an experiment. The outcomes of the experiment will not accurately represent the real-life situation if it is not correctly set up to imitate it. Similar to how the results will not accurately reflect the real world if the numerical model does not precisely reflect it. The user must determine what information is crucial and how it should be presented. It is important to make sure that the problem you are designing represents the actual situation as much as possible.(*FLOW-3D User Manual*, 2008)

3.3 Flow 3D Approach

Using the Flow 3D (V.11.2) software, divide the flow field into rectangular form-groove sub division meshes, and calculate the numerical flow value to solve the Navier-Stokes equations in cartesian coordinates (Ibrahim Al Shaikhli et al., 2022). The most important aspect of any numerical model is selecting an appropriate mesh domain that responds appropriately to how the phenomenon behaves to obtain different numerical approximations of the control equations, control volumes are created around each variable position, based on the values of other variables in the area, it is possible to calculate surface fluxes, surface stresses, and body strengths for each control volume. After that, the sums are put together to produce an approximation for the protection rules suggested by the movement equations. (*FLOW-3D User Manual*, 2008)

3.4 Steps of working on the software can be summarize:

1. Using Auto CAD software and SketchUp to create the channel's 3D model.
2. Importing the 3D model's file into the Flow 3D software and generating the final mesh.
3. Selecting the fundamental equations to be solved.
4. Identity fluid properties.
5. Identify boundary conditions, it is significant that this software has a wide variety of boundary conditions when defining the boundary conditions.
6. Initializing the flow field.
7. Adjusting the output.

8. Changing the control settings and selecting a calculating technique and formula.
9. Running the simulation and results evaluation.
10. Post-processing the results, once the simulation has been completed, use Flow3D's built-in tools or third-party software to post-process the results. Visualize the results, extract data, and analyze the flow characteristics.

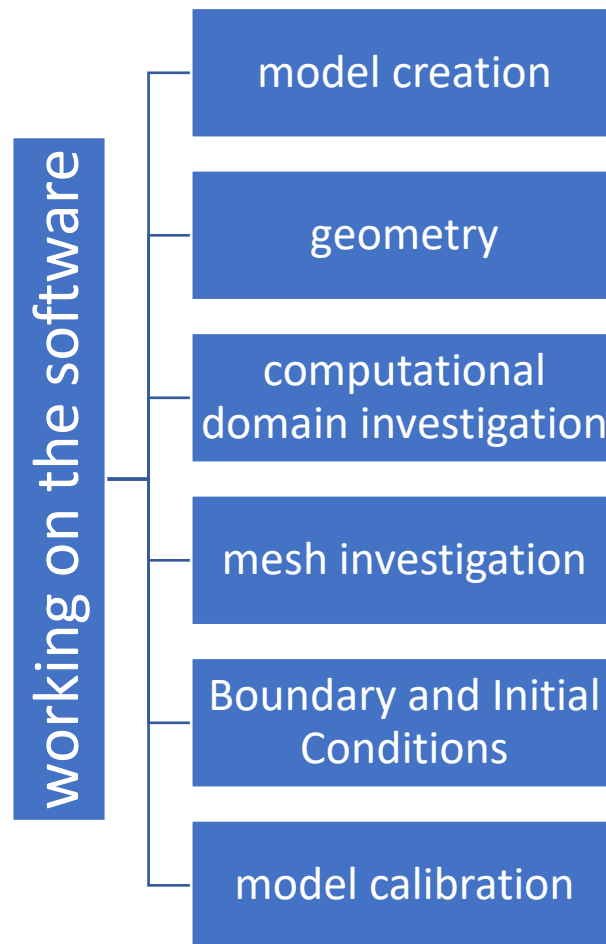


Figure 3.1 : working on the software

3.5 Turbulence Models

Turbulence is the disordered, insecure flow of liquids produced by a lack of stable viscosity forces. Based on the values of other variables in the region, surface fluxes, surface stresses, and body strengths can be estimated for each control volume. The quantities are then added together to obtain an estimate for the protection rules suggested by the movement equations.

Turbulence cannot be disregarded in numerical flow modeling because it is a ubiquitous phenomenon. To model the full range of turbulent variations, it is necessary to maintain constant values of the mass and momentum equations. This can only be achieved if the mesh resolution is high enough to capture such details, but due to constraints in computer memory and processing time, such high resolution is typically not feasible. Therefore, modeling is simplified by describing the effects of turbulence on average flow properties. (*FLOW-3D User Manual*, 2008)

3.6 The Complexity of the Turbulence Model

Depending on the details that should be considered and investigated through these numerical simulations, the complexity of different turbulence models might vary substantially. The Navier-Stokes equation is designed in such a way that this is the case (N-S equation). The N-S equation is a three-dimensional, partial differential equation PDE that is nonlinear and time-dependent. The fact that vortex formations travel together with turbulent flow is another significant characteristic. They usually have a lengthy lifetime. As a result, some volatile volumes are unable to be categorized as local. Turbulence is also considered to be a random process in time. As a result, no deterministic strategy is practicable. Statistical techniques might be used to

discover certain characteristics of turbulence. These relationships cannot be predicted in advance. (Mohammed et al., 2015)

3.7 Mathematical Model and Numerical Solution Technique

Today, a variety of techniques can be used to calculate turbulent flows. Using models that are appropriate for turbulent values, one can either directly calculate the Reynolds intermediate Navier-Stokes equations or solve them.

In this investigation of the Flow-3D software, the fluid velocities are described using the Navier-Stokes equations, demonstrating the value of the k-equation turbulence model in modeling the properties of the hydraulic jumps in the model's complicated water flow. To understand the features of energy dissipation in the model, they employed the volume of fluid (VOF) RNG k- and Mixture RNG k- turbulence models. Additionally, modeling can save time and money when compared to experimental effort. (Karim & Ali, 2000), (Lin et al., 2008)

3.7.1 Governing Equations

The Reynolds-averaged Navier-Stokes equations are the continuity equation, turbulence kinetic energy equation (TKE), momentum equation, and turbulence energy dissipation rate equation, and they are displayed in the following ways:

3.7.1.1 VOF Turbulence Model

The Navier-Stokes equation can give an accurate mathematical representation even though the flow pattern is exceedingly complex and computationally affordable. (WANG et al., 2009)

The flows' hydraulic characteristics are determined using the k- ϵ RNG model (kinetic-energy). The anisotropy of high-velocity jets can be accurately

simulated by this approach. The momentum equation, continuity equation, ε - equation, and k-equation are the governing equations for the VOF turbulence model, respectively. (Chen et al., 2010)

Continuity equation :

$$\left[\frac{\partial \rho}{\partial t} \right] + \left[\frac{\partial \rho u_i}{\partial x_i} \right] = 0 \dots\dots\dots(3-1)$$

where :

$\partial \rho / \partial t$ is the time derivative of density, $(\partial \rho u_i) / (\partial x_i)$ is the divergence of mass flux density, x_i is the spatial coordinate in the I direction, and u_i is the velocity component in the I direction.

Momentum equation :

$$\left[\frac{d \rho u_i}{dt} \right] + \left[\frac{\partial}{\partial x_i} \right] (\rho u_i u_j) = - \frac{\partial \rho}{\partial x_i} + \frac{\partial}{\partial x_i} [(\mu + \mu_t) + \left(\frac{\partial u_i}{\partial x_j} + \frac{\partial u_j}{\partial x_i} \right)] \dots(3-2)$$

Where :

ρ is the fluid density

u_i is the velocity component in the horizontal direction

t is time

x_i is the coordinate in the horizontal direction

μ is the fluid viscosity

μ_t is the turbulent viscosity

$\partial / \partial x_i$ is the partial derivative concerning the coordinate x_i

$\partial u_i / \partial x_j$ and $\partial u_j / \partial x_i$ are the velocity gradients in the j and I directions, respectively.

K - equation:

$$\frac{\partial(\rho k)}{\partial t} + \frac{\partial}{\partial x_i} (p u_i k) = \frac{\partial}{\partial x_i} \left[\left(\mu + \frac{\mu_t}{\sigma_k} \right) \frac{\partial k}{\partial x_i} \right] + Gk - \rho \varepsilon \dots\dots\dots(3-3)$$

Where :

K is the turbulent kinetic energy density, which represents the energy associated with the turbulent fluctuations in the flow

p is the fluid pressure

ε is the dissipation rate of the turbulent kinetic energy

Gk is the production rate of the turbulent kinetic energy, which represents the rate at which the mean flow does work on the turbulent fluctuations.

ε - equation:

$$\frac{\partial(\rho \varepsilon)}{\partial t} + \frac{\partial}{\partial x_i} (p u_i \varepsilon) = \frac{\partial}{\partial x_i} \left[\left(\mu + \frac{\mu_t}{\sigma_\varepsilon} \right) \frac{\partial \varepsilon}{\partial x_i} \right] + c1 \varepsilon \rho \left(\frac{\varepsilon}{k} \right) Gk - c2 \varepsilon \rho \left(\frac{\varepsilon^2}{k} \right) \dots\dots\dots(3-4)$$

Where :

ε is the rate at which turbulent kinetic energy is transformed into thermal energy as a result of viscous and turbulent phenomena, is known as the turbulent dissipation rate.

$c1\varepsilon$ and $c2\varepsilon$ are model constants

3.7.1.2 Mixture turbulence model

To simulate multistage flow with various velocities, the mixture model is a streamlined version of the multistage flow model. At short-term spatial scales, the equilibrium is thought to remain stable. Along with the correlations between phase volume fractions and slip velocity, the model also

incorporates the energy equation, continuity equation, and mixed phase momentum equation. The following are some ways in which the mixed turbulence model and VOF turbulence model diverge:

1. Inter-phase penetration is supported by the mixture model, with volume fractions in the control volume ranging from zero to one.
2. It permits slip velocity between phases.

3.8 CFD Simulation

To accurately replicate the data wherever it was required for this study, only two of the various physics options were chosen. When it was determined that the vertical direction was moving at a negative 9.81 m/s^2 , the acceleration of gravity option was enabled. The viscosity and turbulence option are also available, which selects an appropriate turbulence model and apply newtonian viscosity to the flow. Once the Flow-3D model was completed, only one turbulence model was used, as long as the renormalized group (RNG) model was chosen.

Although there are numerous other physical options available, for accurate simulations of the data needed for this research, just two of them needed to be active. When the vertical gravity acceleration, commonly known as the z-direction, hit -9.81 m/s^2 , the gravity option was turned on. When the flow was subjected to newtonian viscosity and a suitable turbulence model, the option to activate viscosity and turbulence at the same time was activated. According to the user's manual for FLOW 3D, the software's best model for simulating breaking waves is the $(k-\epsilon)$ turbulent model. It is also the best model available right now.

3.9 Geometry of Regulator

Six models were taken and worked on, which are the width of gates 15, 25, 35, and 50 cm for the single opening of the gate, as well as 3*10 cm and 3*20 cm were taken for the multiple openings and with a different high of the gates. Models were created in the shape of a level bottom regulator with a vertical sliding gate and a straight connection, measuring 12 mm thick and 30 cm tall. The Figures in Appendix A to Appendix F show the number of experiments conducted on these six models with different gate openings. Figures (3-1) and (3-2) display the numerical model's geometric representation..

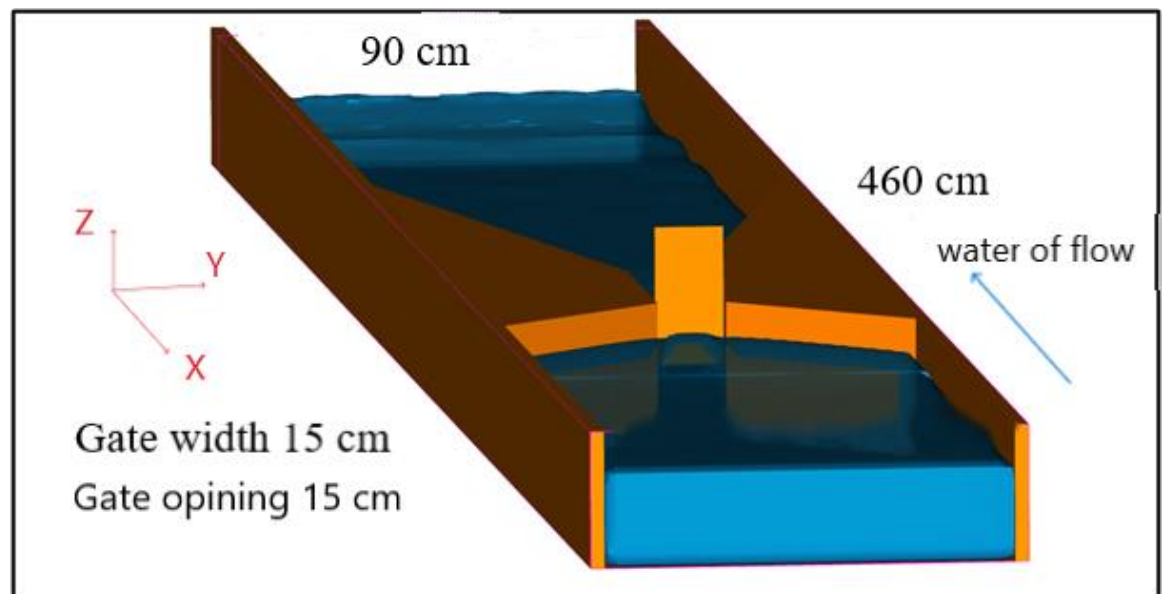


Figure 3.2: Geometric model configured by the FLOW 3D software with one gate

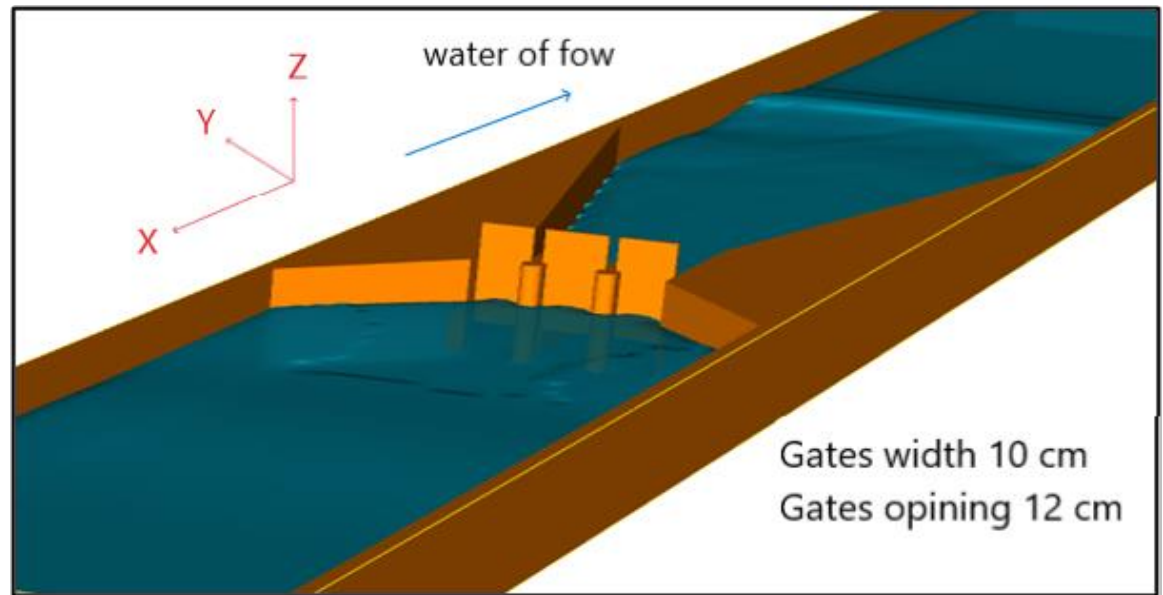


Figure 3.3: Geometric model conFигured by the FLOW 3D software software with three gate

The experimental investigation's results indicate that the simulations' geometry came in the form of a stereo lithography, or STL, picture. The STL version of this picture was created in AutoCAD or SketchUp. If the required network can be constructed. Since it was anticipated that the typical value of concrete hardness for the flume geometry would not be taken into consideration as part of this investigation, the geometry component remained the default setting for all models that were constructed.

3.10 Mesh, Numerical Modeling and Analysis

One of the most significant factors of Flow-3D is the grid. If a high-quality mesh is constructed, the numerical model can be used to apply a precise solution and produce verifiable results. Setting a cell's mesh size is an important step in any numerical model simulation. The simulation duration and accuracy may be affected by cell size and grid. As shown in the Figure

(3-3), as the number of cells rises, so does the accuracy of the results. Starting with a somewhat large cell grid and gradually reducing the mesh size until the result no longer changes noticeably is an excellent technique for determining the crucial cell size. Placing several cells will accelerate the numerical advancement. Because computation is completed for each cell, the number of cells increases the computation time. As a result, the best cell counts must be chosen. Since the cells are perpendicular at first, the optimal cell size must be obtained to build a system that is nearly identical to the real one. This can be done by favoring the option. (*FLOW-3D User Manual*, 2008)

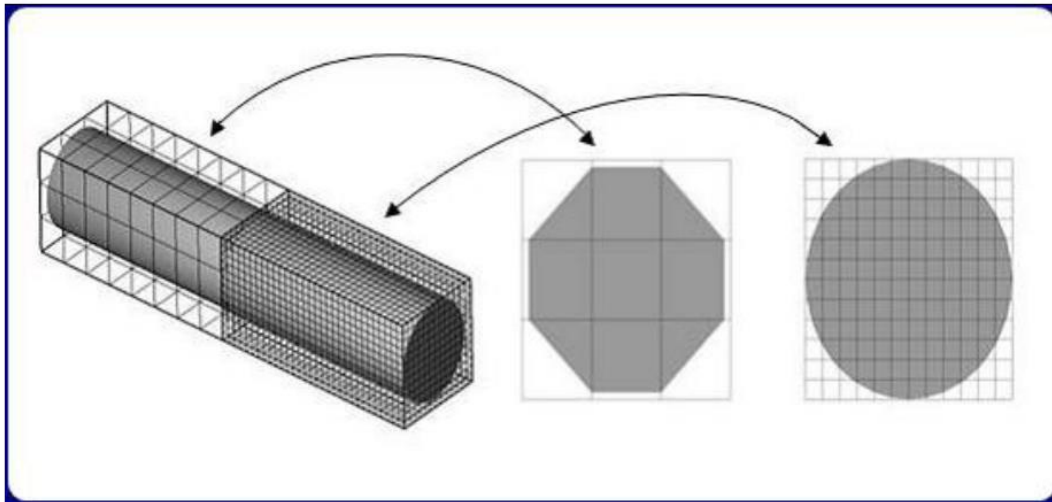


Figure 3.4: Favor option with different cell sizes (Mohammed et al., 2015)

One of the influences on the simulation process is taken into account by the cubic-shaped cells in the mesh of the Flow-3D software. To find the best cell size that meets the parameters of the phenomena, many cell sizes are chosen, including (2,1.8,1,0.5) cm.

In this study, The model utilized has a width of 1 m and a crest elevation of 7.5 m. Hexahedral cells with a 0.03 m diameter were employed in the

investigation. 80,000 meshes make up the entire mesh count (Figure 3-4). The analysis was carried out for another 100 sec, or until the flow was entirely steady. By supplying fluid elevation, turbulence model assessments using the Renormalized Group (RNG) were resolved. The flow began at different elevations, according to the width and gate opening at the inlet, and began to decrease at the outlet, according to the data set and compared to the real case. The channel border conditions were identified as (Symmetry). Boundary conditions for the inlet and outflow are (Specified Pressure) and (Wall) for the channel floor, respectively. A one-meter downstream water inflow is defined to create downstream circumstances and detect hydraulic jumps.(Ulu et al., 2021)

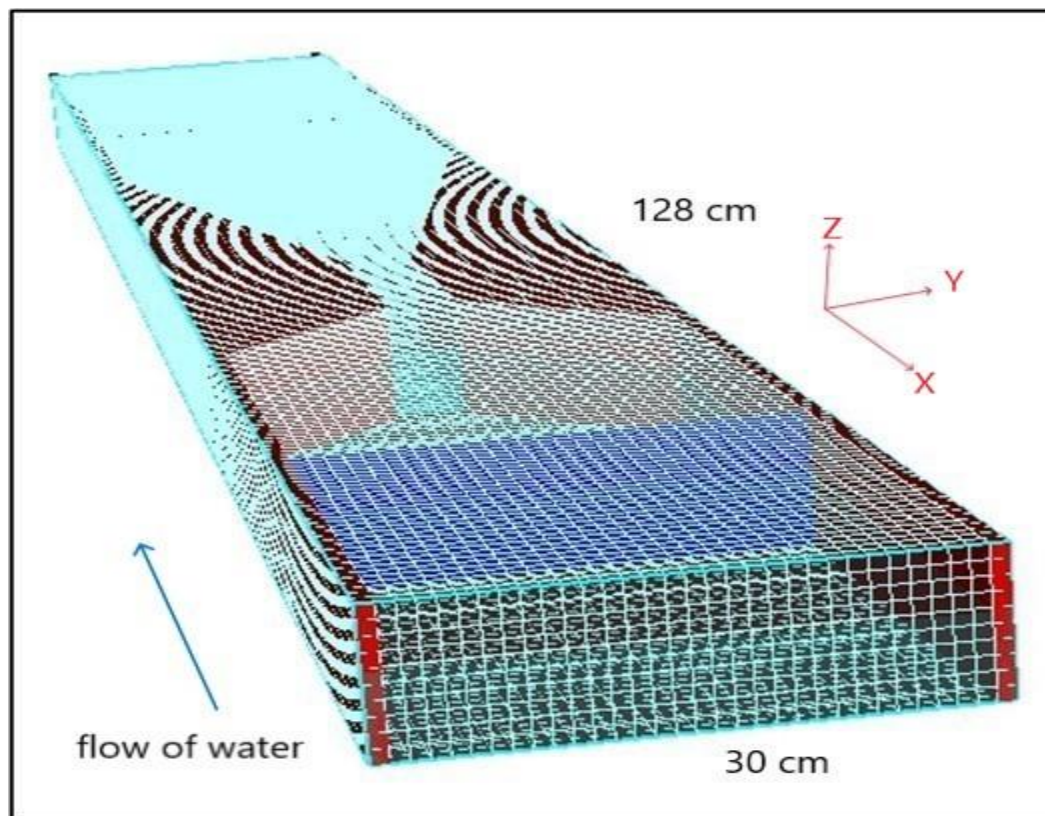


Figure 3.5: Total mesh in model

3.11 Boundary and Initial Conditions

Choosing the suitable boundary conditions, which should accurately reflect the physical circumstances of the issues, is one of the most crucial jobs in numerical flow analysis. The boundary conditions applied in this study are listed below, along with an example of each, Figure (3-5) shows the locations of the boundary conditions.

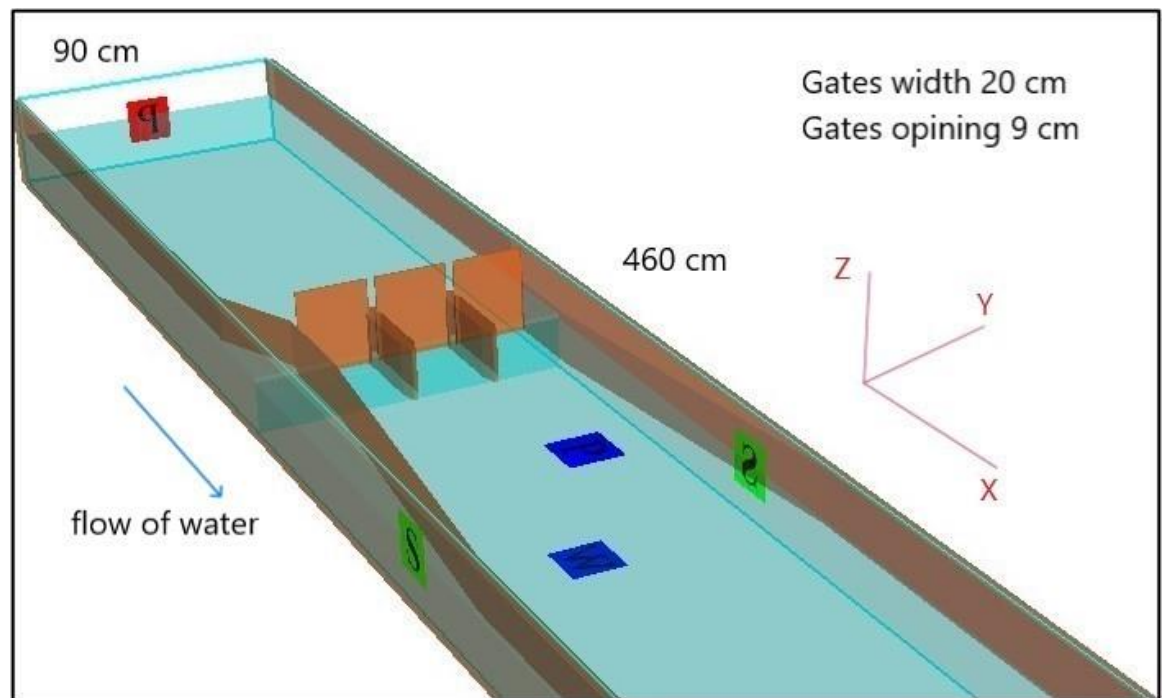


Figure 3.6: Boundary conditions

1. Upstream boundary (X-min): For various uses of fluid elevation, pressure (P) in Pascal is set on the upstream mesh plane (inlet boundary).
2. Downstream boundary (X-max): For various fluid elevation uses, pressure (P) in Pascal is also provided in the downstream mesh plane.

3. Bottom boundary (Z-min): The channel's ground is represented by the wall condition (W).
4. Top boundary (Z-max): This barrier denotes air pressure at the channel's top.
5. Cross boundary (Y-min): Symmetric ailment (S).
6. Cross boundary (Y-max): Symmetric ailment (S).

In a flow that is bounded by a wall, the near-wall zone and the free-stream region are dominated by different sizes and physical processes. The near-wall region's modeling has a considerable impact on the interior flow's numerical solution's fidelity in terms of velocity and pressure drop. It is well established that at the near-wall region, the mesh density and element size must be high enough to capture flow behavior. Even with the continuous advancement of computer power, results a balance between computing resources and mean flow amount accuracy is still difficult.(Al-waeli, 2019)

According to the Navier law, the regular element of the velocity at the fluid-solid interface is continuous (the waterproofness state), and the quantity of slip in the tangential part of the velocity is comparative to the tangential part of the regular stress that the fluid is exerting on the boundary. The term "slip length" refers to the proportionality coefficient. It is necessary to suppose that the slip length disappears (i.e., assume no-slip boundary conditions) in order for theoretical and experimental conclusions to be significant. (Gérard-Varet et al., 2015)

3.12 Solver Option

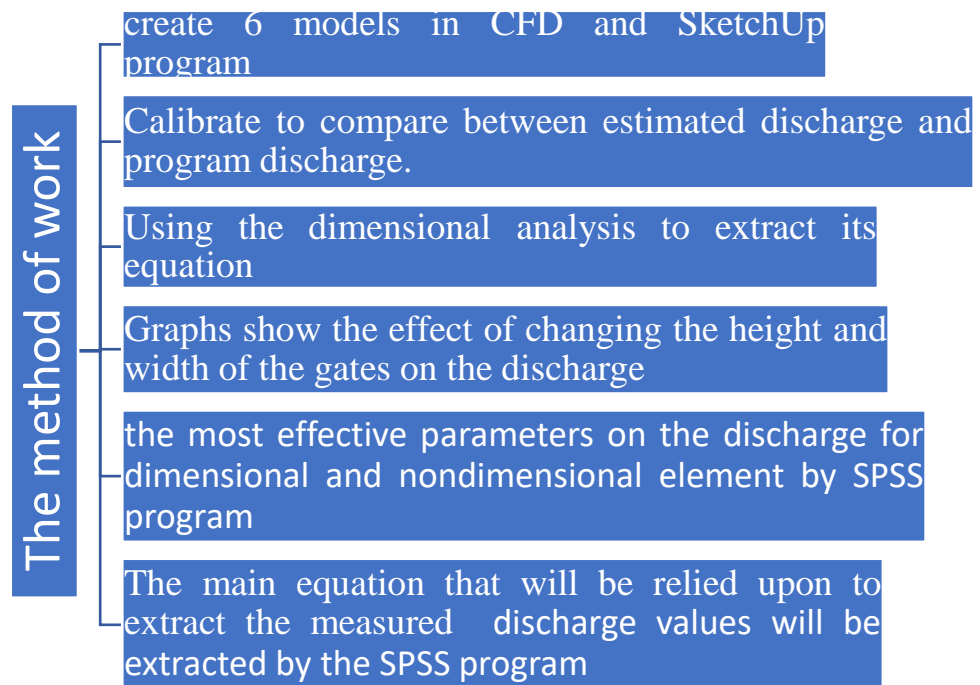
Convergence parameters, numerical approximations, and time step size are some of the variables that affect simulation results. It's important to

balance run time and simulation accuracy. Therefore, providing the best and most efficient solutions for simulation and choosing appropriate model options are crucial. The number of options are listed under the numeric tab. Since just one fluid was solved, it is assumed throughout all simulations to be incompressible. The generalized minimal residual method (GMRES) algorithm is an iterative method that can be applied to a variety of issues, according to the Flow-3D user manual. For all kinds of flow issues, there are several possibilities for passing fluid interfaces. Using programmed choices to follow the fluid interface, the volume of fluid advection model. The most often applied and precise Flow-3D model for acute contact with a single free surface fluid flow is the softwaremed option.

3.13 The method of work

Using the dimensional analysis to extract its equation, a comparison was made between the non-dimensional elements using the Spss software to extract the most influential on discharge. This was achieved after the calibration that was carried out between Q estimated and Q software, and also after making six models with widths and heights of different gates, making simulations, and extracting discharge values for each model to obtain adequate information for analysis and comparison with laboratory measurements. Initial levels were chosen based on the previous research for the different six models with different heights and widths of the gates, with a total of 85 models made as shown in Appendix G, 55 of which were used in this study, to calculate the discharge. Therefore, choosing the correct initial conditions in the inlet and outlet is very important to extract values that are identical or close to the actual situation in the laboratory channel.

After that, the non-dimensional element values were extracted and analyzed with a discharge to know the effect of each change in the width and gate opening on the flow. Finally, using the Spss software, the main equation that was relied upon was extracted.



3.14 Dimensional Analysis

Dimensional analysis is the more effective approach for formulating the issues. To correlate the various relationships between the various parameters that affect flow that result from changes in the (regulator shape, Froude number, change in height of gate, and width of the gate in the model), a theoretical study relies on the fundamentals of dimensional analysis. The categories of time (T), length (L), and mass (M) could be written as displayed in Table (4-1).

Table 3-1: The classification of parameters that affect on the flow of water

characterizing the fluid flow		Dimensions
ρ	The density	ML^{-3}
Q	The discharge	L^3T^{-1}
g	Gravitational acceleration	LT^{-2}
μ	Dynamic viscosity of the fluid	$ML^{-1}T^{-1}$
Y_1	Depths of the water in the upstream flow	L
V_1	The velocity of the water	LT^{-1}
L	Model's length	L
W	Model's width	L
N	Number of gates	-
B	The gate's width	L
H	Gate opening	L
T	Time	T

This study's discharge coefficient is influenced by the fluid's and the model's geometric and hydraulic properties, respectively. Thus, according to Buckingham's Π theory, can be recast as:

$$Q = f_1(Y_1, V_1, g, W, N, L, B, \rho, \mu, H) \dots \dots \dots (3-5)$$

which Buckingham's Π theory permits to be rewritten:

$$f_1 = (Q, Y_1, V_1, g, W, N, L, B, \rho, \mu, H) \dots \dots \dots (3-6)$$

- Because there are three fundamental units ($m=3$) and eleven variables ($n=11$), there are nine ($n-m = 11-3 = 8$) dimensionless parameters.

- Every term must have $(m+1) = (3+1) = 4$ variables when the common variables, Y_1 , and g are taken into account. The Buckingham theorem may be used to write the equation.

$$F_2(\pi_1, \pi_2, \pi_3, \pi_4, \pi_5, \pi_6, \pi_7, \pi_8) = 0 \dots \dots \dots (3-7)$$

Where :

$$\pi_1 = \rho, g, y_1, Q \dots \dots \dots (3-8)$$

$$\pi_2 = \rho, g, y_1, V \dots \dots \dots (3-9)$$

$$\pi_3 = \rho, g, y_1, W \dots \dots \dots (3-10)$$

$$\pi_4 = \rho, g, y_1, N \dots \dots \dots (3-11)$$

$$\pi_5 = \rho, g, y_1, L \dots \dots \dots (3-12)$$

$$\pi_6 = \rho, g, y_1, B \dots \dots \dots (3-13)$$

$$\pi_7 = \rho, g, y_1, H \dots \dots \dots (3-14)$$

$$\pi_8 = \rho, g, y_1, \mu \dots \dots \dots (3-15)$$

- Taking each term and evaluating:

$$\pi_1 = \rho^{a_1}, g^{b_1}, Y_1^{c_1}, Q \dots \dots \dots (3-16)$$

- Expression these in dimension terms to give:

$$M^0 L^0 T^0 = (ML^{-3})^{a_1} (LT^{-2})^{b_1} (L)^{c_1} L^3 T^{-1}$$

For M

$$0 = a_1$$

For L

$$0 = -3a_1 + b_1 + c_1 + 3$$

For T

$$0 = -2b_1 - 1$$

$$a_1=0 \quad , \quad b_1=-1/2 \quad , \quad c_1=-2.5$$

$$\therefore \pi_1 = \frac{Q}{\sqrt{g} \cdot Y_1^{2.5}}$$

In the same way, another parameter is showed in the Table (4-2):

Table 3-2: parameter influence of flow rate

$\pi_1 = \frac{Q}{\sqrt{g} \cdot Y_1^{2.5}}$	$\pi_2 = \frac{v}{\sqrt{g \cdot Y_1}}$	$\pi_3 = \frac{W}{Y_1}$
$\pi_4 = N$	$\pi_5 = \frac{L}{Y_1}$	$\pi_6 = \frac{B}{Y_1}$
$\pi_7 = \frac{H}{Y_1}$	$\pi_8 = \frac{\sqrt{g \cdot \rho \cdot Y_1^{1.5}}}{\mu}$	

The general effects can be simplified as follows:

- If the area of the cross-section of the channel is a rectangle, then the term π_2 will be:

$$Fr = \frac{v}{\sqrt{g \cdot Y_1}}$$

- If the flow is completely turbulent, the term $\pi_8 = \frac{\sqrt{g \cdot \rho \cdot Y_1^{1.5}}}{\mu}$ is typically a negligible parameter and can be ignored from the equation because its effect is small. (Pagliara et al., 2008)
- Since the model's length and width are taken to be constant across all runs, the effect of the basin's length and width on the water flow (L/Y, W/Y) can be ignored.

After the aforementioned equations were simplified, the constant and negligible parameter values were removed, and the assumption was been applied:

$$F3 (\pi_1, \pi_2, \pi_4, \pi_6, \pi_7) = 0 \dots \dots \dots (3-17)$$

It is possible to express the functional connection that explains the discharge as follows:

$$Q = \sqrt{g} \cdot Y_1^{2.5} F4(Fr, \frac{B}{Y_1}, \frac{H}{Y_1}) \dots \dots \dots (3-18)$$

$$Q = F4(g^{0.5} \cdot Y_1^{2.5}, Fr, \frac{B}{Y_1}, \frac{H}{Y_1}) \dots \dots \dots (3-19)$$

3.15 The standard performance measures

The following common statistical metrics are used to assess the accuracy of forecasts:

- Root mean square error (RMSE)

$$RMSE = \left(\sqrt{\frac{\sum_{i=1}^n (Q_m - Q_p)^2}{n}} \right) * 100 \dots \dots \dots 3-20$$

- Mean absolute error (MAE)

$$MAE = \left| \frac{\sum_{i=1}^n (Q_m - Q_p)}{n} \right| \dots\dots\dots 3-21$$

Where:

Q_m is measured discharge

Q_p is software discharge

n is the number of discharge

According to theory, the RMSE allows for a term-by-term comparison of the real difference among the calculated and observed values, which offers information about a system's short-term performance. (Iqbal, 1984). The system performs better when the value is smaller. This test's drawback is that it does not differentiate between underestimation and overestimation, which can result in a significant increase in RMSE with just a few significant errors.

Chapter Four

Results and Discussion

Chapter Four

Results and Discussion

4.1 Introduction

This chapter discusses the outcomes of numerical model simulations completed by means of the Flow-3D software to examine the effects of variables, such as channel geometry, position, and gate opening. The information from the numerical models was utilized to create formulas that would forecast the highest ratio of discharge employing the dimensional analysis technique and SPSS V23.0 statistics package. In order to confirm the accuracy of the Flow-3D software's outputs, the numerical model results were compared with information gathered from earlier research. The results of the calibration between the various models were then examined. To evaluate the effectiveness of the channel and the most effective parameter on the discharge, this chapter compares the maximum flow rates for numerous test runs on various models.

4.2 Results and their evaluation

The depth of the water at the inlet (Y_1) affect the discharge coefficient contained in the symbol (h_i), which is the variance among the depth of the water at the inlet and the depth at the outlet. This is controlled by the degree of narrowing of the waterway about the channel, the transition from the width of the regulator to the width of the channel of the regulator or model.

Each model has a bond among the flow rate (Q) and the ratio of the width of the gate to the depth of water at the inlet (B/Y) and the ratio of high of the gate to the depth of water at the inlet (H/Y) that differs from the other

models, and since the studied models differ among themselves in width and the number of openings only, so the flow rate coefficient turns with the change in the width and number of openings in the model.

The results extracted from the software in which the (Q_p) discharge software is calculated for each of the six models used for the two cases of flow at the total full opening of the gate and the submerged flow at the gate partially opening. As shown in Figure (4-1), the determination coefficient R^2 between Q_P and Q_E is 84.76%, it is an acceptable outcome, so the results of the software can be depended upon. Data were taken from (Labeed A. Jawad Al-Taher, 1987) and the CFD software as shown in Appendix A to Appendix F.

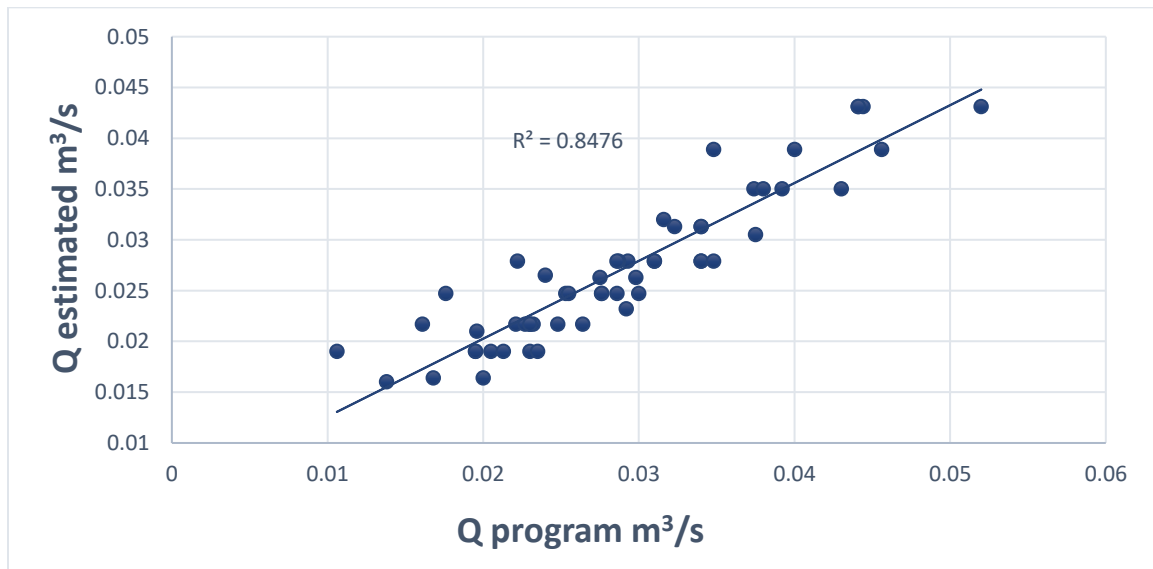


Figure 4.1: Software calibration with Labeed's study

Figures 4-2 and 4-3 show the difference in parameters with a height of gate opening of 16 cm and full opening of the gate and other Figures in Appendix F. It is noted that the discharge is approximately 0.2 to 0.3 m³/s at an opening of 16 cm while when the gate is fully opened 0.3 to 0.4 m³/s an growth in the flow rate is observed with an rise in the gate opening.

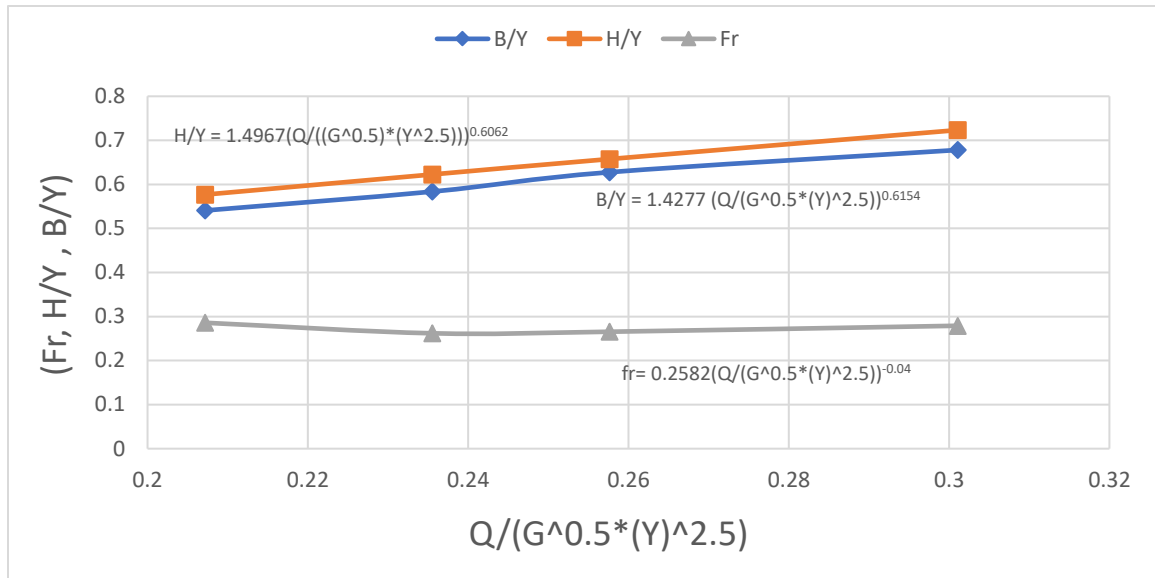


Figure 4.2: Equations of 15 cm width and 16 cm open of the gate

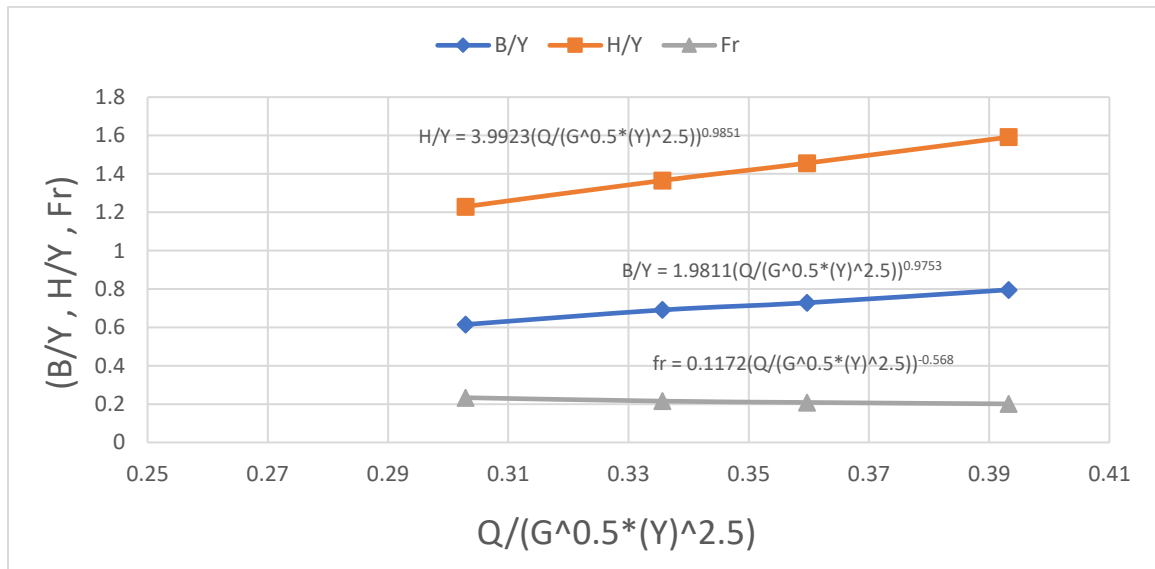


Figure 4.3: Equations of 15 cm width and full opening of the gate

Also, in Figures 4.4 and 4.5, it is noted that the full opening of the gate has the greatest effect on increasing the amount of discharge.

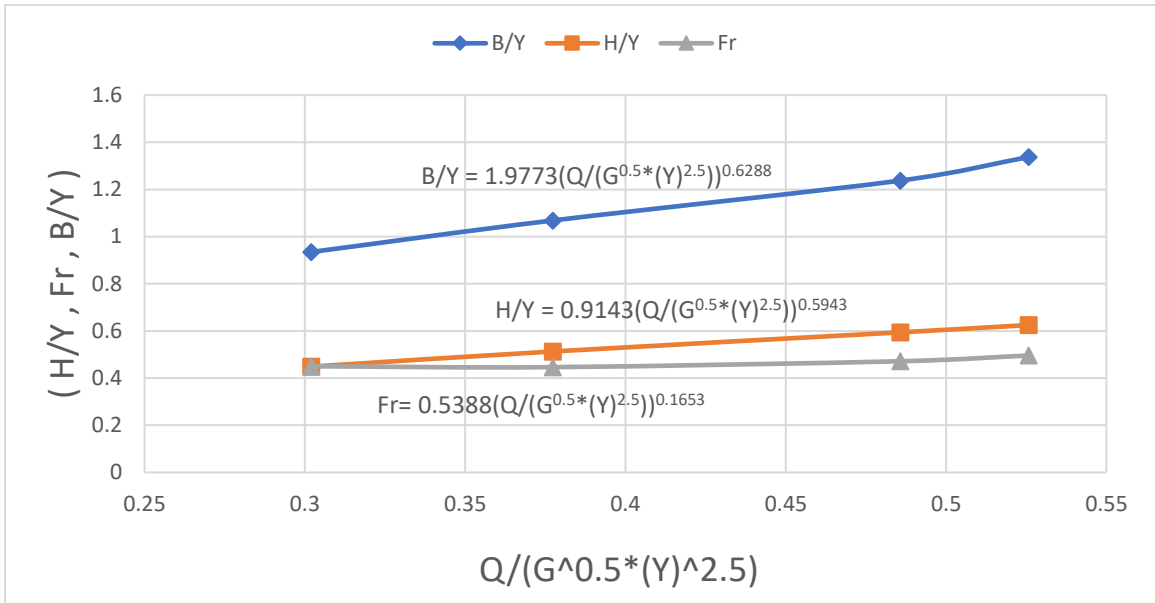


Figure 4.4 : Equations of 25 cm width and 12 cm open of the gate

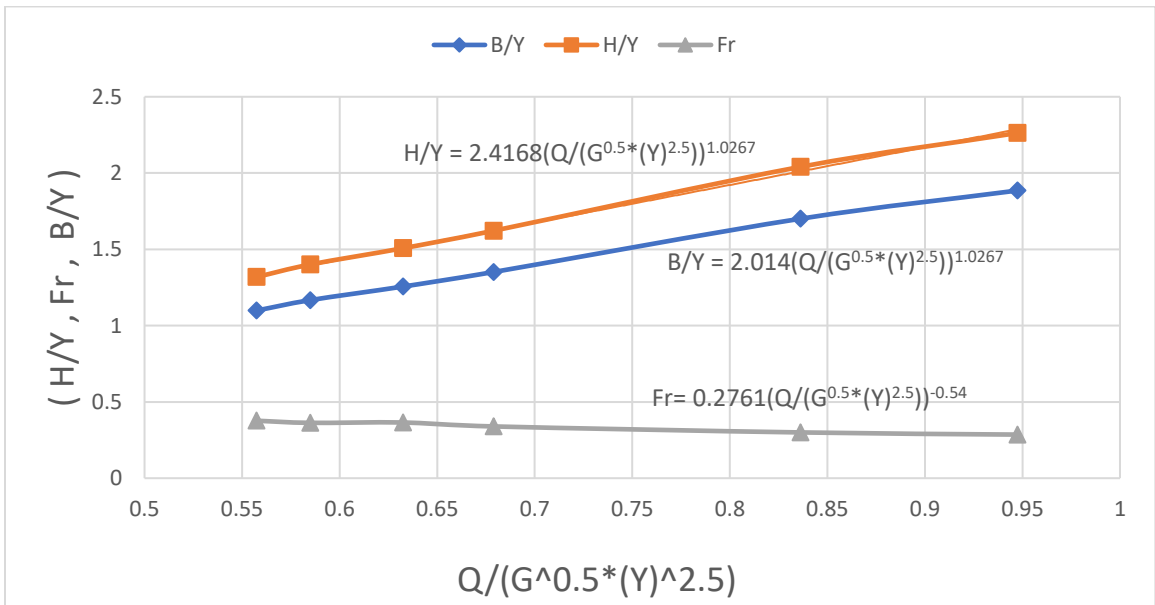


Figure 4.5 : Equations of 25 cm width and full opening of the gate

4.3 Nonlinear multiple regression analysis

There are many functional correlations were tested, and those with low R^2 were disregarded. The last functional connection was chosen and will take the power form;

$$\frac{Q}{\sqrt{g} Y^{2.5}} = a \left(\frac{B}{Y}\right)^b \left(\frac{H}{Y}\right)^c (Fr)^d \dots\dots\dots(4-1)$$

Using the more recent Spss software V.24, the multiple nonlinear regression analysis was carried out. Only functional forms that precisely describe the connection between the dependent and independent variables can lead to convergence. To obtain good results, it is also crucial to choose the appropriate coefficient and exponent beginning values in the suggested functional relationship. Poor initial values might prevent the suggested relationship from converging until the proper functional relationship is found. As a result, the initial coefficient and exponent values were determined via an iterative process. (Al-waeli, 2019)

In this investigation, a beginning value of 0.1 proved more practical. The empirical formula is stated as follows in its final and more trustworthy form:

$$\frac{Q}{\sqrt{g} Y^{2.5}} = 0.723 \left(\frac{B}{Y}\right)^{0.586} \left(\frac{H}{Y}\right)^{0.519} (Fr)^{0.46} \dots\dots\dots(4-2)$$

Where;

$$Fr = \frac{v}{\sqrt{gh}} \dots\dots\dots(4-3)$$

And $v = \frac{Q}{bY}$ when $b = 0.3$

Then the final formula for calculating discharge is;

$$Q_m = 0.548 * \left(\frac{B}{Y}\right)^{1.085} * \left(\frac{H}{Y}\right)^{0.96} * \frac{g^{0.925} * y^{4.629}}{(0.3 * Y * \sqrt{g * h})^{0.851}} \dots\dots\dots(4-4)$$

Where;

Q_m : measured discharge

h : water level under the gate

v : velocity

4.4 Validation of the formulation

The developed empirical formula has been evaluated by Table 4-3 comparing the discharge extracted from the equation (measured discharge Q_m) based on data taken from (Labeed A. Jawad Al-Taher, 1987) and the discharge extracted from the software Q_p . Figure 4-4 compares the discharge statistics that were measured and calculated. The R^2 determination coefficient was used in this comparison. It demonstrates that there is good contract among the results of the proposed formula and the estimated values. $R^2=0.7558$, which indicates that there is an agreement, suggests that using this formula is a realistic method for calculating discharge.

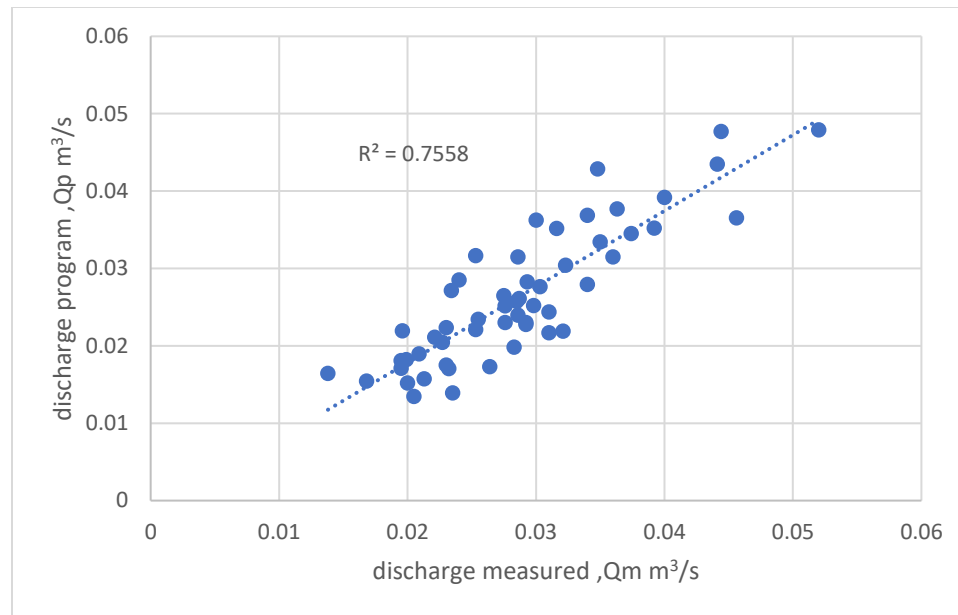


Figure 4.6: correlation coefficient between discharge software and discharge measured

Table 4-1: Data to validation the estimated value and measured

No	B/Y	H/Y	Q_p m ³ /s	Q_m m ³ /s	ΔQ
1	0.795756	1.591512	0.0195	0.018102	0.0014
2	0.761421	0.761421	0.0205	0.013474	0.0070
3	0.728155	1.456311	0.0221	0.021105	0.0010
4	0.678119	0.723327	0.0232	0.017042	0.0062
5	0.65388	0.65388	0.0230	0.017532	0.0055
6	0.583658	0.622568	0.0253	0.022088	0.0032
7	0.558451	0.558451	0.0276	0.023030	0.0046
8	0.614754	1.229508	0.0293	0.028282	0.0010
9	0.590551	0.787402	0.0310	0.024394	0.0066
10	0.638298	1.276596	0.0275	0.026503	0.0010
11	0.540735	0.576784	0.0298	0.025207	0.0046
12	0.872093	1.744186	0.0168	0.015450	0.0013
13	0.626043	0.417362	0.0201	0.015209	0.0048
14	1.88537	2.262443	0.0195	0.017108	0.0024
15	1.552795	0.559006	0.0230	0.022340	0.0007
16	1.70068	2.040816	0.0227	0.020446	0.0023
17	1.28866	0.463918	0.0264	0.017324	0.0091
18	1.572327	1.886792	0.0255	0.023417	0.0021
19	0.919118	0.441176	0.0300	0.036256	-0.0063
20	1.068376	0.384615	0.0286	0.023956	0.0046
21	1.476669	1.772002	0.0287	0.026101	0.0026

22	1.237624	0.594059	0.0310	0.021675	0.0093
23	0.912409	0.328467	0.0286	0.031471	-0.0029
24	1.351351	1.621622	0.0323	0.030426	0.0019
25	1.28866	0.773196	0.0292	0.022781	0.0064
26	1.068376	0.512821	0.0340	0.027950	0.0060
27	1.256281	1.507538	0.0374	0.034516	0.0029
28	1.152074	0.691244	0.0303	0.027650	0.0026
29	0.934579	0.448598	0.0392	0.035225	0.0040
30	1.167134	1.40056	0.0401	0.039201	0.0008
31	0.980392	0.588235	0.0456	0.036548	0.0091
32	1.098901	1.318681	0.0441	0.043504	0.0006
33	3.333333	2.857143	0.0138	0.016435	-0.0026
34	2.820306	2.417405	0.0196	0.021941	-0.0023
35	2.423823	2.077562	0.0240	0.028511	-0.0045
36	2.147239	1.840491	0.0316	0.035156	-0.0036
37	1.914661	1.641138	0.0348	0.042863	-0.0081
38	1.799486	1.542416	0.0444	0.047717	-0.0033
39	1.277372	0.364964	0.0520	0.047892	0.0041
40	1.627907	0.465116	0.0360	0.031490	0.0045
41	2.12766	0.607903	0.0283	0.019822	0.0085
42	1.268116	0.217391	0.0340	0.036882	-0.0029
43	1.666667	0.285714	0.0292	0.022993	0.0062
44	2.229299	0.382166	0.0235	0.013906	0.0096
45	4.45236	2.671416	0.0234	0.027135	-0.0037
46	3.703704	0.444444	0.0213	0.015744	0.0056
47	4.071661	2.442997	0.0253	0.031670	-0.0064
48	3.990423	0.798085	0.0199	0.018199	0.0017
49	3.32668	0.399202	0.0209	0.018956	0.0019
50	3.745318	2.247191	0.0350	0.033455	0.0015
51	3.584229	0.716846	0.0321	0.021911	0.0102
52	2.824859	0.338983	0.0276	0.025149	0.0025
53	3.462604	2.077562	0.0363	0.037760	-0.0014
54	3.263708	0.652742	0.0285	0.025763	0.0027

It is noted from Table 4.3 that the discharge values from the program are always higher with a slight difference, and the reason for this is due to the neglect of some values with little effect such as viscosity, friction and slope in this study.

The results are shown in Table (4-4) and demonstrate that Artificial Neural Network model produced acceptable R^2 with low MAE and RMSE values for the testing data and training data. As a result, this model provides a good discharge estimation.

Table 4-2: parameters of the ANN model's statistics

Statistical parameters	Limit	Ratio
MAE	0.1 > Excellent 0.25 Good 0.25 – 0.5 Acceptable 0.5 < Unacceptable	0.412
RMSE	0.1 > Excellent 0.25 Good 0.25 – 0.5 Acceptable 0.5 < Unacceptable	0.4872
R^2	0.9 < Excellent 0.8 – 0.9 Good 0.7 – 0.8 Acceptable 0.7 < Unacceptable	0.7558

From Table (4-3) the results show that, the gate opening had the greatest influence on discharge, whereas width of the gate had the least significant impact, and the least effect is Froude number.

Table 4-3 : The factors most affecting the discharge

Q_m m ³ /s	B/Y	Fr	H/Y
0.018102	0.021255	0.014608	0.044462
0.013474	0.019037	0.018692	0.033861
0.021105	0.02577	0.017605	0.053011
0.017042	0.024488	0.023073	0.044048
0.017532	0.025302	0.024592	0.045783
0.022088	0.032015	0.029863	0.059291
0.023030	0.034978	0.033639	0.062578
0.028282	0.037956	0.025638	0.074134
0.024394	0.036829	0.030621	0.06504
0.026503	0.034817	0.023577	0.068815
0.025207	0.038771	0.035981	0.068977
0.015450	0.017266	0.011939	0.037083
0.015209	0.022547	0.026968	0.040433
0.017108	0.012448	0.011816	0.022149
0.022340	0.01274	0.022297	0.017416
0.020446	0.015616	0.01472	0.027168
0.017324	0.018025	0.031155	0.025198
0.023417	0.018562	0.017406	0.031737
0.036256	0.034734	0.050551	0.057141
0.023956	0.024871	0.042452	0.036529
0.026101	0.021563	0.020135	0.035939
0.021675	0.022427	0.033297	0.031693
0.031471	0.031618	0.053401	0.049935
0.030426	0.026056	0.024186	0.042842
0.022781	0.021884	0.029016	0.032847

0.027950	0.029265	0.043024	0.042412
0.034516	0.031144	0.028769	0.049502
0.027650	0.026395	0.034736	0.04101
0.035225	0.038297	0.0558	0.055284
0.039201	0.035927	0.033024	0.057273
0.036548	0.040717	0.053008	0.056457
0.043504	0.041182	0.037702	0.064533
0.016435	0.007445	0.008743	0.01395
0.021941	0.011281	0.0131	0.019425
0.028511	0.015592	0.017923	0.026224
0.035156	0.021276	0.024259	0.033338
0.042863	0.026479	0.02996	0.041838
0.047717	0.032549	0.036676	0.04731
0.047892	0.042913	0.083577	0.052742
0.031490	0.025058	0.049602	0.032624
0.019822	0.014929	0.030086	0.019195
0.036882	0.030789	0.078131	0.041046
0.022993	0.018944	0.04896	0.023886
0.013906	0.011014	0.029026	0.013425
0.027135	0.010514	0.015148	0.015937
0.015744	0.008367	0.027453	0.009955
0.031670	0.012486	0.017881	0.019024
0.018199	0.008392	0.021228	0.011195
0.018956	0.009766	0.031813	0.012314
0.033455	0.01646	0.023442	0.022448
0.021911	0.012311	0.030918	0.013848
0.025149	0.014233	0.045857	0.017024
0.037760	0.018861	0.02672	0.026224
0.025763	0.013441	0.033543	0.016671

4.5 Artificial Neural Network (ANN) Model by parameters of dimensional analysis

Model was developed for each type of model; as shown in Table 4-5, around 67.3% of the data were utilized to build (train) the model, 20% were used to test the model, and the remaining 12.7% were held back to (holdout).

Table 4-4:MLP-ANN model synopsis

Case Processing synopsis			
		N	ratio
Sample	Training	37	67.3%
	Testing	11	20.0%
	Holdout	7	12.7%
Valid		55	100.0%
Excluded		1	
Total		56	

4.5.1 Network Information and Results

The amount of layers and the amount of neurons in every layer are displayed in Table 4-6, three independent variables are present in the input layer, the gate's opening, width, and water level at the intake. For covariates, the standardized rescaling approach was utilized. The hidden layer was assigned to a single layer with three nodes by automatic architecture selection, while the output layer had a single node for the dependent variable course result.

Table 4-5: Case processing summary

Network Data			
Input Layer	Common variables	1	B/Y
		2	H/Y
		3	Fr
	Quantity of Units		3
	Rescaling Method for Covariates		Standardized
Hidden Layer	Quantity of Hidden Layers		1
	Quantity of Units in Hidden Layer 1 ^a		1
	Activation assignment		Hyperbolic tangent
Output Layer	Dependent Variables	1	$Q/G^{0.5} \cdot Y1^2$.5 Estimated
	Quantity of Units		1
	Rescaling Method for Scale Dependents		Standardized
	Activation Function		Identity
	Error Function		Sum of Squares
a. Excluding the bias unit			

It is safe to assume that the model has not been overtrained because the relative error that is roughly convergent for training is 0.03, testing is 0.26, and holdout is 0.166, and the error discovered by the network in subsequent cases will be comparable to the error listed in Table 4-7. Given that the holdout set was excluded from the construction process, the holdout set's low relative error shows how the model is accurate.

Table 4-6: The relative errors for the ANN model.

Model Synopsis		
Training	The amount of Squares Error	0.534
	Relative Mistake	0.030
	Ending Rule Used	1 successive step(s) without a reduction in inaccuracy
Testing	The amount of Squares Error	0.137
	Comparative Error	0.026
Holdout	Comparative Error	0.166
Dependent Variable: $Q/G^{0.5} * Y1^{2.5}$ Estimated		
a. The testing sample is used as the basis for error calculations.		

As shown in Figure 4-5, the ANN models were trained using a single hidden layer and one neuron. The best ANN architecture was discovered through this iterative procedure.

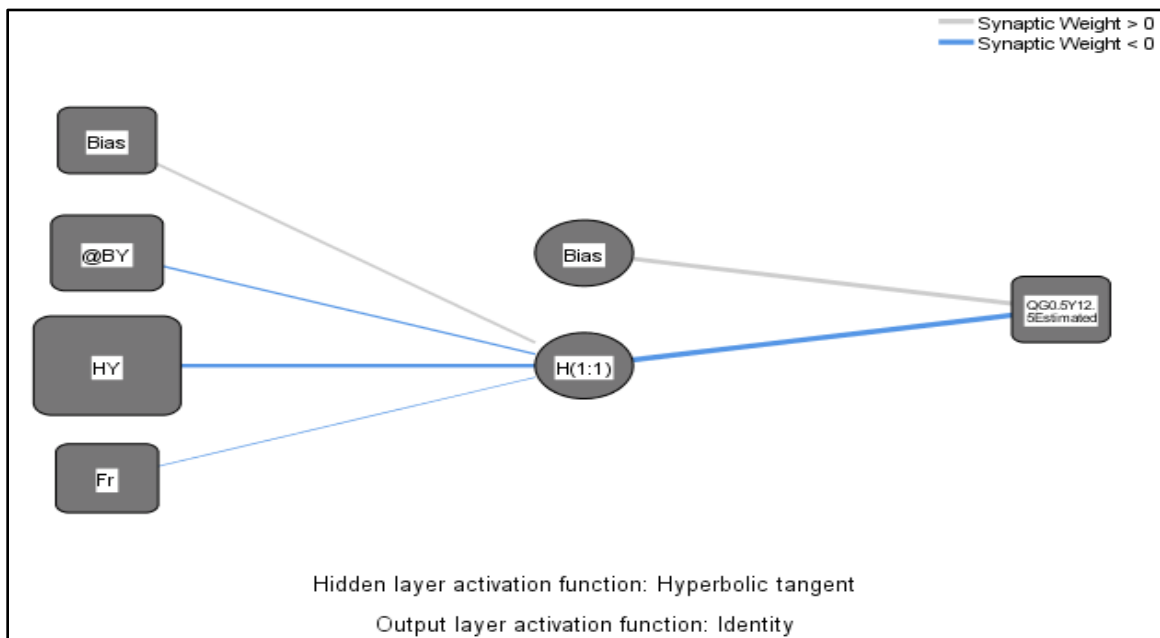


Figure 4.7: Activation layers

Since this model's coefficient of determination (R^2) is (0.971), it can be said that it exhibits extremely perfect arrangement with the actual observation, as depicted in Figure 4-6, between estimated discharge in dimensional analysis and predicted value (dimensionless parameters H/Y , B/Y , Fr).

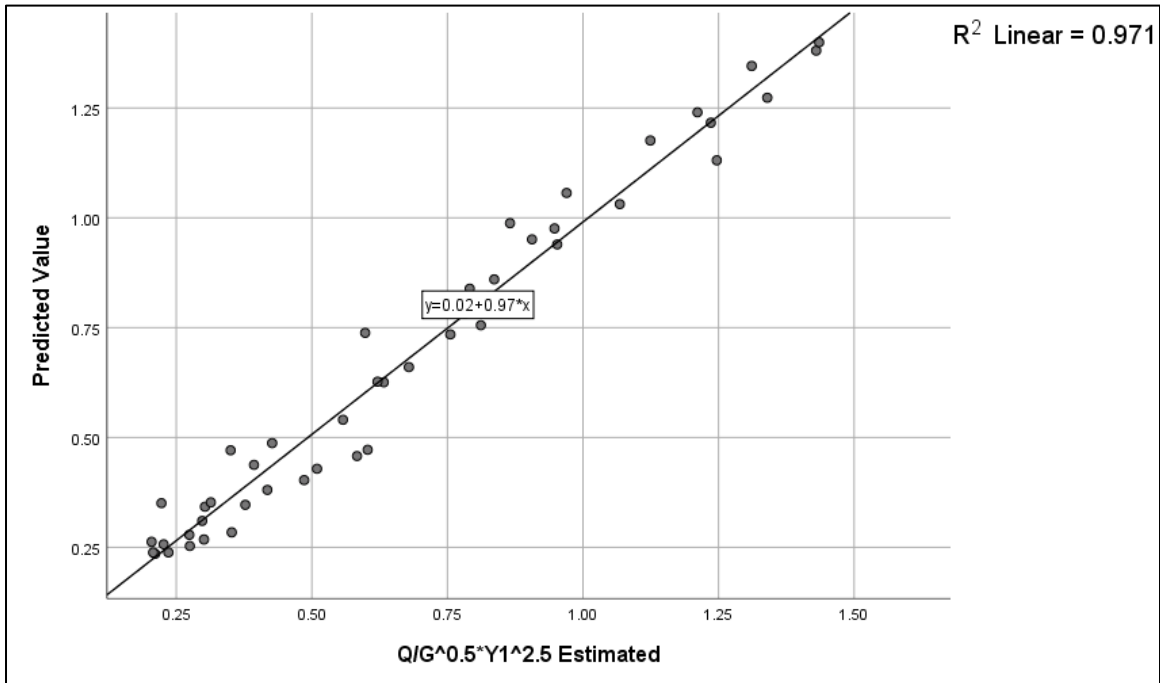


Figure 4.8: Scatter comparison

Table 4-8 and Figure 4-7 illustrate how input factors affect the ANN model's normalized and relative relevance (M1). The results show that, with an important ratio of around 45.8%, the Gate opening had the greatest influence on discharge, whereas the width of the gate had the least significant impact, at around 29.4% and then Froude number in the gate had effect about 24.8%.

Table 4-7: The outcome of independent variables on the estimate of the discharge

Independent Variable Importance		
	Importance	Normalized Importance
B/Y	0.294	64.3%
H/Y	0.458	100.0%
Fr	0.248	54.2%

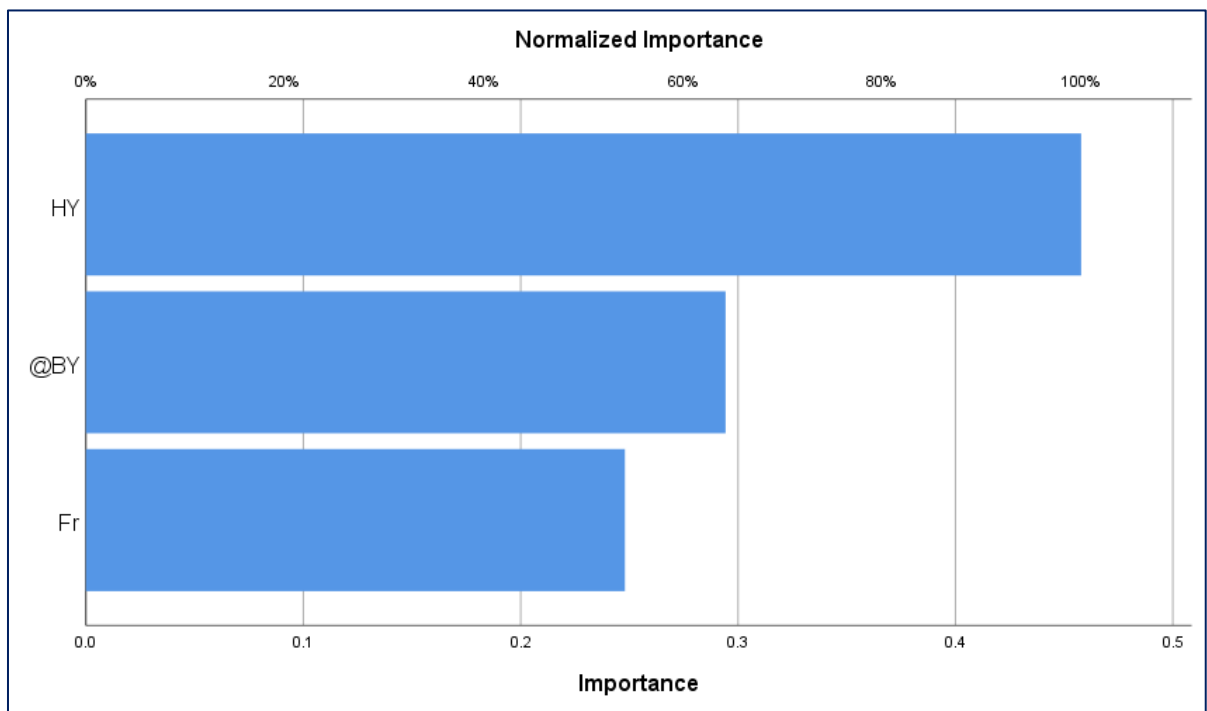


Figure 4.9: The outcome of independent variables on the estimate of the discharge

4.6 Discussion

Analyzing the behaviour of and hydraulic features for the flow across the regulator is a difficult process that consume a lot of effort and money.

Based on the modeling outcomes, it may be said that the CFD approach is a useful tool for modelling the flow pattern in regulators. But also because of the difficulty of using a software and the difficulty of accessing it, this research was done to solve this problem.

Through the dimensional analysis and Spss software, knowing that (H/Y) has the most effect on the flow rate by 45.8%, followed by (B/Y) with a rate of 29.4%, and finally (Fr) with a rate of 24.8%, But it is a difficult method that took a lot of time, so the main equation was used, and by deleting an element after an element, the same result was reached when using SPSS software.

Also, the results of the software were confirmed by a comparison between Q software and Q estimated, in which the value of R^2 reached 0.8476 between them. Finally, the main equation was extracted, which showed good applicability with a value of $R^2=0.7558$ and $RMSE=0.004872$ with $MAE=0.00412$ without the need for softwares, field works, or models, only the initial measurements that can be obtained from state departments

Chapter Five

Conclusion and Recommendations

5.1 introduction

3D numerical simulations of the discharge in a model were carried out to ascertain the discharge that arises from the usage of appropriate appurtenances. The simulation examined the effect of hydraulic properties and produced good agreement. It proved that the turbulence models were accurate.

This chapter provides examples of the research's efficacy and recommendations for enhancing it. Following the results in Chapter 4, the key points are only provided here so that readers may learn more quickly about the project's final suggestions for enhancing the efficacy and efficiency of the research. Include future steps that must be taken to advance the research as well.

5.2 Conclusion

1. Based on the modeling outcomes from calibration, it may be said that the CFD approach is a useful tool for modelling the flow pattern in regulators.
2. The main equation was extracted, which showed good agreement with a value of $R^2=0.756$ and $RMSE=0.004872$ with $MAE=0.00412$ without the need for programs, field works, or models, only the initial measurements that can be obtained from state departments
3. It was concluded that (H/Y) has the most effect on the flow rate by 45.8%, followed by (B/Y) with a rate of 29.4%, and finally (Fr) with a rate of 24.8%.

4. Using the final equation (4-19) from this research is to extract the discharge as it is faster and easier and cheaper than laboratory methods and without the need for a model.

5.3 Recommendations

To provide direction for future research and engineers, several recommendations may be made, including the following:

1. Calibration of irrigation regulators that have a non-horizontal floor or that contain a sill under the gate.
2. The study of the effect of using gates with edges that differ from the existing edge, as well as the use of non-vertical gates.
3. Different gate widths and heights can be used in multi-slot organizations.
4. Using a channel with different cross-sections on the coefficients of the flow calculation equations.
5. Recommendation Flow 3D because it has a range of features that make it stand out from other CFD software. It can simulate a wide range of physics, including fluid-structure interactions, solidification and melting, and cavitation. It also offers a user-friendly interface and advanced meshing capabilities.
6. The newly developed formulas from the present study need to be validated and calibrated to the natural rivers.
7. I recommend the Ministry of Water Resources to study and rely on this equation because it has a significant impact on increasing the speed and accuracy of work.

References

- Abiodun, O. I., Jantan, A., Omolara, A. E., Dada, K. V., Mohamed, N. A. E., & Arshad, H. (2018). State-of-the-art in artificial neural network applications: A survey. *Heliyon*, 4(11), e00938. <https://doi.org/10.1016/j.heliyon.2018.e00938>
- Akoz, M. S., Kirkgoz, M. S., & Oner, A. A. (2009). Experimental and numerical modeling of a sluice gate flow. *Journal of Hydraulic Research*, 47(2), 167–176. <https://doi.org/10.3826/jhr.2009.3349>
- Al-saadi, G. N. H. (2022). *Performance evaluation of drip irrigation lateral with different emitters and distances*. November.
- Al-waeli, L. K. H. (2019). *Pan, Linqi. "A Study on Weakly-Imposed Dirichlet Boundary Conditions in Internal Flows."* (2016) Master's Thesis, Rice University. <https://hdl.handle.net/1911/96612>.
- Al-zwainy, F. M. S. (2016). *The Use of Artificial Neural Network for Estimating Total Cost of Highway Construction Projects Republic of Iraq Ministry of Higher Education and Scientific Research University of Baghdad College of Engineering Department of Civil Engineering A thesis Sub. December 2008*. <https://doi.org/10.13140/RG.2.1.2917.6084>
- Alhamid, A. A. (1999). Coefficient of Discharge for Free Flow Sluice Gates. *Journal of King Saud University - Engineering Sciences*, 11(1), 33–47. [https://doi.org/10.1016/S1018-3639\(18\)30989-9](https://doi.org/10.1016/S1018-3639(18)30989-9)
- Bilhan, O., Aydin, M. C., Emiroglu, M. E., & Miller, C. J. (2018). Experimental and CFD Analysis of Circular Labyrinth Weirs. *Journal of Irrigation and Drainage Engineering*, 144(6), 1–11. [https://doi.org/10.1061/\(asce\)ir.1943-4774.0001301](https://doi.org/10.1061/(asce)ir.1943-4774.0001301)
- Boyacioglu, M. A., Kara, Y., & Baykan, Ö. K. (2009). Predicting bank

- financial failures using neural networks, support vector machines and multivariate statistical methods: A comparative analysis in the sample of savings deposit insurance fund (SDIF) transferred banks in Turkey. *Expert Systems with Applications*, 36(2 PART 2), 3355–3366. <https://doi.org/10.1016/j.eswa.2008.01.003>
- Carrillo, J. M., Matos, J., & Lopes, R. (2020). Numerical modeling of free and submerged labyrinth weir flow for a large sidewall angle. *Environmental Fluid Mechanics*, 20(2), 357–374. <https://doi.org/10.1007/s10652-019-09701-0>
- Chen, J. G., Zhang, J. M., Xu, W. L., & Wang, Y. R. (2010). Numerical simulation of the energy dissipation characteristics in stilling basin of multi-horizontal submerged jets. *Journal of Hydrodynamics*, 22(5), 732–741. [https://doi.org/10.1016/S1001-6058\(09\)60110-4](https://doi.org/10.1016/S1001-6058(09)60110-4)
- Daneshfaraz, R., Norouzi, R., & Abbaszadeh, H. (2022). *Experimental Investigation of Hydraulic Parameters of Flow in Sluice Gates with Different Openings* *Experimental Investigation of Hydraulic Parameters of Flow in Sluice Gates with Different Openings* Keywords : 8(January), 923–939. <https://doi.org/10.22034/jewe.2022.321259.1700>
- Daneshfaraz, R., Norouzi, R., Abbaszadeh, H., & Azamathulla, H. M. (2022). Theoretical and experimental analysis of applicability of sill with different widths on the gate discharge coefficients. *Water Supply*, 22(10), 7767–7781. <https://doi.org/10.2166/ws.2022.354>
- Darsono, S., & Labadie, J. W. (2007). Neural-optimal control algorithm for real-time regulation of in-line storage in combined sewer systems. *Environmental Modelling and Software*, 22(9), 1349–1361. <https://doi.org/10.1016/j.envsoft.2006.09.005>
- Das, S. K. (2013). *Artificial Neural Networks in Geotechnical Engineering*:

- Modeling and Application Issues. In *Metaheuristics in Water, Geotechnical and Transport Engineering* (First Edit, Issue 1994). Elsevier Inc. <https://doi.org/10.1016/B978-0-12-398296-4.00010-6>
- Dehdar-Behbahani, S., & Parsaie, A. (2016). Numerical modeling of flow pattern in dam spillway's guide wall. Case study: Balaroud dam, Iran. *Alexandria Engineering Journal*, 55(1), 467–473. <https://doi.org/10.1016/j.aej.2016.01.006>
- Erdbrink, C. D., Krzhizhanovskaya, V. V., & Sloot, P. M. A. (2014). Free-surface flow simulations for discharge-based operation of hydraulic structure gates. *Journal of Hydroinformatics*, 16(1), 189–206. <https://doi.org/10.2166/hydro.2013.215>
- FLOW-3D User Manual*. (2008).
- Gérard-Varet, D., Hillairet, M., & Wang, C. (2015). The influence of boundary conditions on the contact problem in a 3D Navier-Stokes flow. *Journal Des Mathematiques Pures et Appliquees*, 103(1), 1–38. <https://doi.org/10.1016/j.matpur.2014.03.005>
- Ghaderi, A., Dasineh, M., Abbasi, S., & Abraham, J. (2020). Investigation of trapezoidal sharp-crested side weir discharge coefficients under subcritical flow regimes using CFD. *Applied Water Science*, 10(1), 1–12. <https://doi.org/10.1007/s13201-019-1112-8>
- Ghare, A. D., Mhaisalkar, V. A., & Porey, P. D. (2008). An Approach to Optimal Design of Trapezoidal Labyrinth Weirs. *World Applied Sciences Journal*, 3(6), 934–938. <https://pdfs.semanticscholar.org/6cbf/a8d27cd17901217aec339cffe43b834dcad4.pdf>
- Hamed, M. M., Khalafallah, M. G., & Hassanien, E. A. (2004). Prediction of wastewater treatment plant performance using artificial neural networks.

- Environmental Modelling and Software*, 19(10), 919–928.
<https://doi.org/10.1016/j.envsoft.2003.10.005>
- Hasan Ibrahim Al Shaikhli, & Prof. Dr. Saleh Issa Khassaf. (2022). Stepped Mound Breakwater Simulation by Using Flow 3D. *Eurasian Journal of Engineering and Technology*, 6(SE-Articles), 60–68.
<https://www.geniusjournals.org/index.php/ejet/article/view/1368>
- Ibrahim Al Shaikhli, H., Issa Khassaf, S., & Ibrahim Al-Shaikhli, H. (2022). CFD Simulation of Waves over Mound Breakwater Spatial Distribution Analysis and Mapping of Groundwater Quality for the Hilla City by G.I.S View project CFD Simulation of Waves over Mound Breakwater. *Journal of Global Scientific Research*, 7(5), 2022–2283.
<https://doi.org/10.5281/zenodo.6570572>
- Iqbal, M. (1984). *STATISTICAL COMPARISON OF SOLAR RADIATION CORRELATIONS*. 33(2), 143–148.
- Karami, S., Heidari, M. M., & Rad, M. H. A. (2020). Investigation of Free Flow Under the Sluice Gate with the Sill Using Flow-3D Model. *Iranian Journal of Science and Technology - Transactions of Civil Engineering*, 44(1), 317–324. <https://doi.org/10.1007/s40996-019-00310-x>
- Karim, O. A., & Ali, K. H. M. (2000). Prediction of flow patterns in local scour holes caused by turbulent water jets. *Journal of Hydraulic Research*, 38(4), 279–287. <https://doi.org/10.1080/00221680009498327>
- Kavzoglu, T. (1999). Determining Optimum Structure for Artificial Neural Networks. *In Proceedings of the 25th Annual Technical Conference and Exhibition of the Remote Sensing Society, September*, 675–682.
- Labeed A. Jawad Al-Taher. (1987). *Calibration Of Horizontal Ground Irrigation Systems*.
- Levesque, R. (2005). SPSS programming and data management: A guide for

- SPSS and SAS users. In *Ibm Spss*.
<http://dl.acm.org/citation.cfm?id=1199139>
- Lin, L. U., Yu-cheng, L. I., Bin, T., & Bing, C. (2008). *Numerical Simulation of Turbulent Free Surface Flow*. *M*(4), 414–423.
- Mahmoudi, J., Arjomand, M. A., Rezaei, M., & Mohammadi, M. H. (2016). Predicting the Earthquake Magnitude Using the Multilayer Perceptron Neural Network with Two Hidden Layers. *Civil Engineering Journal*, 2(1), 1–12. <https://doi.org/10.28991/cej-2016-00000008>
- Marugán, A. P., Márquez, F. P. G., Perez, J. M. P., & Ruiz-Hernández, D. (2018). A survey of artificial neural network in wind energy systems. *Applied Energy*, 228(April), 1822–1836. <https://doi.org/10.1016/j.apenergy.2018.07.084>
- Mohammadian, A., Gildeh, H. K., & Nistor, I. (2020). CFD modeling of effluent discharges: A review of past numerical studies. *Water (Switzerland)*, 12(3). <https://doi.org/10.3390/w12030856>
- Mohammed, S. R., Khalil, B., Waqed, N., & Hassan, H. (2015). *Dissipation of Hydraulic Energy of Sewage Networks Using New Shapes of Baffle Blocks*.
- Muk-Pavic, E., Chin, S., & Spencer, D. (2006). *Validation of the CFD code Flow-3D for the free surface flow around the ships' hulls*.
- Negm, A. M., & Saleh, O. (2014). *Investigating scour characteristics downstream of sudden expanding stilling basins*. May 2014.
- Norouzi, R., Daneshfaraz, R., & Ghaderi, A. (2019). Investigation of discharge coefficient of trapezoidal labyrinth weirs using artificial neural networks and support vector machines. *Applied Water Science*, 9(7), 1–10. <https://doi.org/10.1007/s13201-019-1026-5>
- Nouri, M., & Hemmati, M. (2020). Discharge coefficient in the combined

- weir-gate structure. *Flow Measurement and Instrumentation*, 75, 101780.
<https://doi.org/10.1016/j.flowmeasinst.2020.101780>
- Pagliara, S., Das, R., & Palermo, M. (2008). Energy Dissipation on Submerged Block Ramps. *Journal of Irrigation and Drainage Engineering*, 134(4), 527–532. [https://doi.org/10.1061/\(asce\)0733-9437\(2008\)134:4\(527\)](https://doi.org/10.1061/(asce)0733-9437(2008)134:4(527))
- Pourshahbaz, 28 *ISH Journal of Hydraulic Engineering* 53 (2022).
<https://doi.org/10.1080/09715010.2020.1830000>
- Rahimpour, M., Keshavarz, Z., & Ahmadi, M. mehdi. (2011). Flow over trapezoidal side weir. *Flow Measurement and Instrumentation*, 22(6), 507–510. <https://doi.org/10.1016/j.flowmeasinst.2011.08.004>
- Rajaratnam, N. (1978). Closure to “Free Flow Immediately Below Sluice Gates.” *Journal of the Hydraulics Division*, 104(10), 1462–1463.
<https://doi.org/10.1061/jyceaj.0005091>
- Saleh, L. A. (2018). Studying the seepage phenomena under a concrete dam using SEEP/W and Artificial Neural Network models. *IOP Conference Series: Materials Science and Engineering*, 433(1).
<https://doi.org/10.1088/1757-899X/433/1/012029>
- Salmasi, F., & Abraham, J. (2021). Prediction of discharge coefficients for sluice gates equipped with different geometric sills under the gate using multiple non-linear regression (MNL). *Journal of Hydrology*, 597, 125728. <https://doi.org/10.1016/j.jhydrol.2020.125728>
- Salmasi, F., Yıldırım, G., Masoodi, A., & Parsamehr, P. (2013). Predicting discharge coefficient of compound broad-crested weir by using genetic programming (GP) and artificial neural network (ANN) techniques. *Arabian Journal of Geosciences*, 6(7), 2709–2717.
<https://doi.org/10.1007/s12517-012-0540-7>

- Savage, B. M., & Johnson, M. C. (2001). Flow over Ogee Spillway: Physical and Numerical Model Case Study. *Journal of Hydraulic Engineering*, 127(8), 640–649. [https://doi.org/10.1061/\(asce\)0733-9429\(2001\)127:8\(640\)](https://doi.org/10.1061/(asce)0733-9429(2001)127:8(640))
- Shahin, M. A., Jaksa, M. B., & Maier, H. R. (2009). Recent Advances and Future Challenges for Artificial Neural Systems in Geotechnical Engineering Applications. *Advances in Artificial Neural Systems, 2009*, 1–9. <https://doi.org/10.1155/2009/308239>
- Shen, Y., Gao, Y., Qian, W., Ruse, N. D., Zhou, X., Wu, H., & Haapasalo, M. (2010). Three-dimensional Numeric Simulation of Root Canal Irrigant Flow with Different Irrigation Needles. *Journal of Endodontics*, 36(5), 884–889. <https://doi.org/10.1016/j.joen.2009.12.010>
- Silva, C. O., & Rijo, M. (2017). Flow Rate Measurements under Sluice Gates. *Journal of Irrigation and Drainage Engineering*, 143(6). [https://doi.org/10.1061/\(asce\)ir.1943-4774.0001177](https://doi.org/10.1061/(asce)ir.1943-4774.0001177)
- Supercritical, O. F., & Gate, B. S. (1994). *FLOW*. 120(3), 332–346.
- Ulu, A. E., Cihan Aydın, M., & Işık, E. (2021). *A study on the flow velocities and energy dissipation potential of flow separator placed in spillway flip bucket.*
- Upport, I. N. S., Cosystem, O. F. E., & Anagement, A. M. (2011). *S Imulation M Odels of a Ntarctic M Arine E Cosystems. May.*
- WANG, K., JIN, S., & LIU, G. (2009). Numerical modelling of free-surface flows with bottom and surface-layer pressure treatment. *Journal of Hydrodynamics*, 21(3), 352–359. [https://doi.org/10.1016/S1001-6058\(08\)60156-0](https://doi.org/10.1016/S1001-6058(08)60156-0)
- Weyer, E. (2001). System identification of an open water channel. *Control Engineering Practice*, 9(12), 1289–1299. <https://doi.org/10.1016/S0967->

0661(01)00099-5

- Yen, J. F., Lin, C. H., & Tsai, C. T. (2001). Hydraulic characteristics and discharge control of sluice gates. *Journal of the Chinese Institute of Engineers, Transactions of the Chinese Institute of Engineers, Series A/Chung-Kuo Kung Ch'eng Hsueh K'an*, 24(3), 301–310.
<https://doi.org/10.1080/02533839.2001.9670628>
- Z. Zacharis, N. (2016). Predicting Student Academic Performance in Blended Learning Using Artificial Neural Networks. *International Journal of Artificial Intelligence & Applications*, 7(5), 17–29.
<https://doi.org/10.5121/ijaia.2016.7502>

Appendices

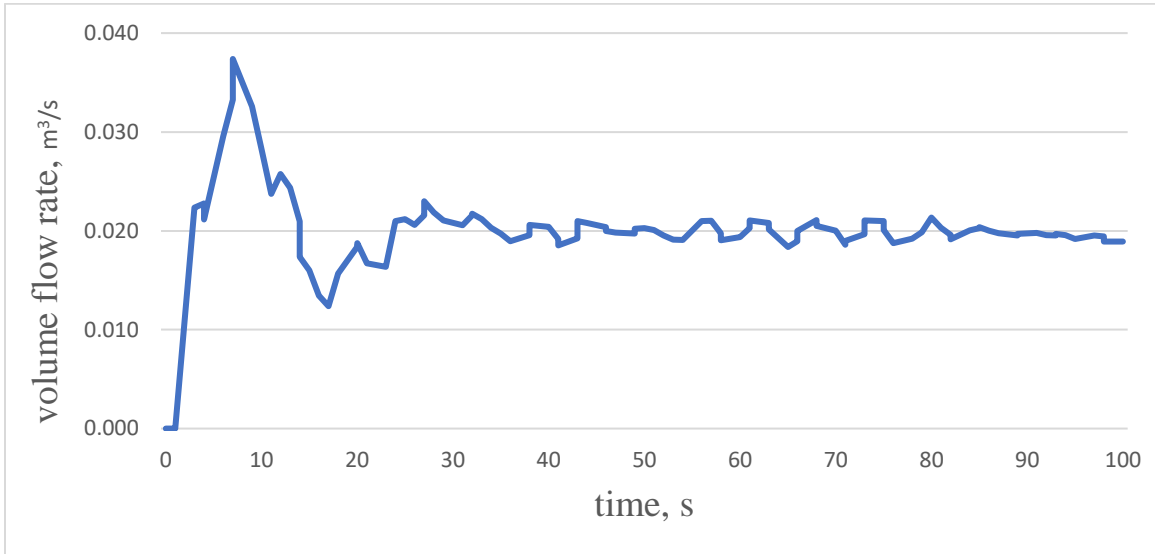
Appendix**Numerical Work Results****Appendix A. The discharge for the model with 15 cm wide**

Figure A-1 Relationship between time and volume flow rate depending on the full opening of the gate (Experiment 1)

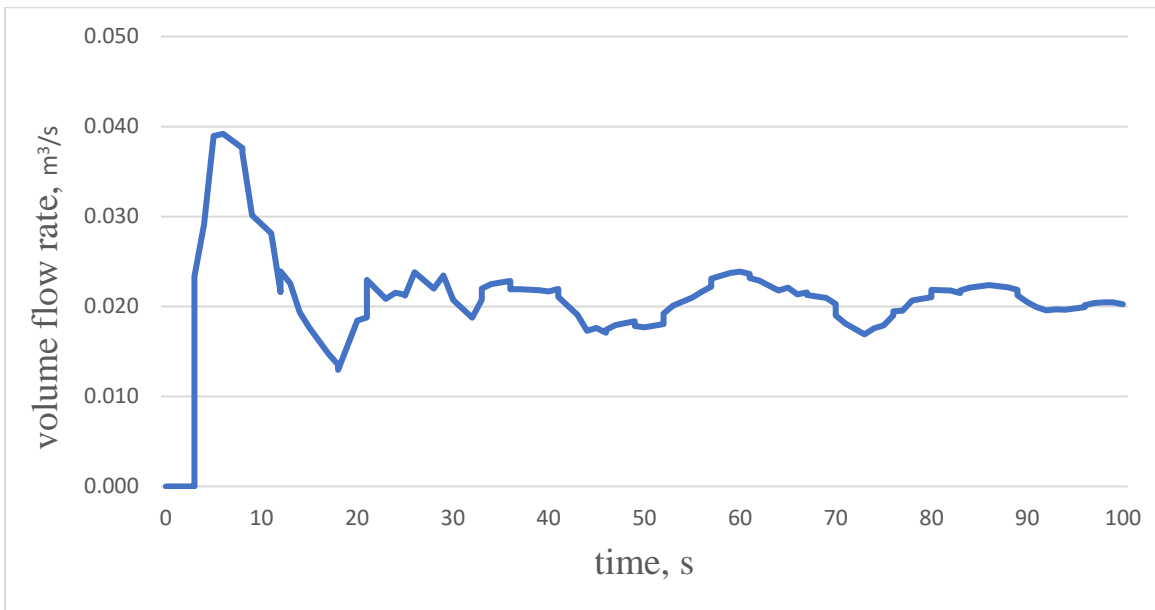


Figure A-2 Relationship between time and volume flow rate depending on the gate opening 15 cm (Experiment 1)

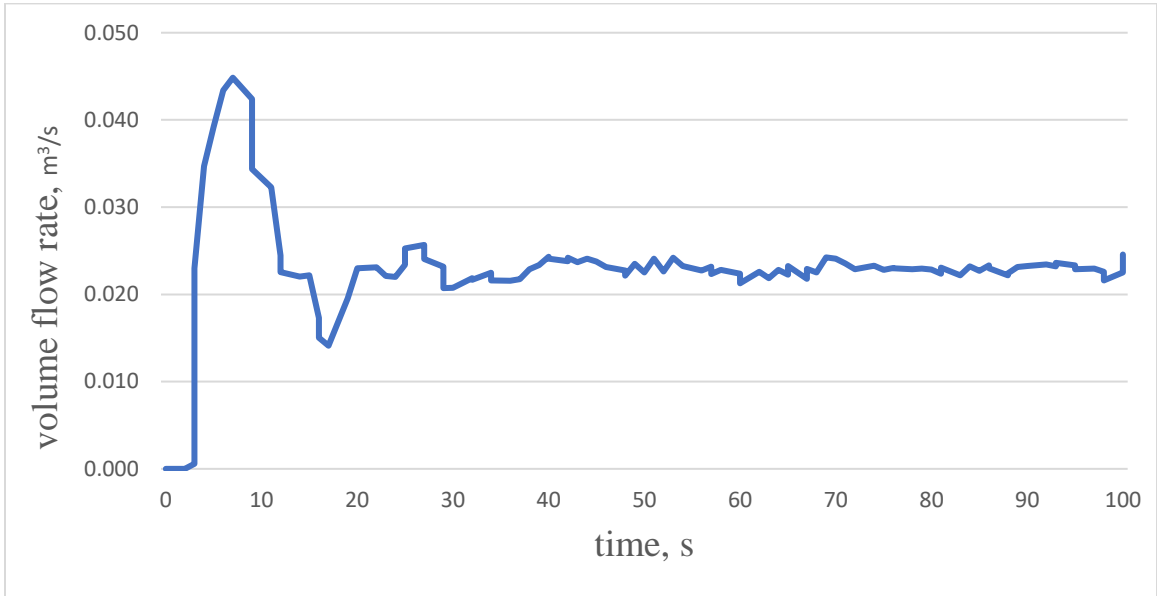


Figure A-3 Relationship between time and volume flow rate depending on the gate opening 15 cm (Experiment 2)

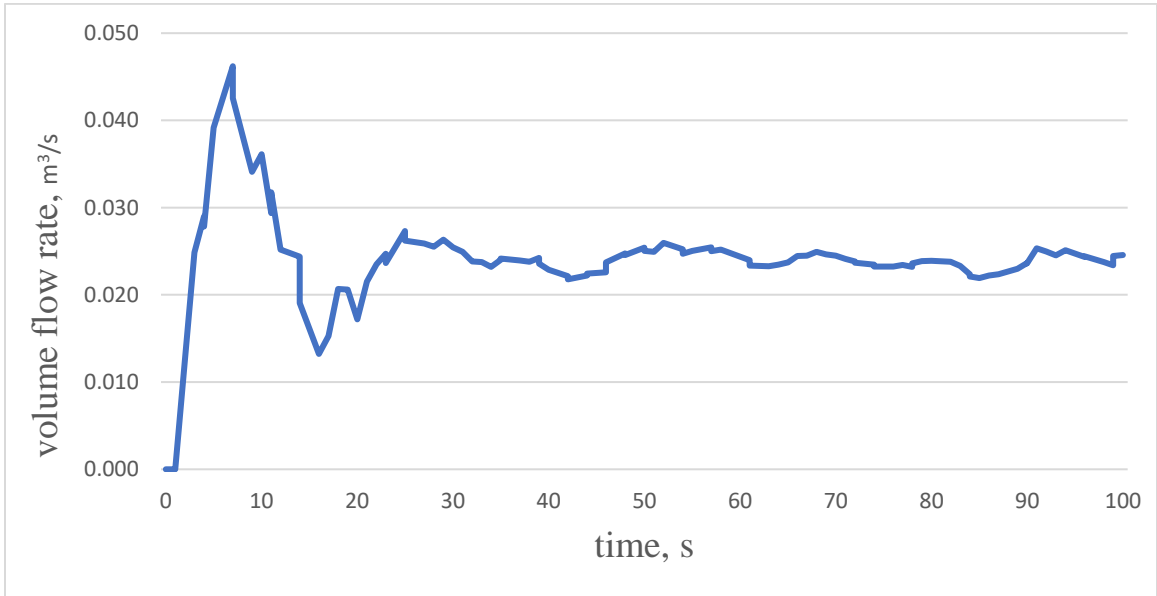


Figure A-4 Relationship between time and volume flow rate depending on the gate opening 16 cm (Experiment 2)

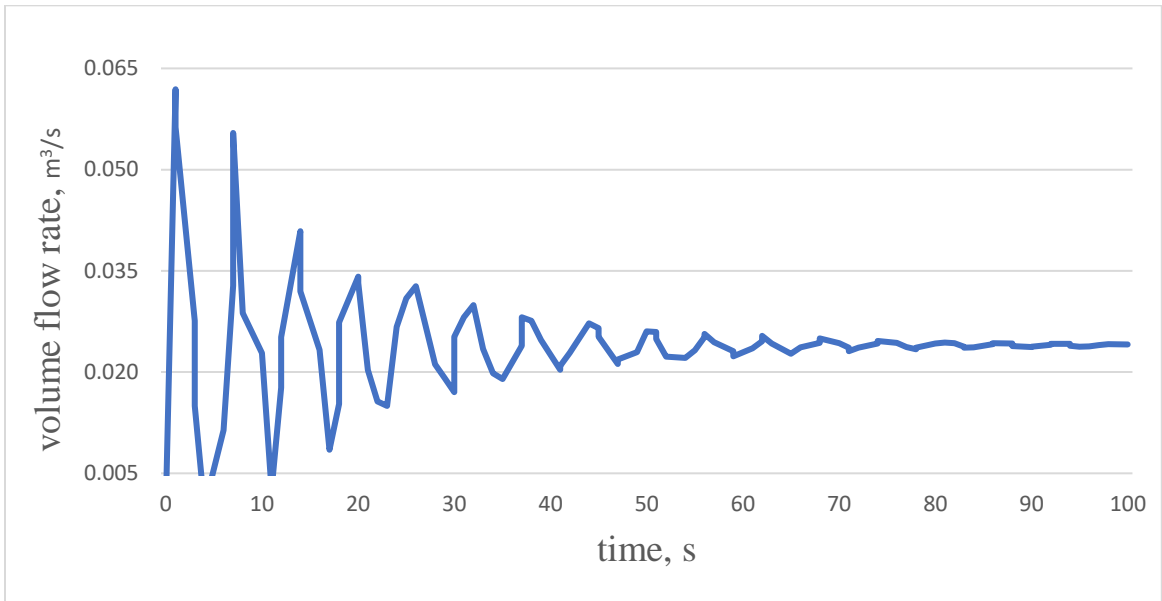


Figure A-5 Relationship between time and volume flow rate depending on the gate opening 15 cm (Experiment 2)

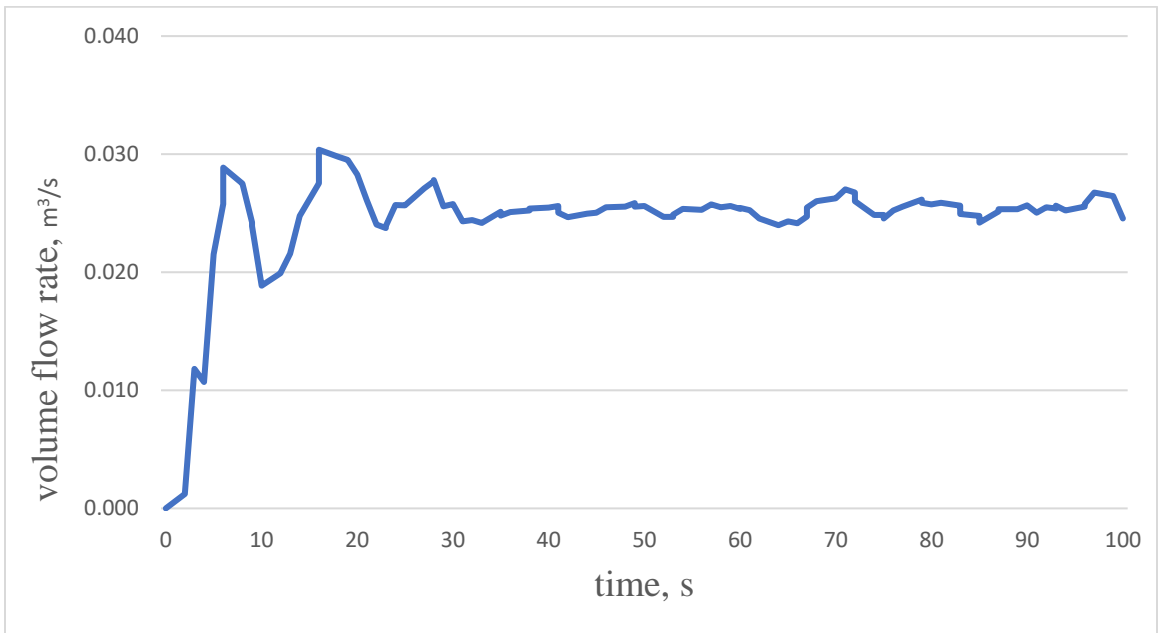


Figure A-6 Relationship between time and volume flow rate depending on the gate opening 16 cm (Experiment 3)

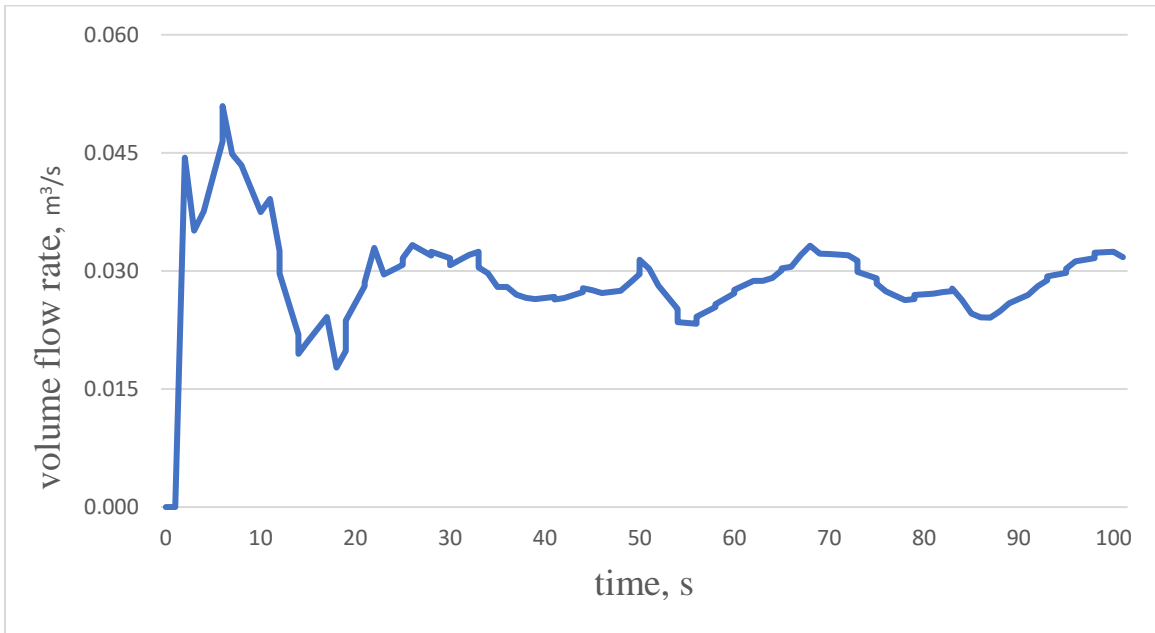


Figure A-7 Relationship between time and volume flow rate depending on the gate opening 15 (Experiment 3)

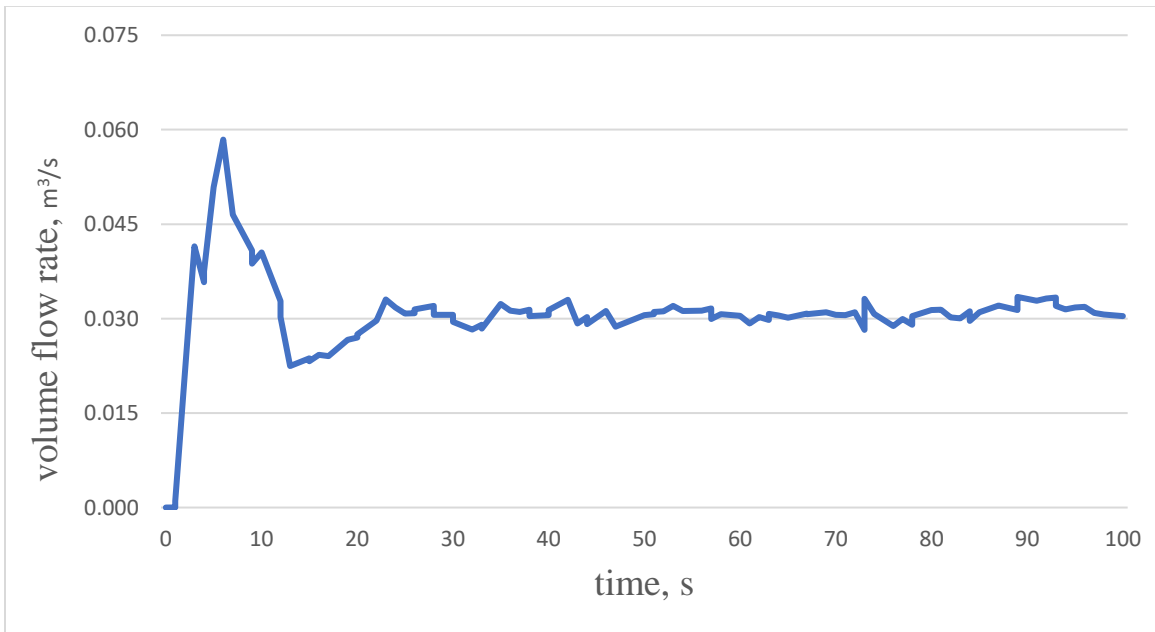


Figure A-8 Relationship between time and volume flow rate depending on the gate opening 20 cm (Experiment 4)

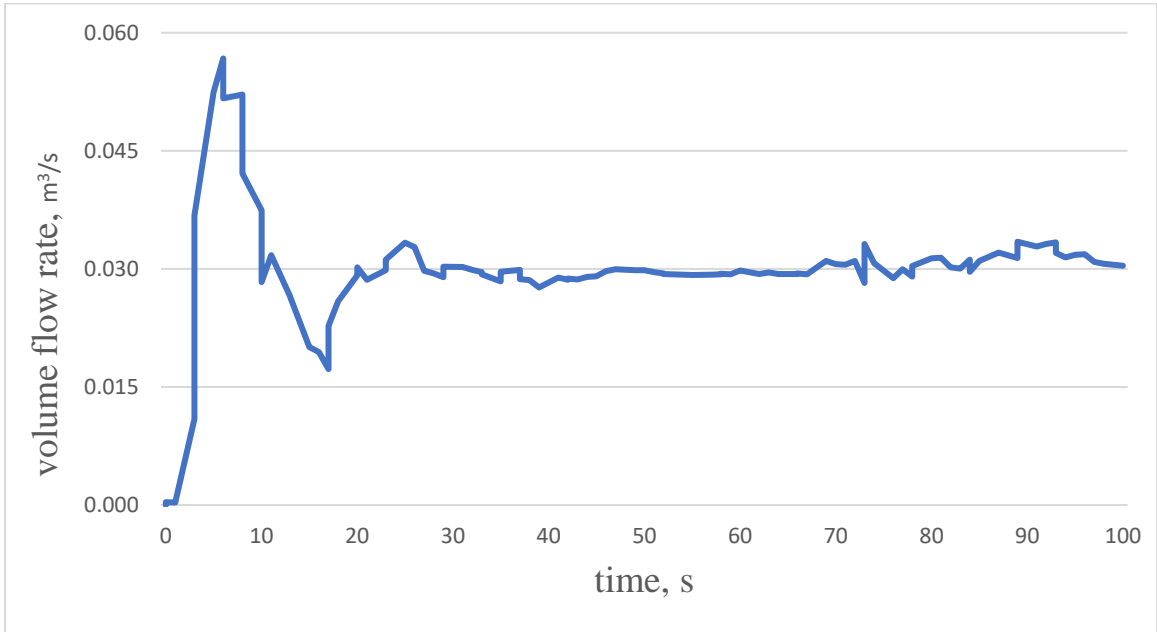


Figure A-9 Relationship between time and volume flow rate depending on the gate opening 15 cm (Experiment 4)

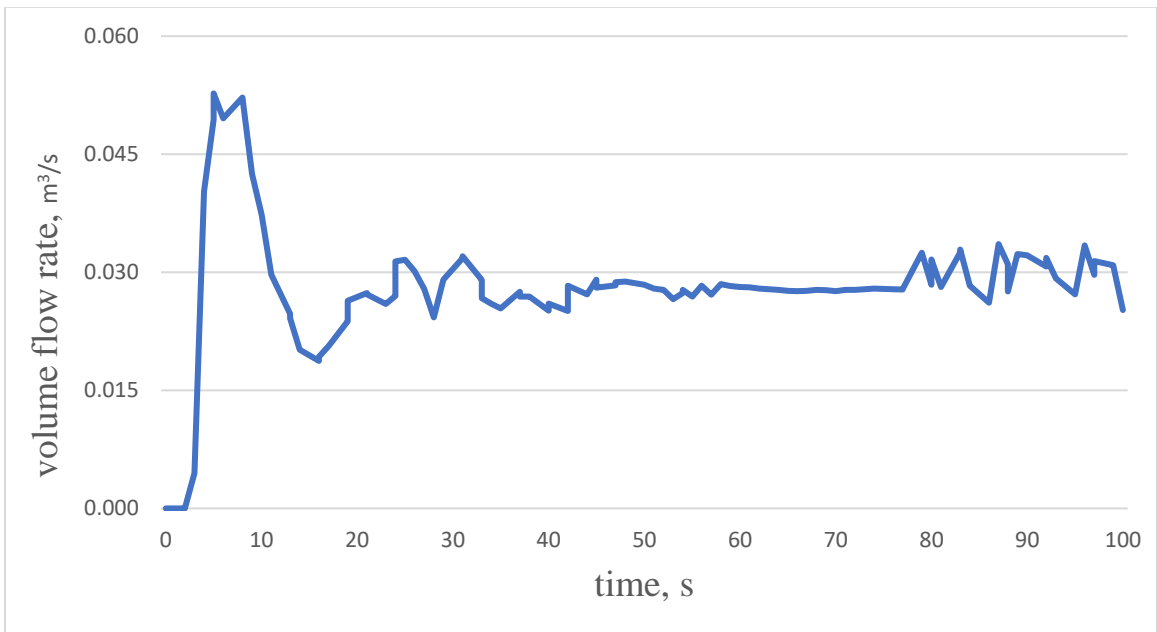


Figure A-10 Relationship between time and volume flow rate depending on the gate opening 15 cm (Experiment 5)

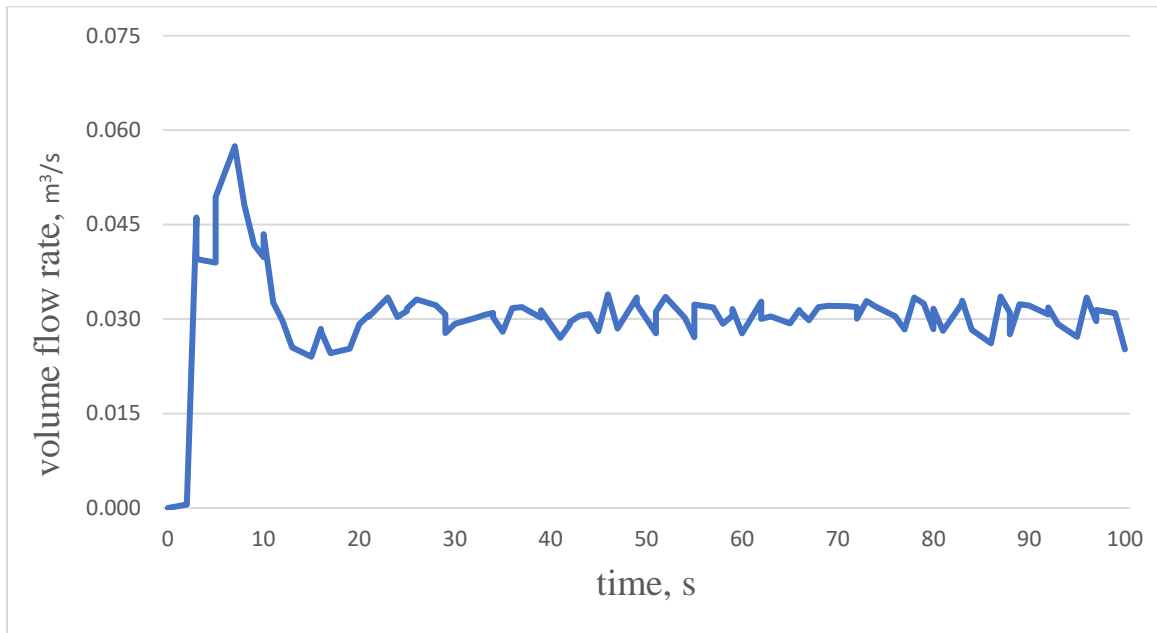


Figure A-11 Relationship between time and volume flow rate depending on the gate opening 16 cm (Experiment 5)

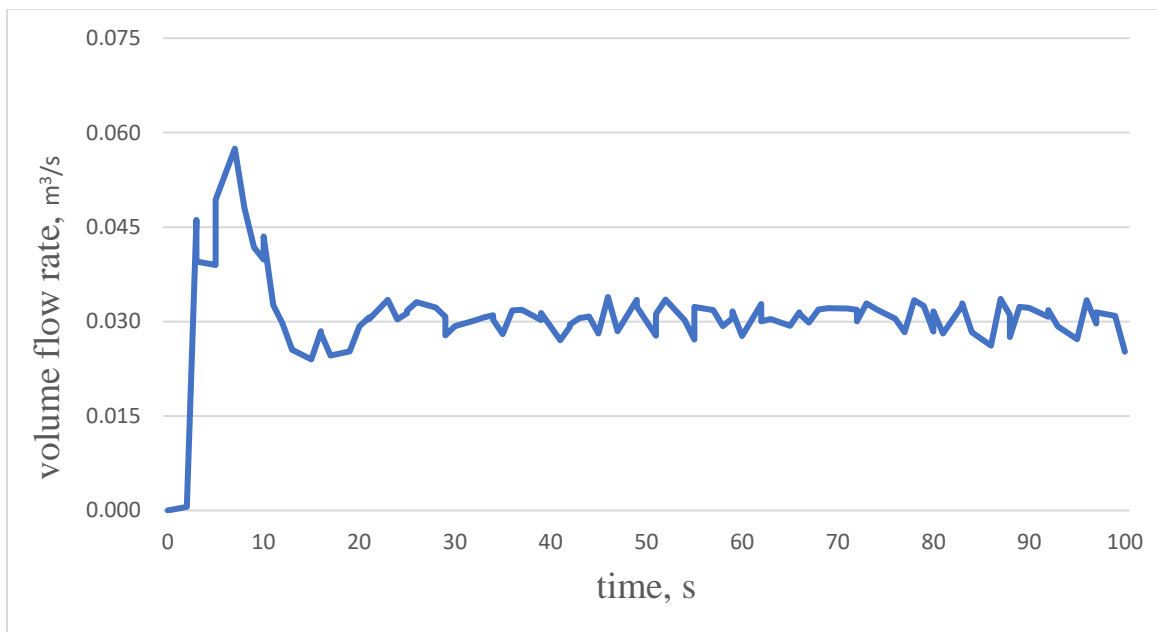


Figure A-12 Relationship between time and volume flow rate depending on the gate opening 15 cm (Experiment 6)

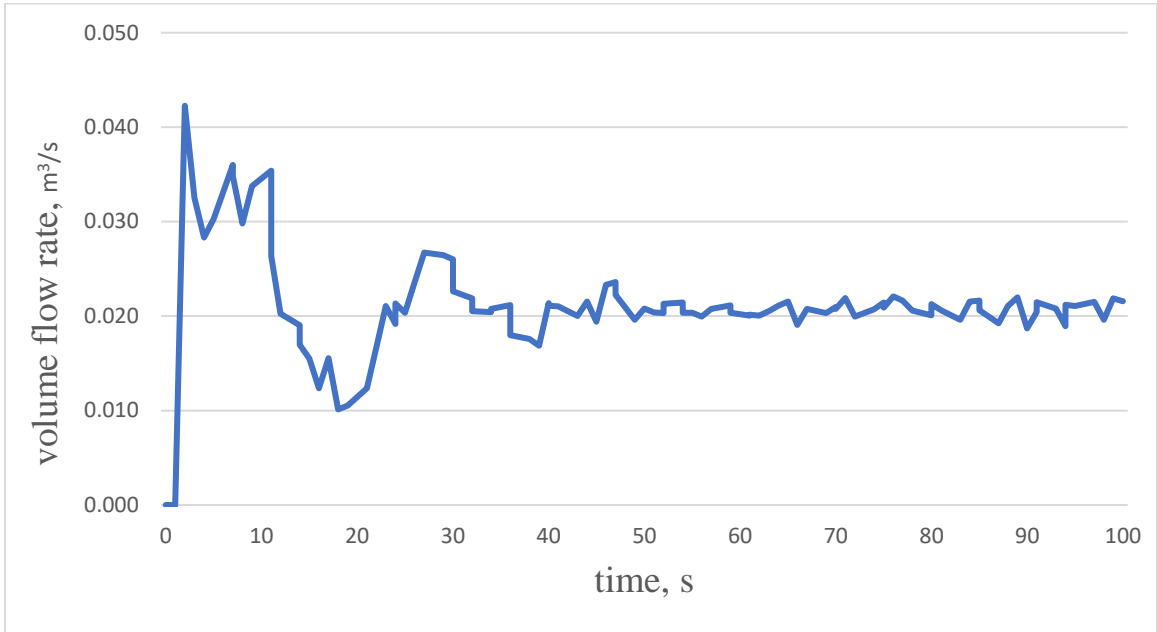


Figure A-13 Relationship between time and volume flow rate depending on the gate opening 10 cm (Experiment 6)

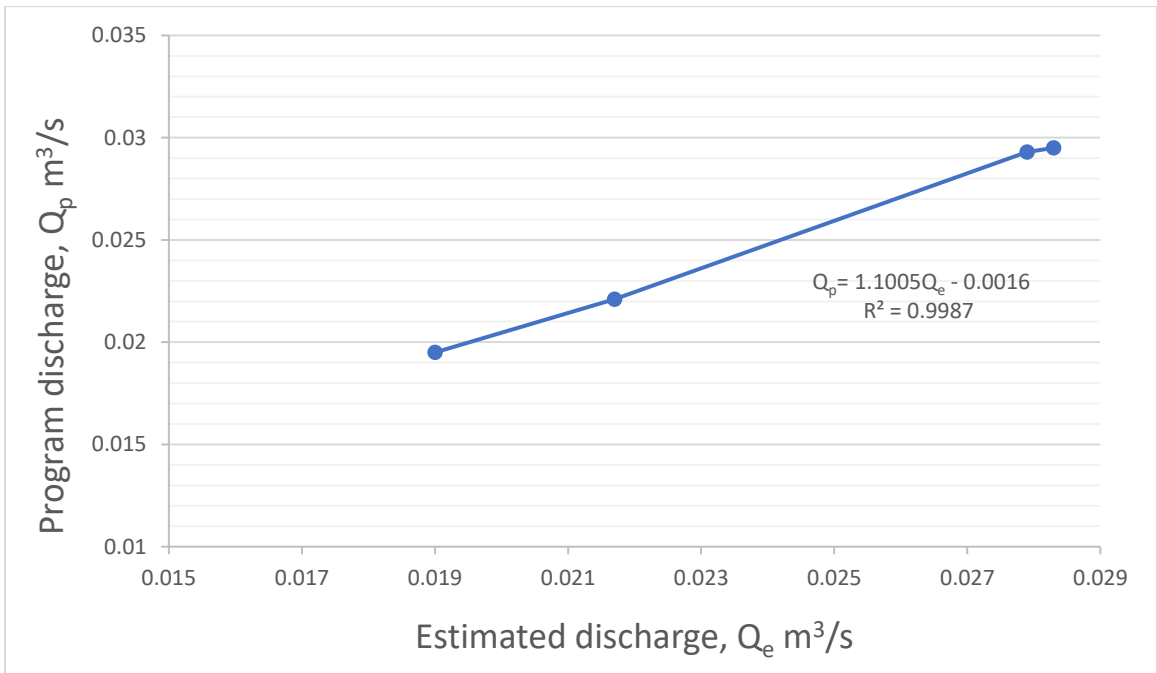


Figure A-14 Relationship between estimated discharge and software discharge in 15 cm wide and full opening of the gate

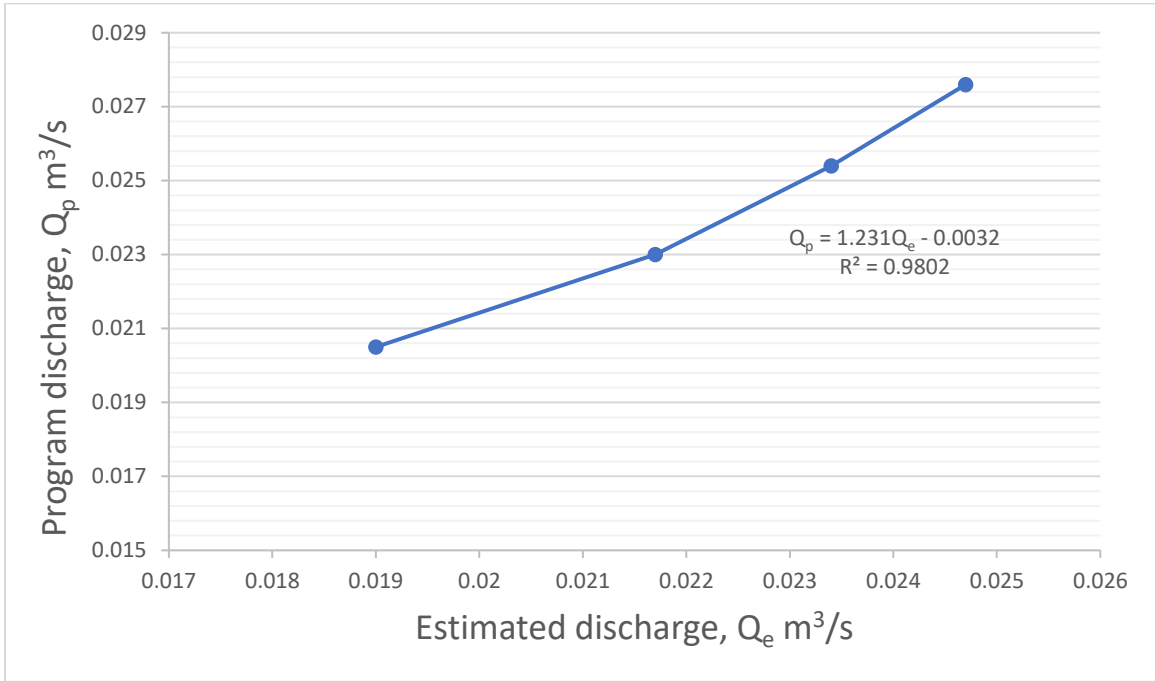


Figure A-15 Relationship between estimated discharge and software discharge in 15 cm wide and 15 cm opening

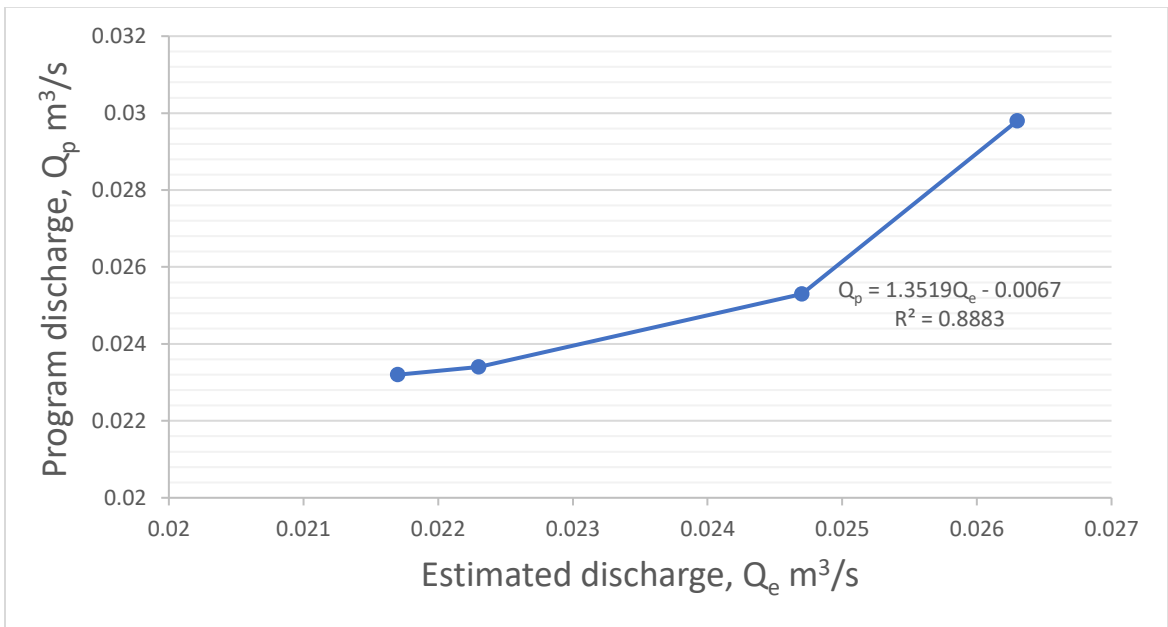


Figure A-16 Relationship between estimated discharge and software discharge in 15 cm wide and 16 cm opening

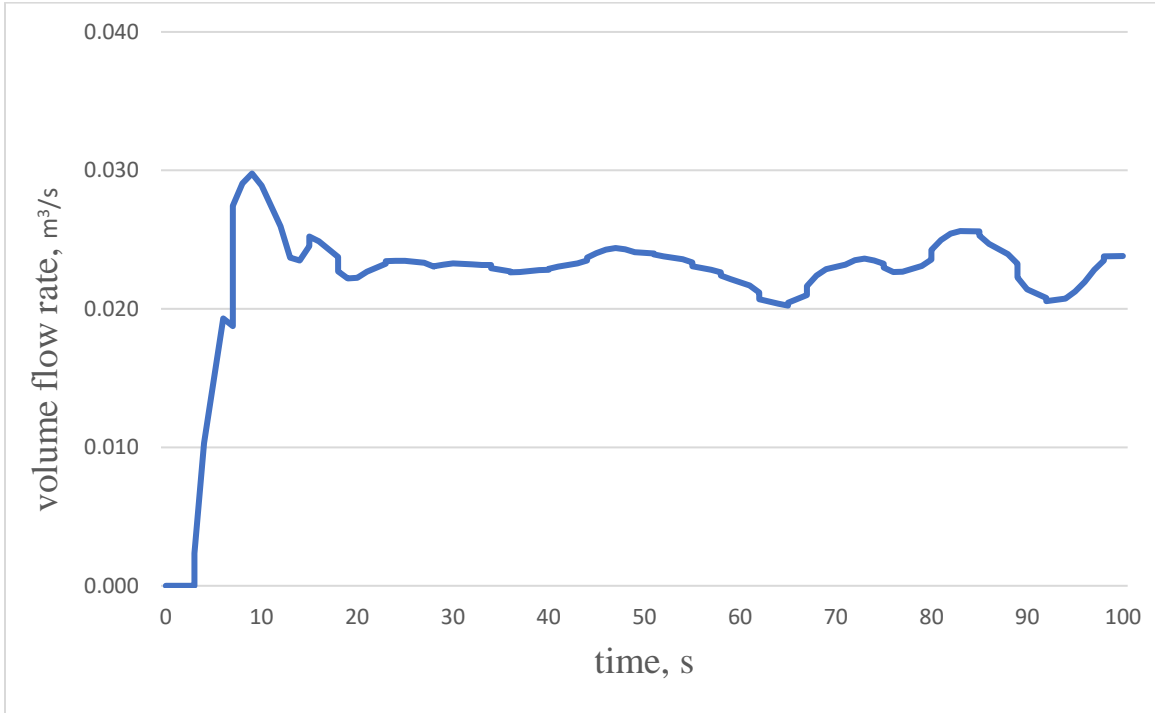
Appendix B. The discharge for the model with 25 cm wide

Figure B-1 Gate opening is 9 cm (Experiment 1)

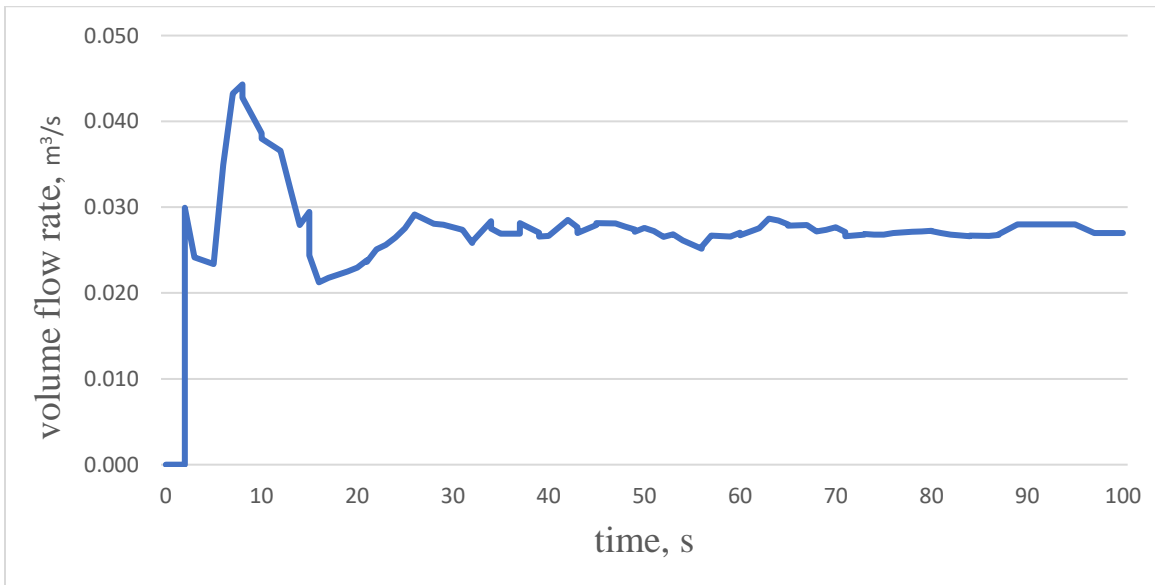


Figure B-2 Gate opening is 9 cm (Experiment 2)

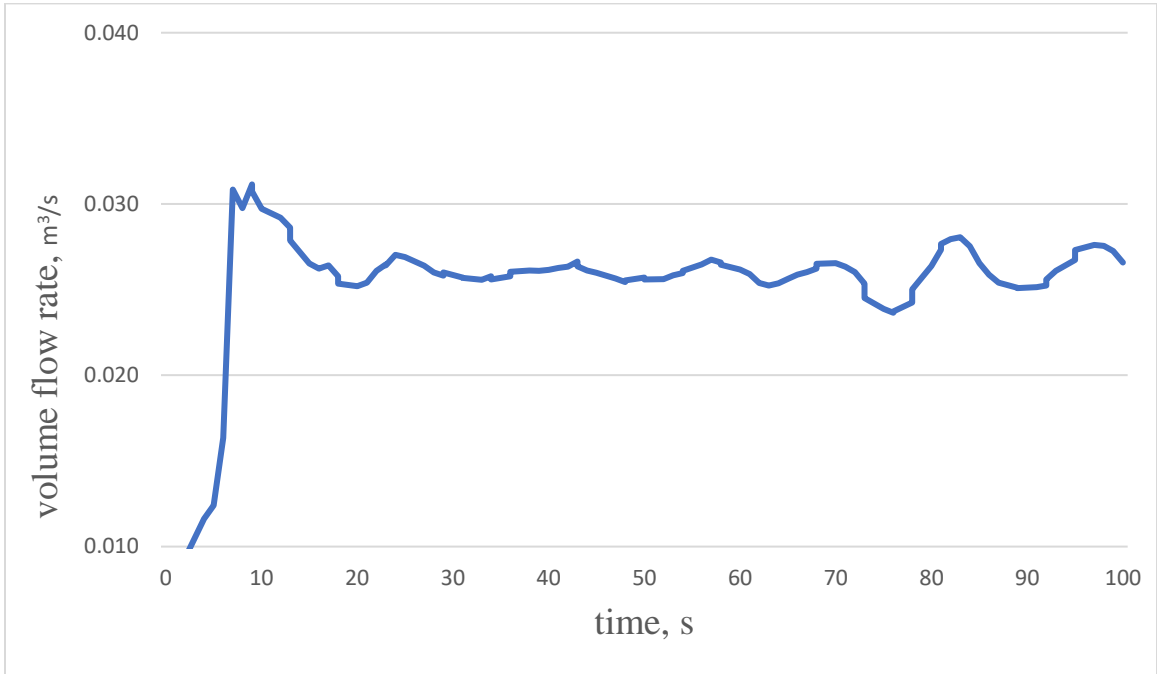


Figure B-3 Full opening of the gate (Experiment 3)

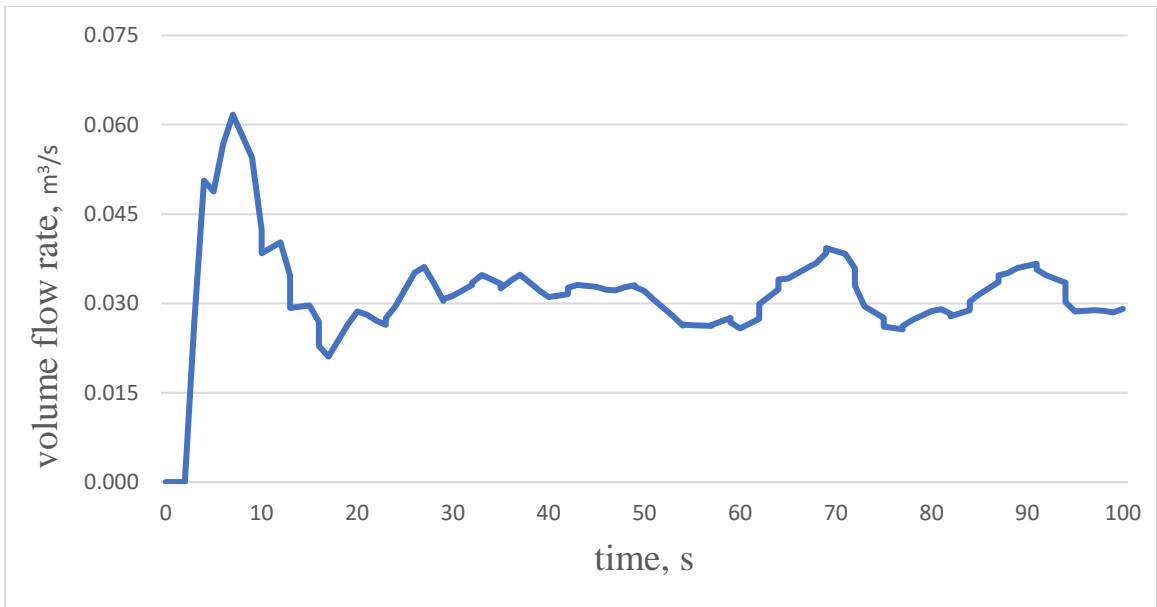


Figure B-4 Gate opening is 9 cm (Experiment 3)

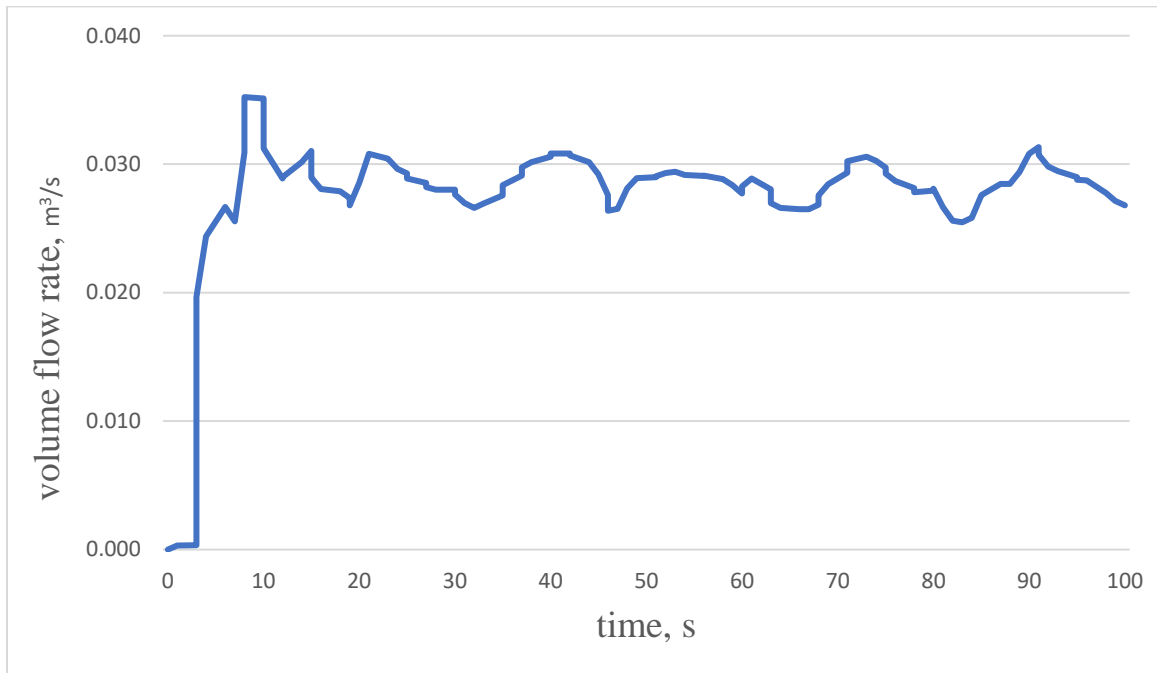


Figure B-5 Full opening of the gate (Experiment 4)

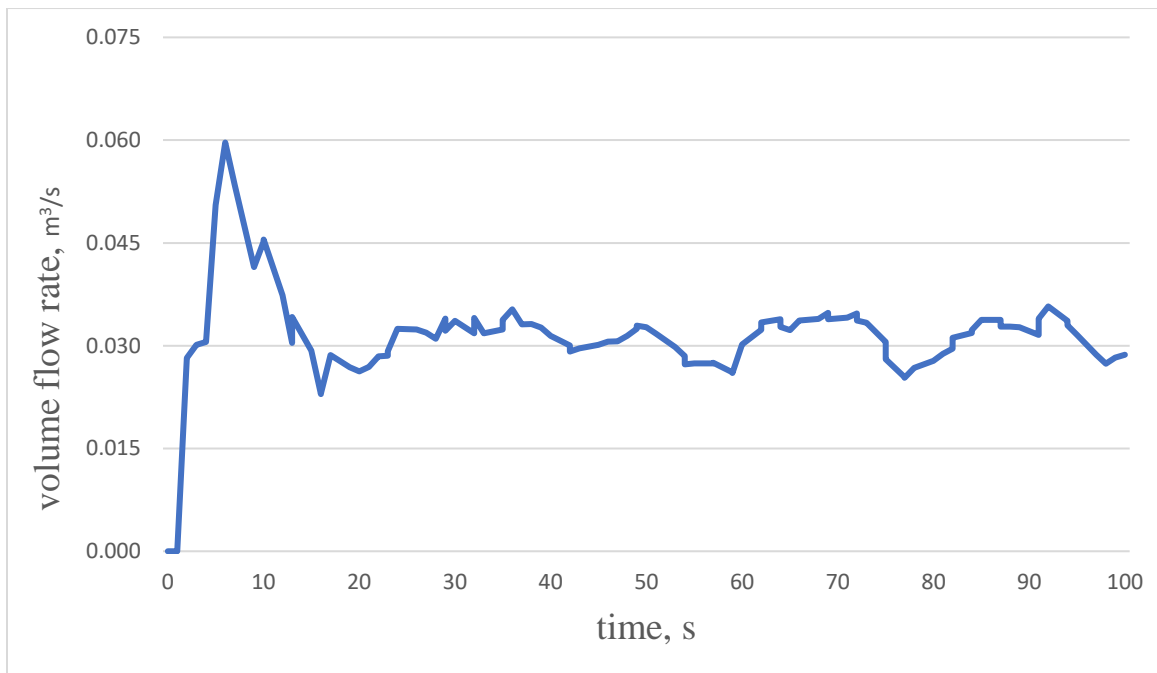


Figure B-6 Gate opening is 9 cm (Experiment 4)

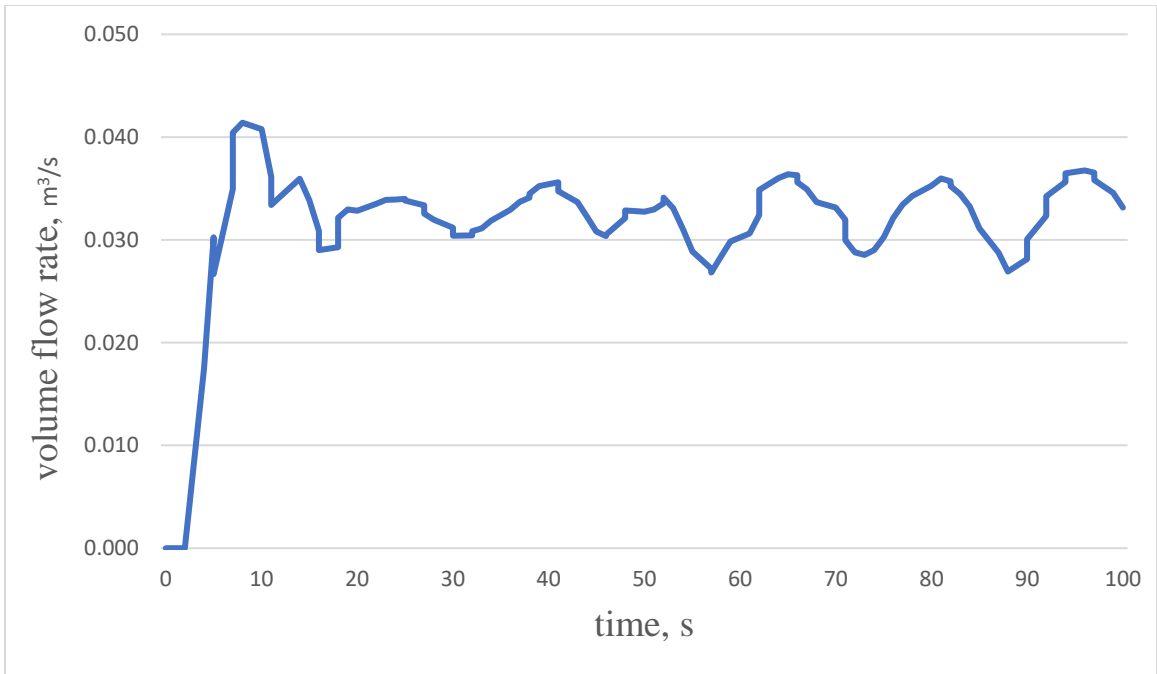


Figure B-7 Full opening of the gate (Experiment 5)

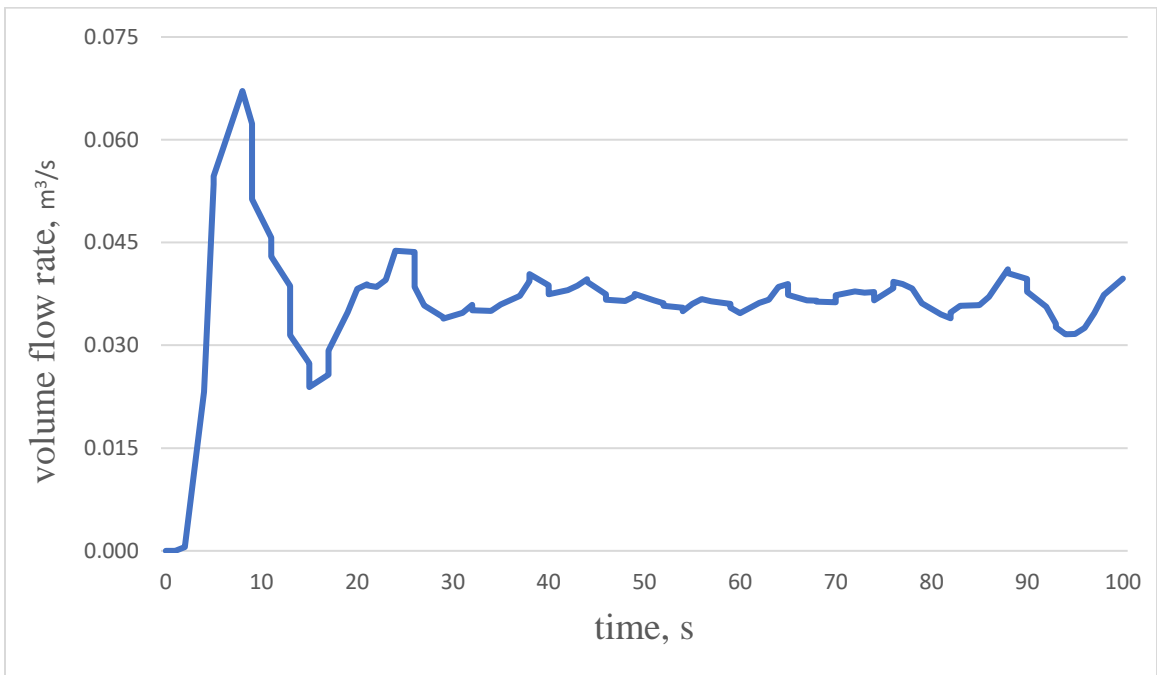


Figure B-8 Gate opening is 12 cm (Experiment 5)

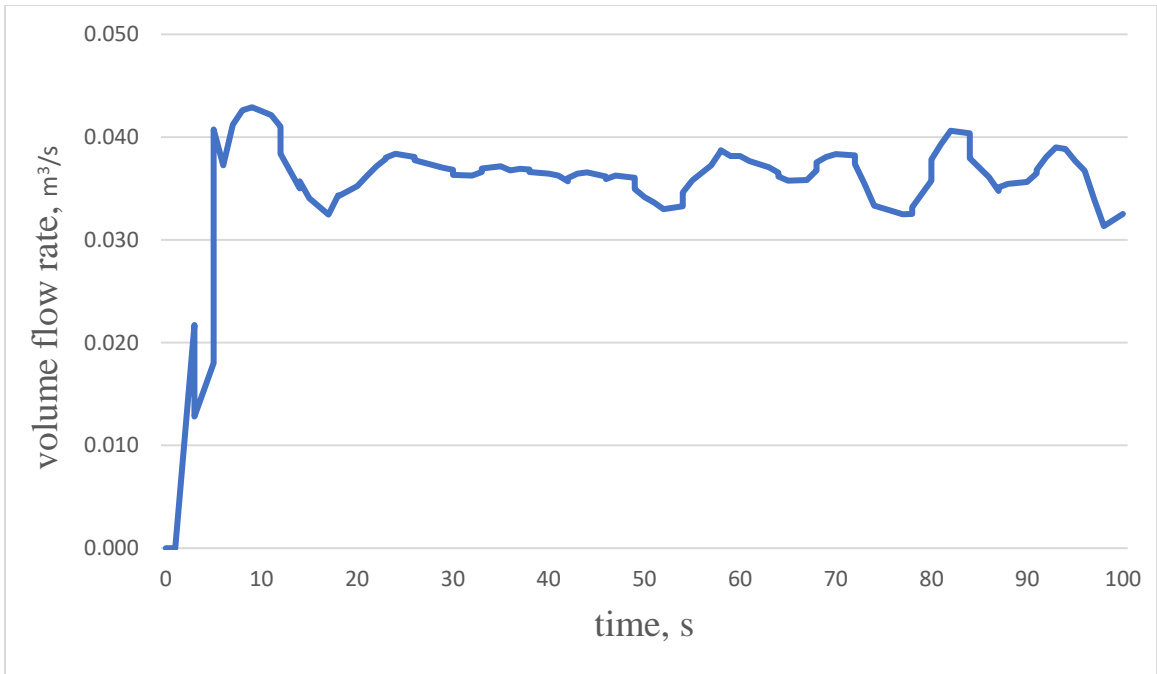


Figure B-9 Full opening of the gate (Experiment 6)

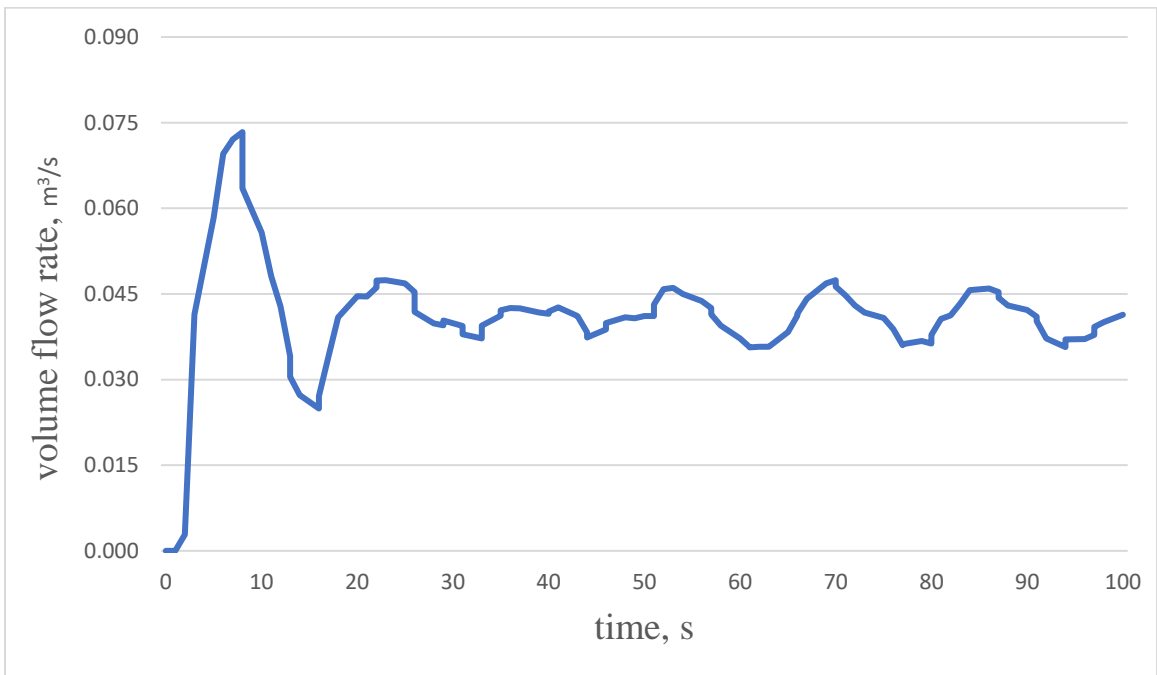


Figure B-10 Gate opening is 12 cm (Experiment 6)

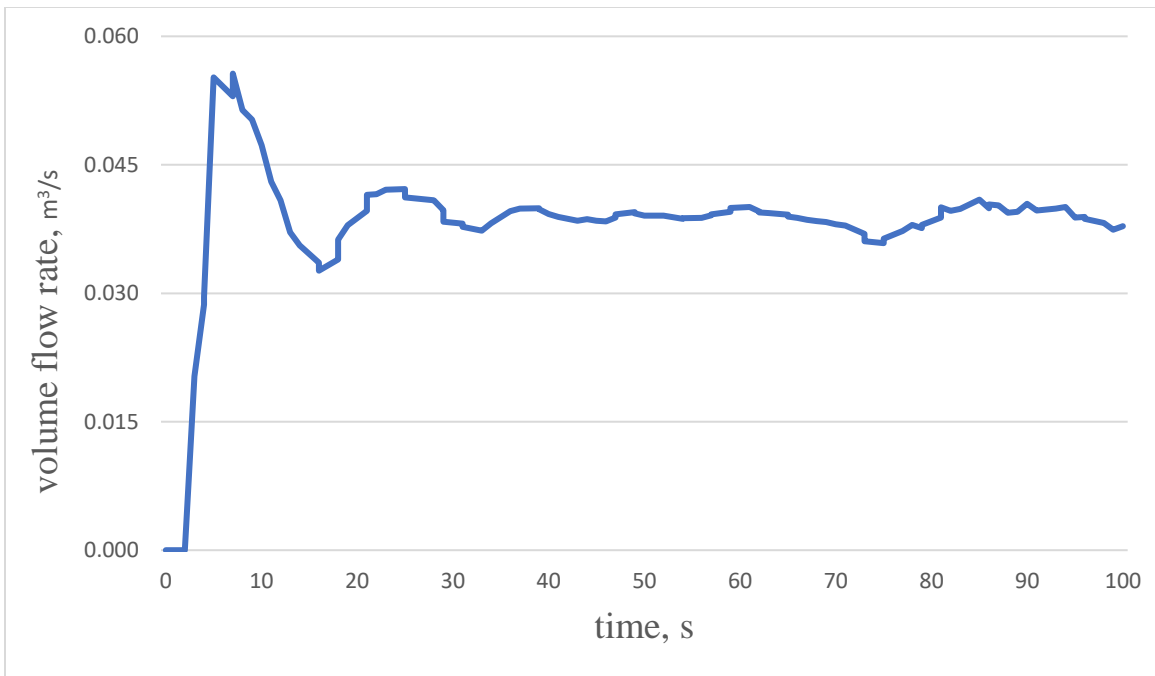


Figure B-11 Gate opening is 15 cm (Experiment 6)

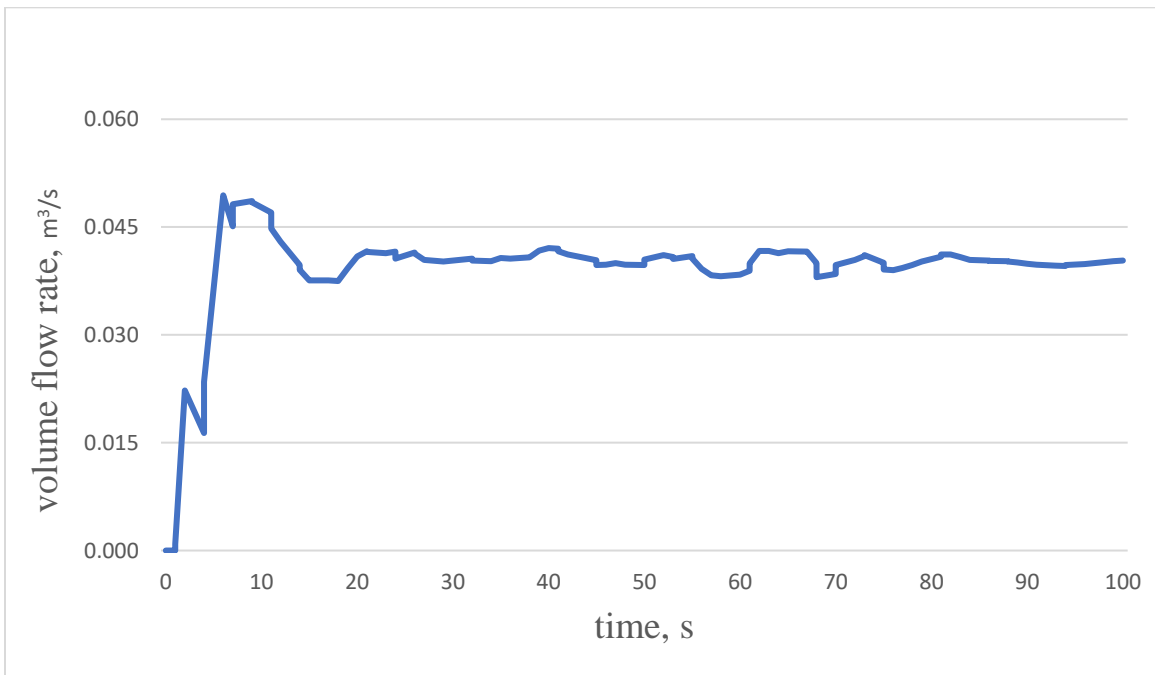


Figure B-12 Full opening of the gate (Experiment 7)

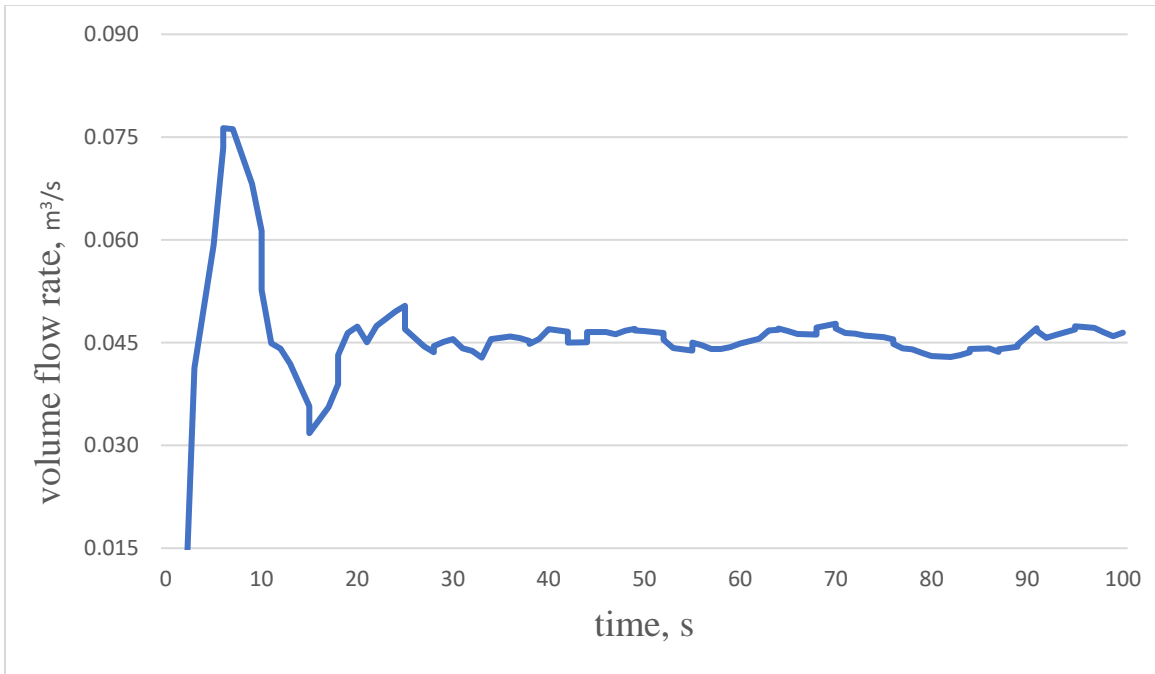


Figure B-13 Gate opening is 15 cm (Experiment 7)

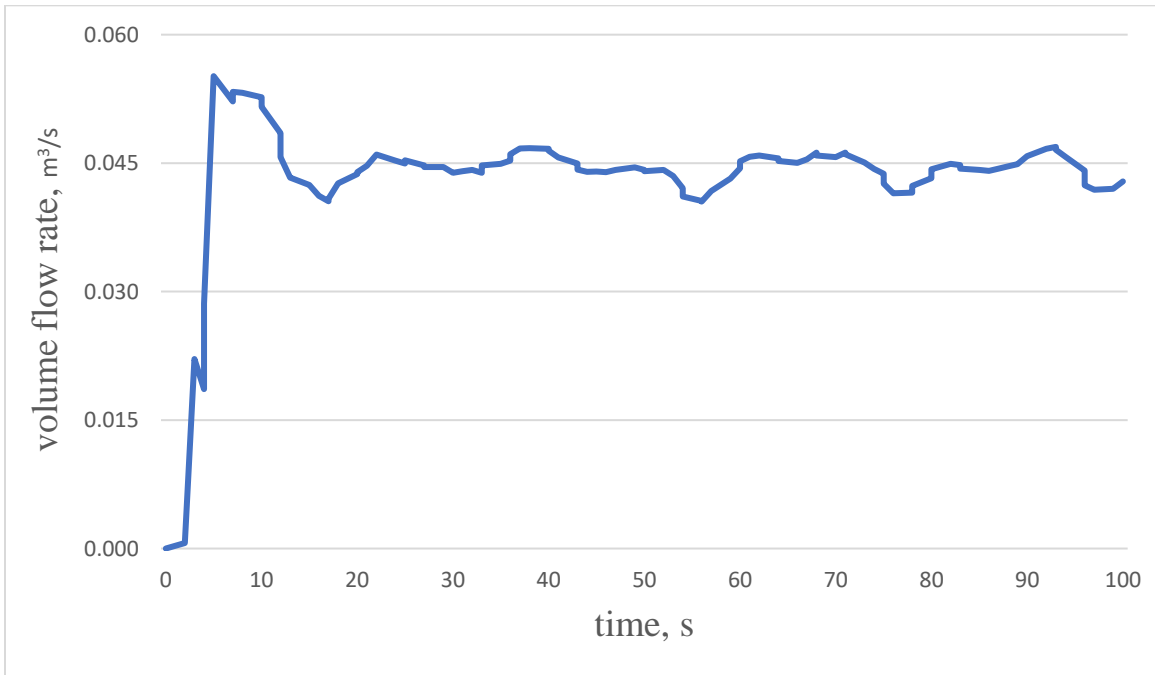


Figure B-14 Full opening of the gate (Experiment 8)

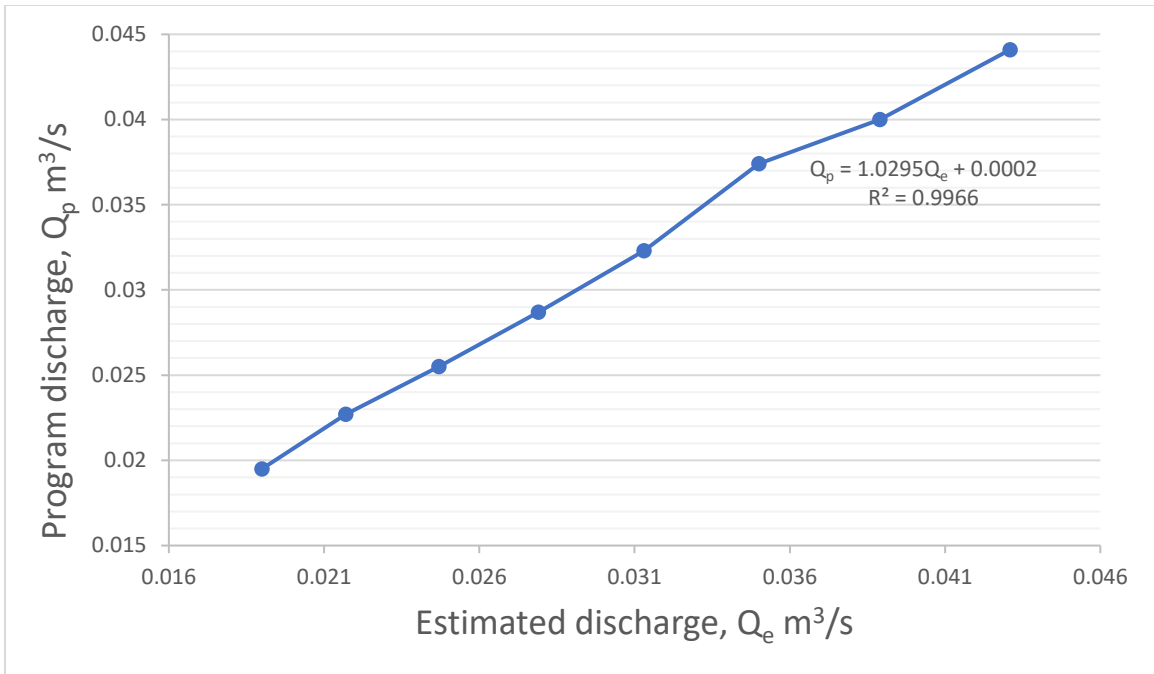


Figure B-15 Relationship between estimated discharge and software discharge in 25 cm wide and full opening

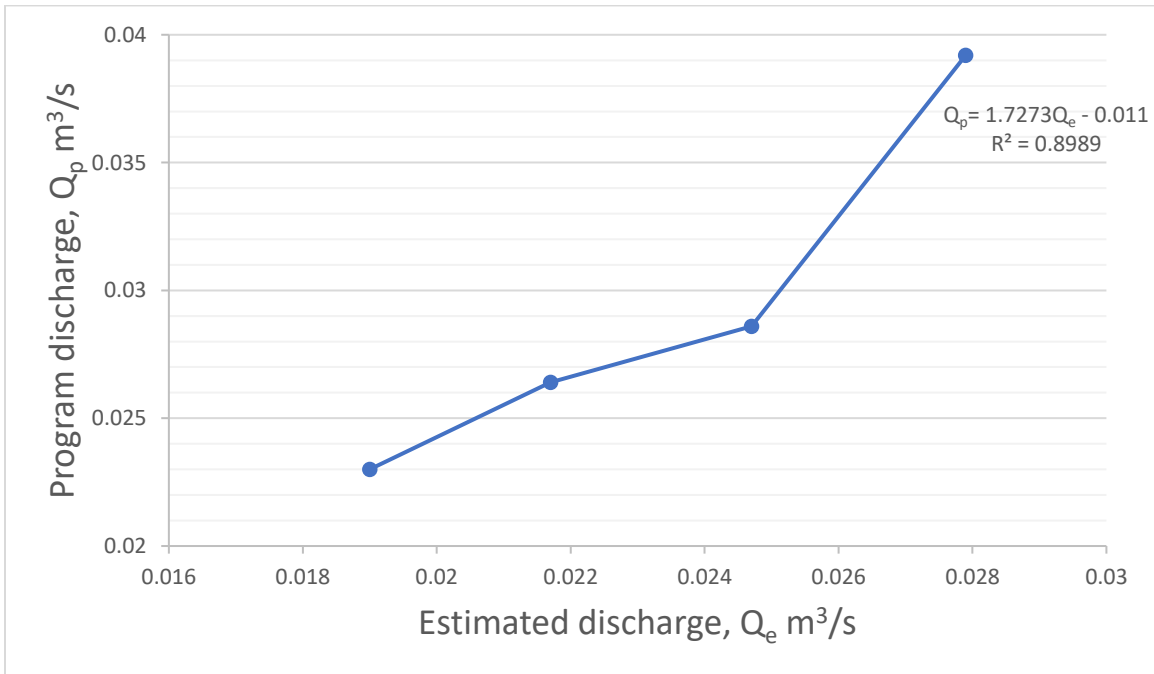


Figure B-16 Relationship between estimated discharge and software discharge in 25 cm wide and 9 cm opening

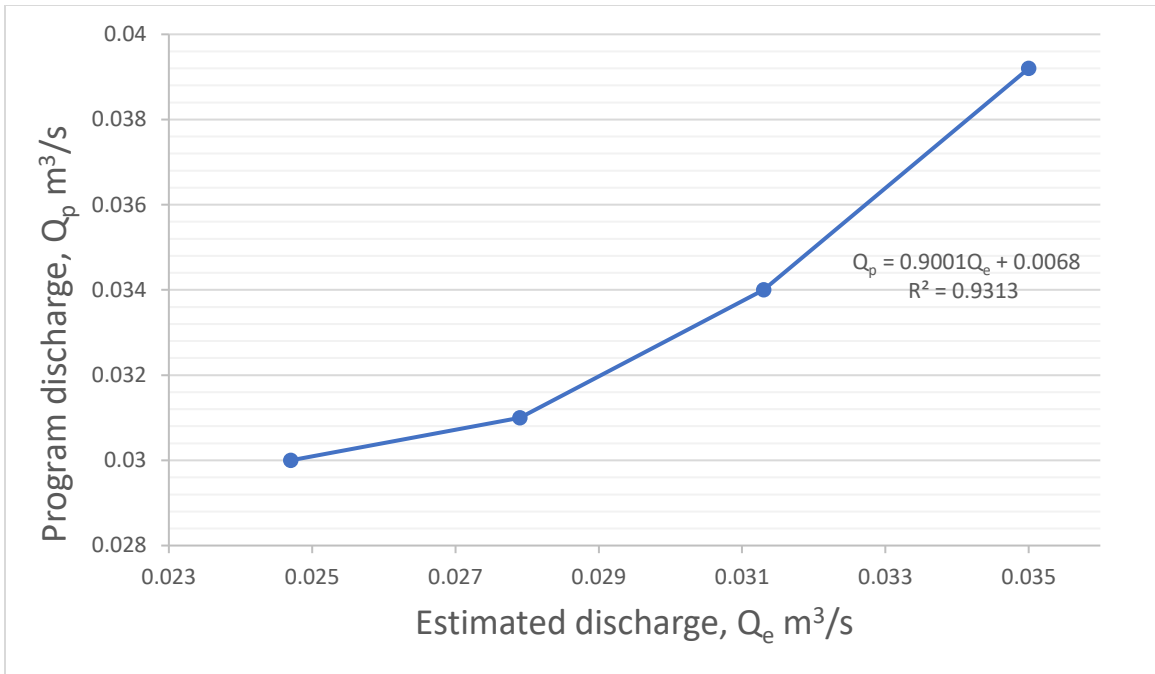


Figure B-17 Relationship between estimated discharge and software discharge in 25 cm wide and 12 cm opening

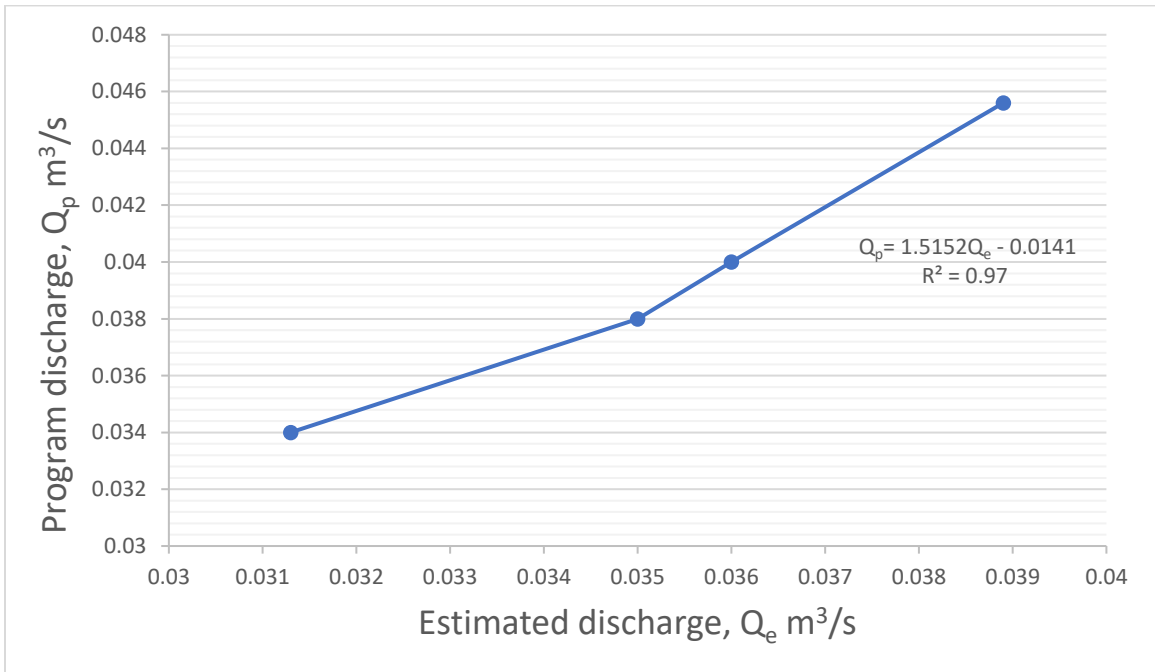


Figure B-18 Relationship between estimated discharge and software discharge in 25 cm wide and 15 cm opening

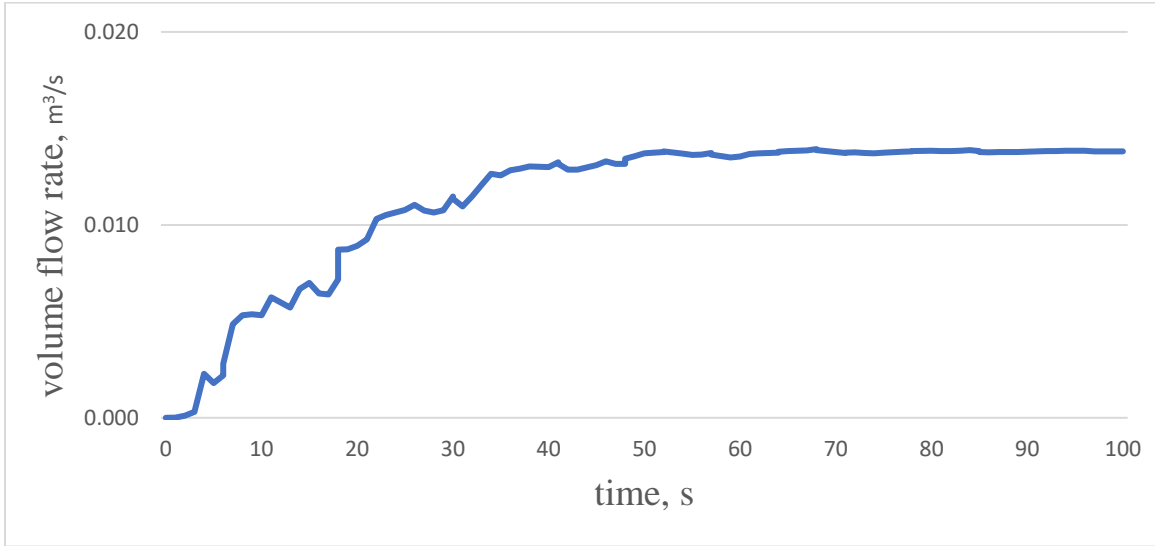
Appendix C. The discharge for the model with 35 cm wide

Figure C-1 Full opening of the gate (Experiment 1)

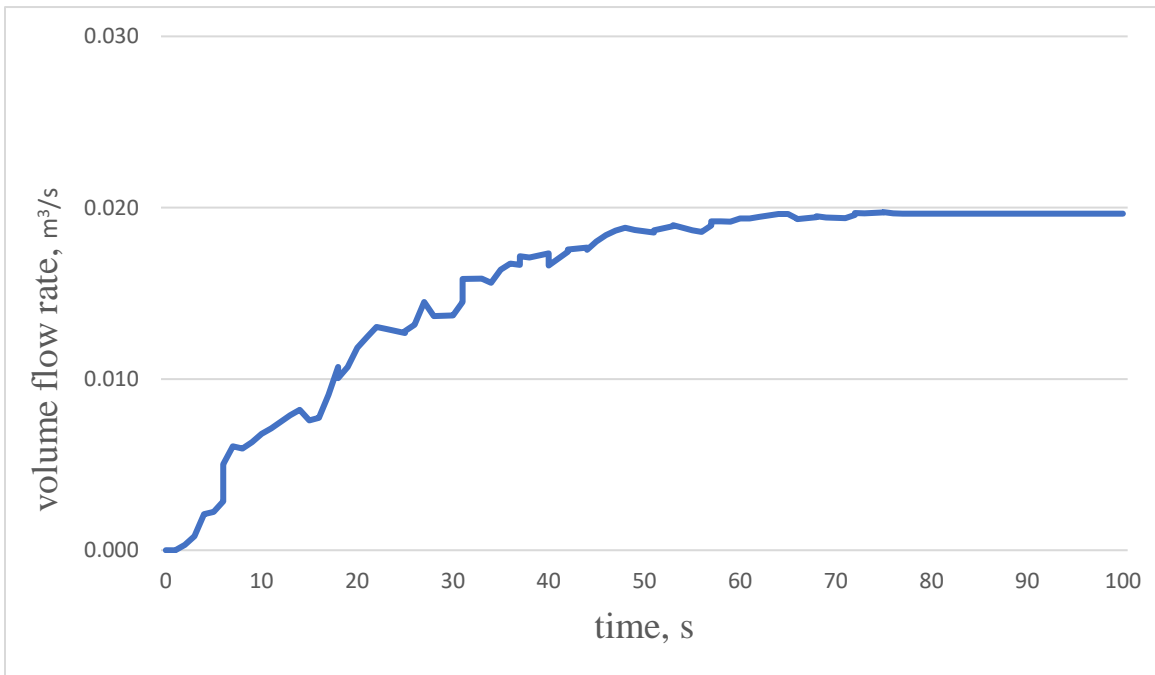


Figure C-2 Full opening of the gate (Experiment 2)

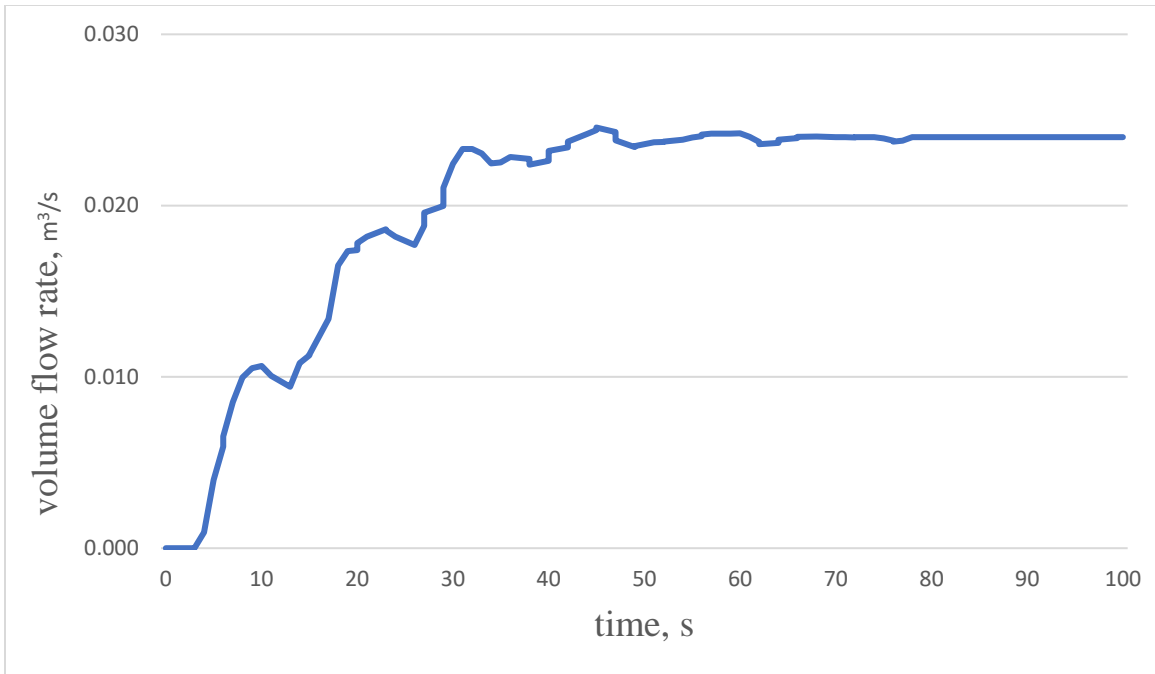


Figure C-3 Full opening of the gate (Experiment 3)

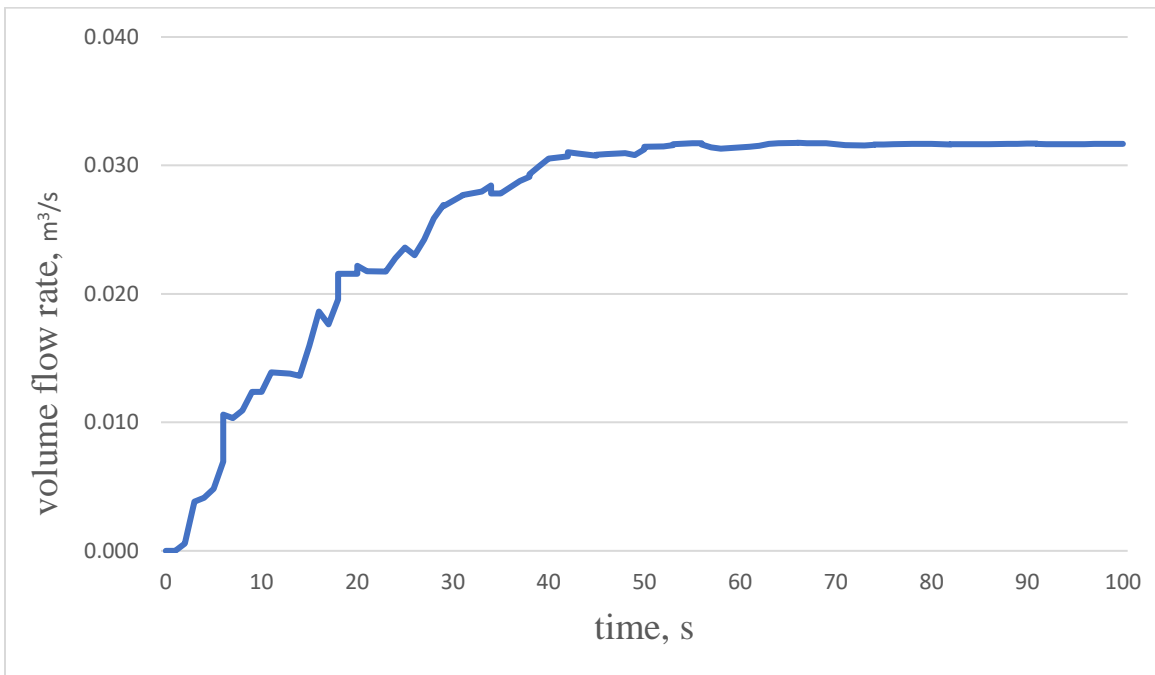


Figure C-4 Full opening of the gate (Experiment 4)

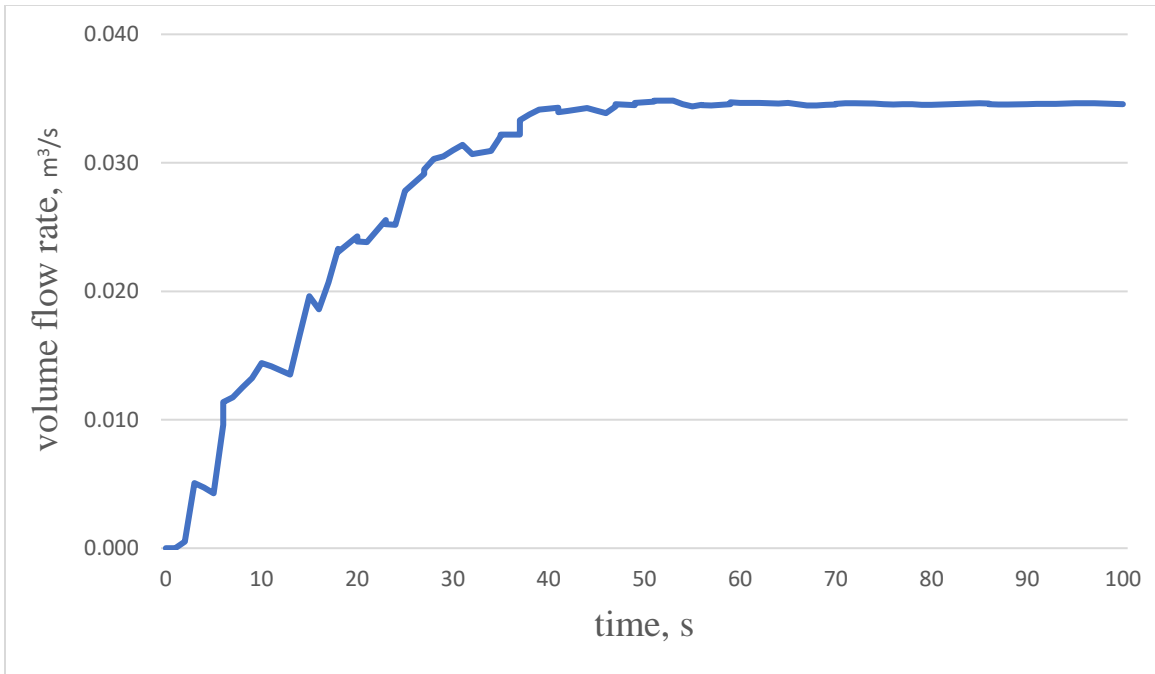


Figure C-5 Full opening of the gate (Experiment 5)

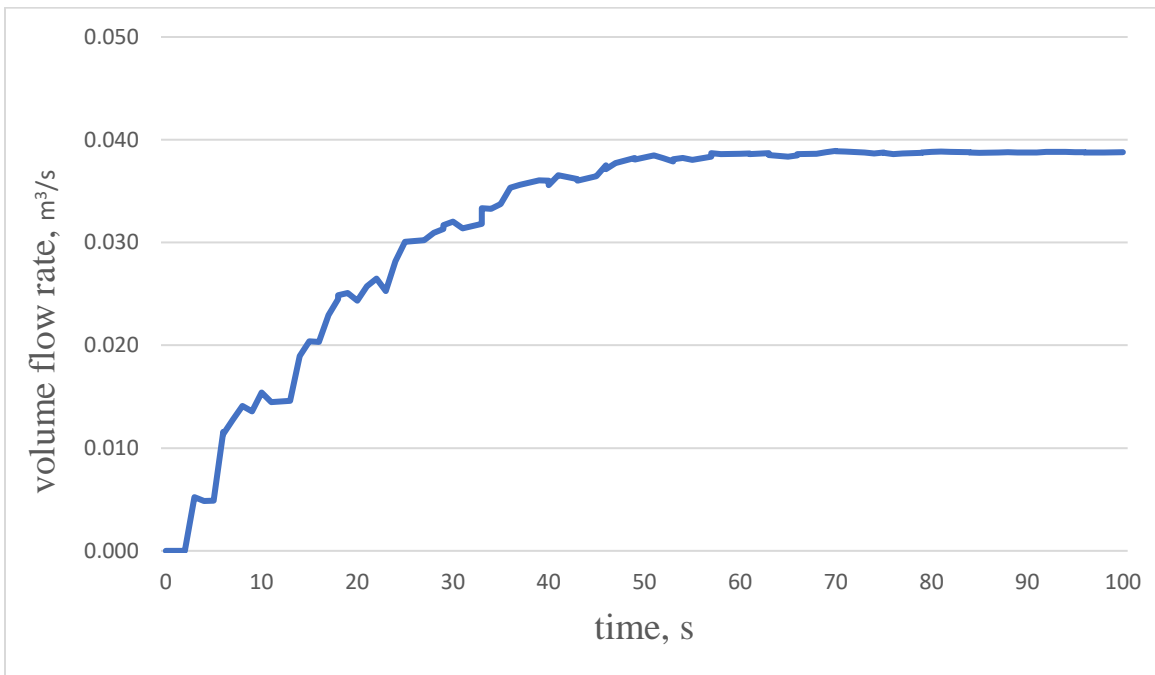


Figure C-6 Full opening of the gate (Experiment 6)

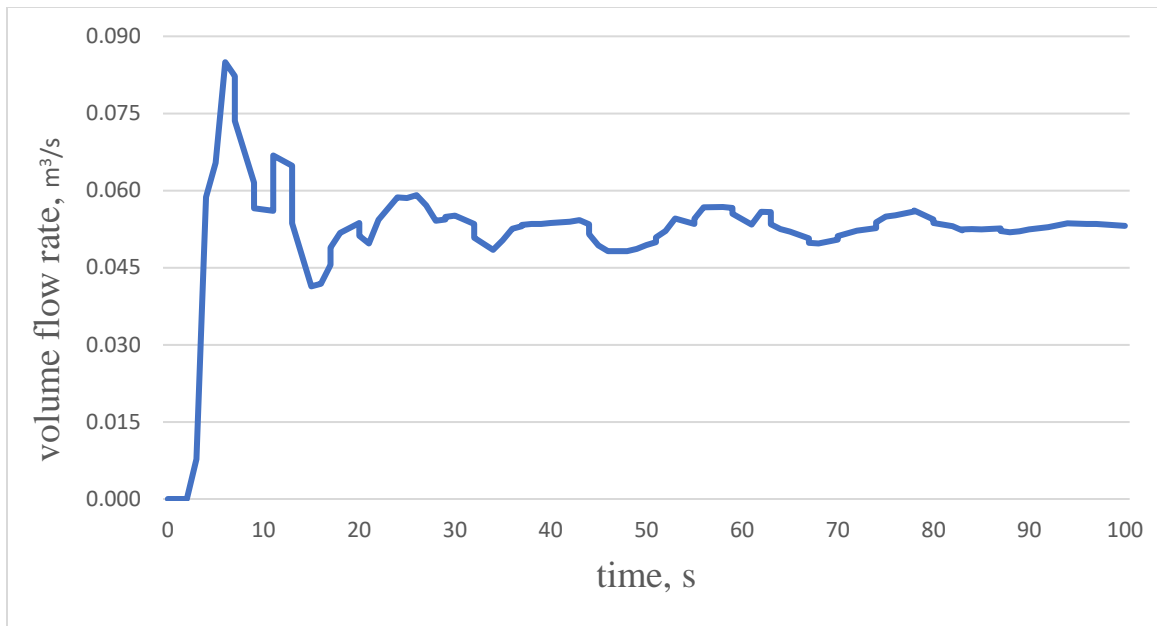


Figure C-7 Gate opening is 10 cm (Experiment 6)

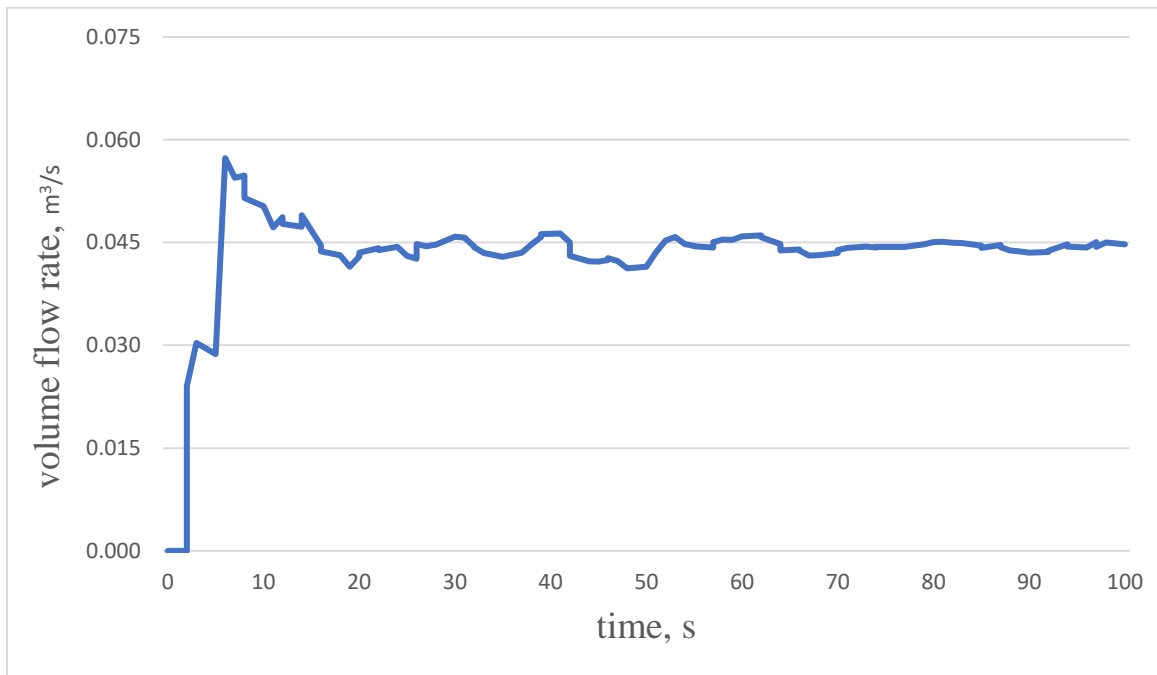


Figure C-8 Gate opening is 10 cm (Experiment 7)

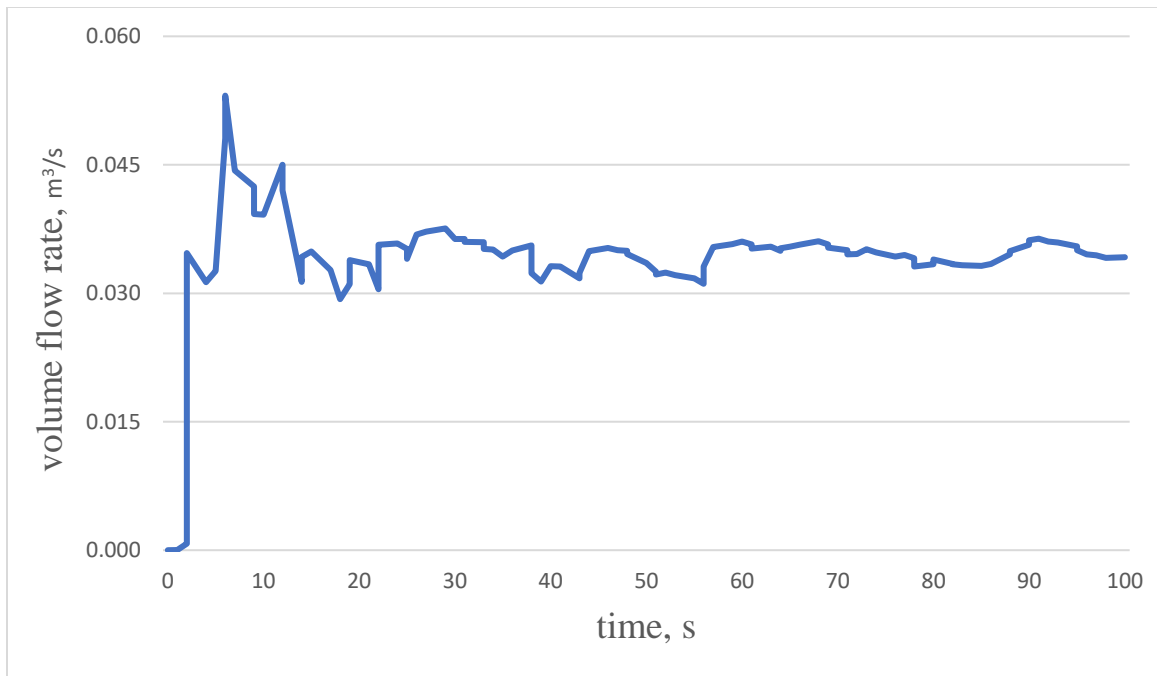


Figure C-9 Gate opening is 6 cm (Experiment 8)

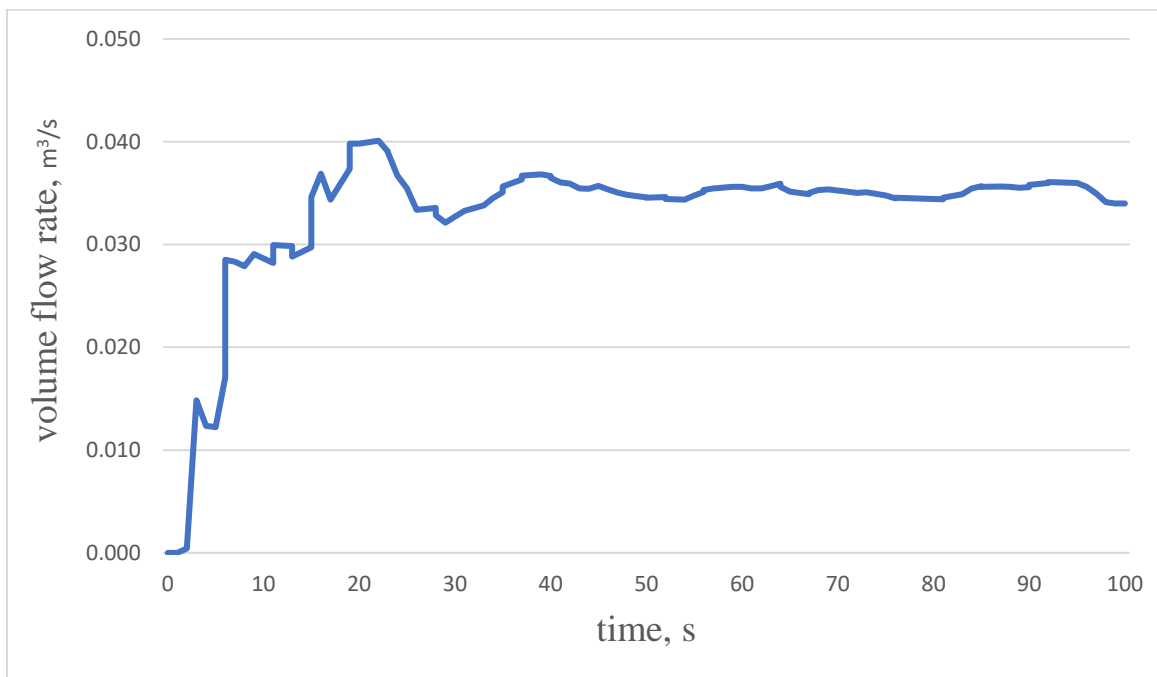


Figure C-10 Gate opening is 10 cm (Experiment 8)

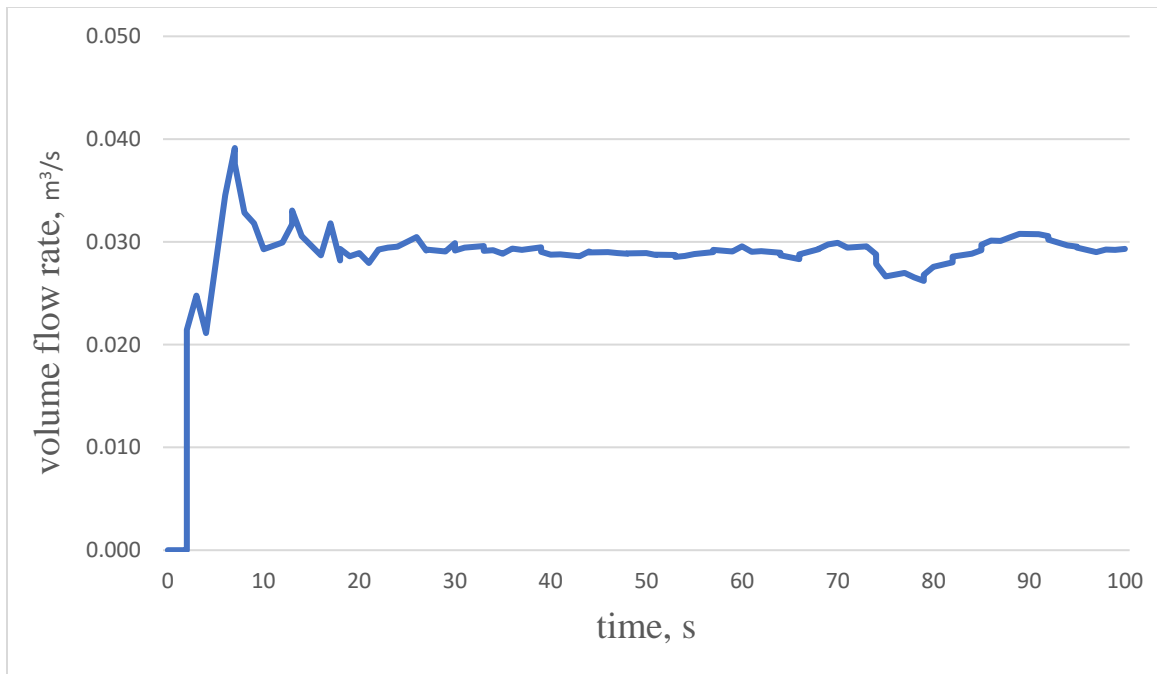


Figure C-11 Gate opening is 6 cm (Experiment 9)

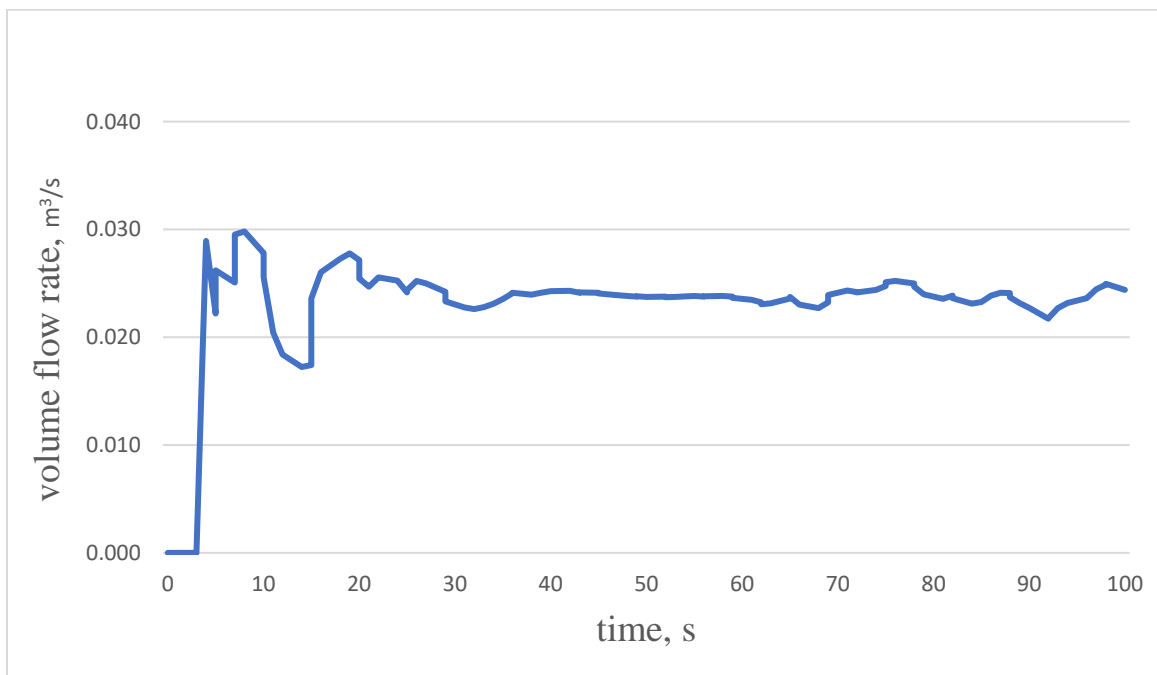


Figure C-12 Gate opening is 6 cm (Experiment 10)

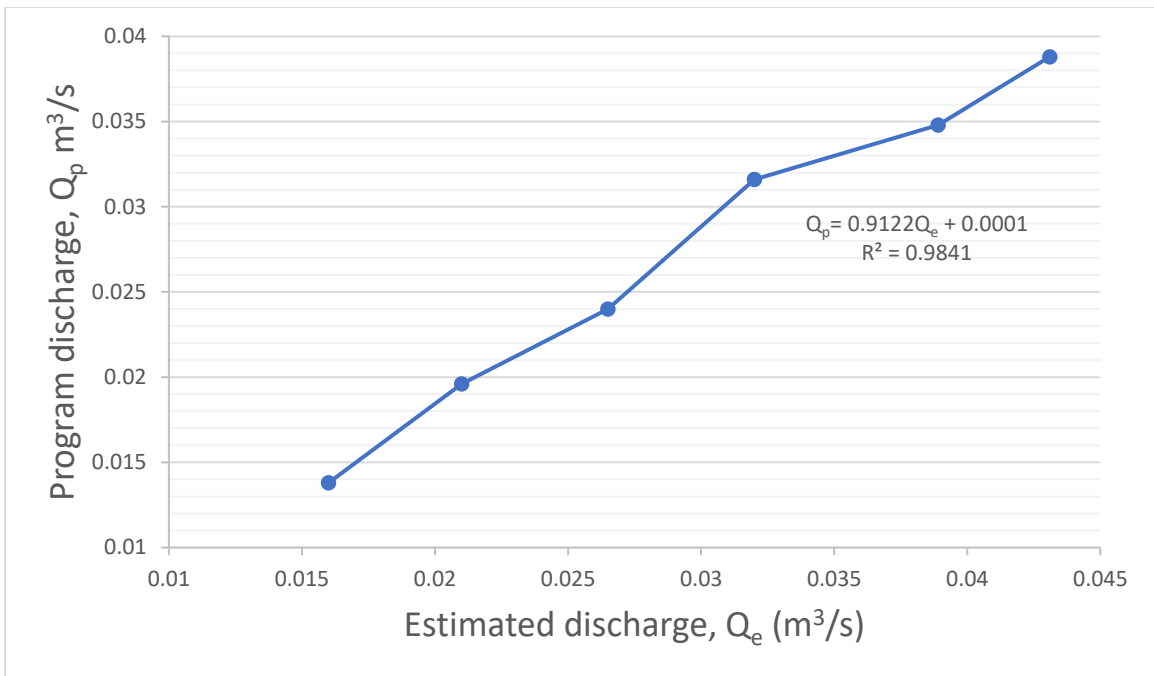


Figure C-13 Relationship between estimated discharge and software discharge in 35 cm wide and full opening

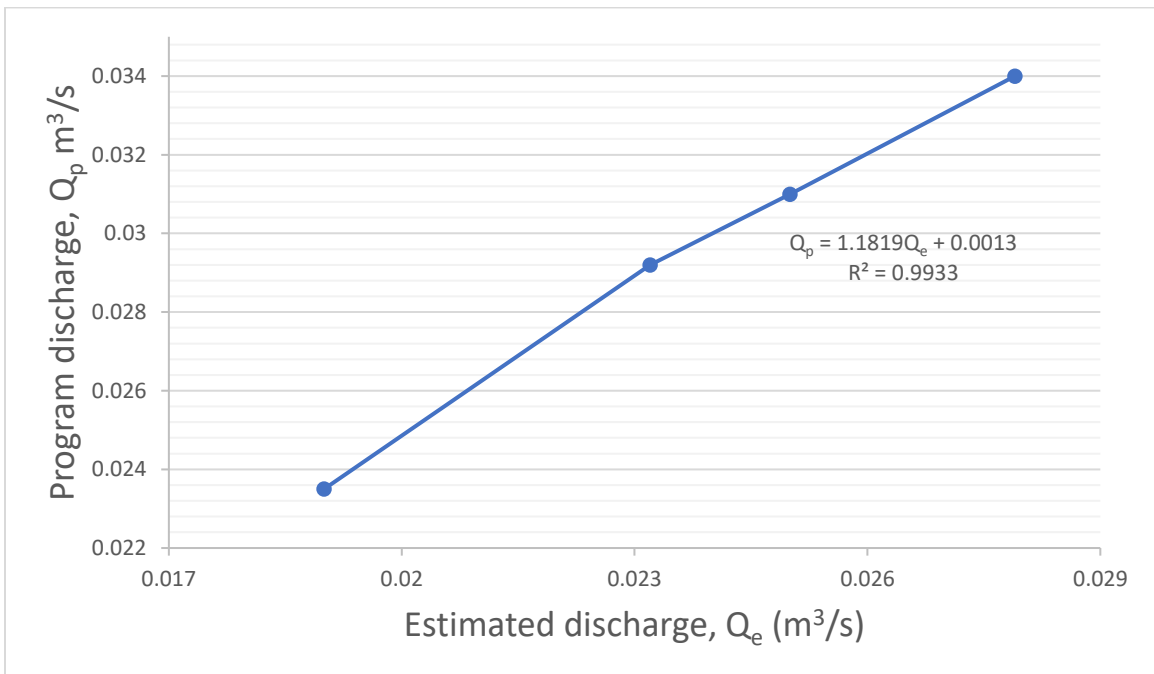


Figure C-14 Relationship between estimated discharge and software discharge in 35 cm wide and 6 cm opening

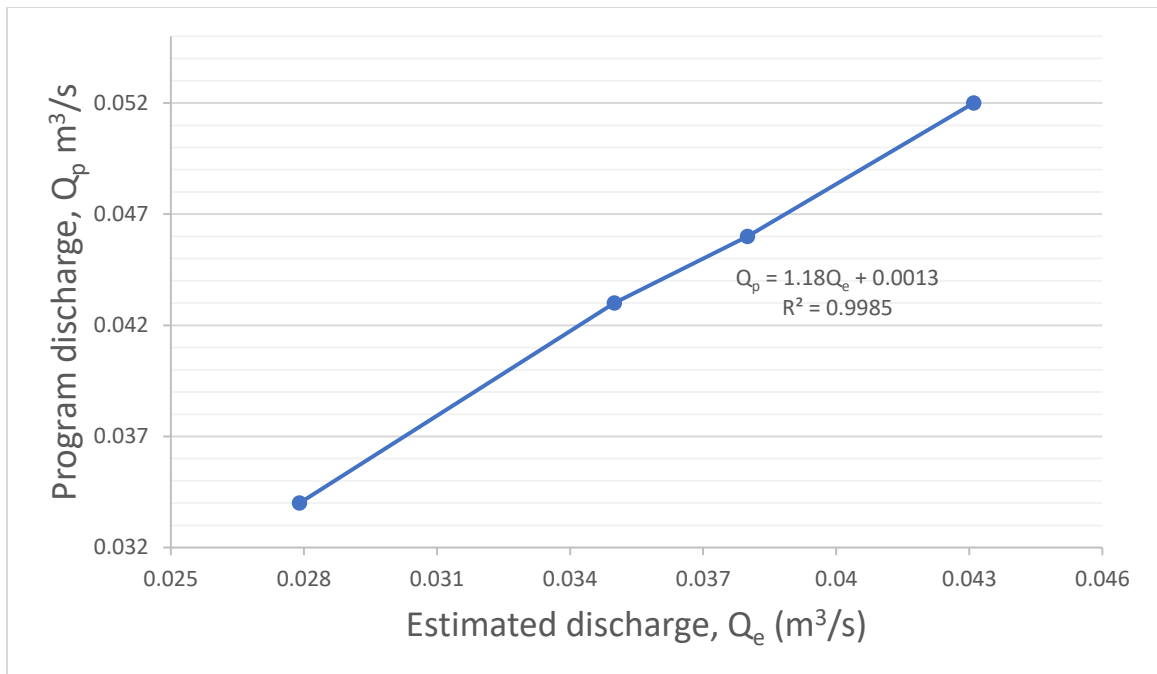


Figure C-15 Relationship between estimated discharge and software discharge in 35 cm wide and 10 cm opening

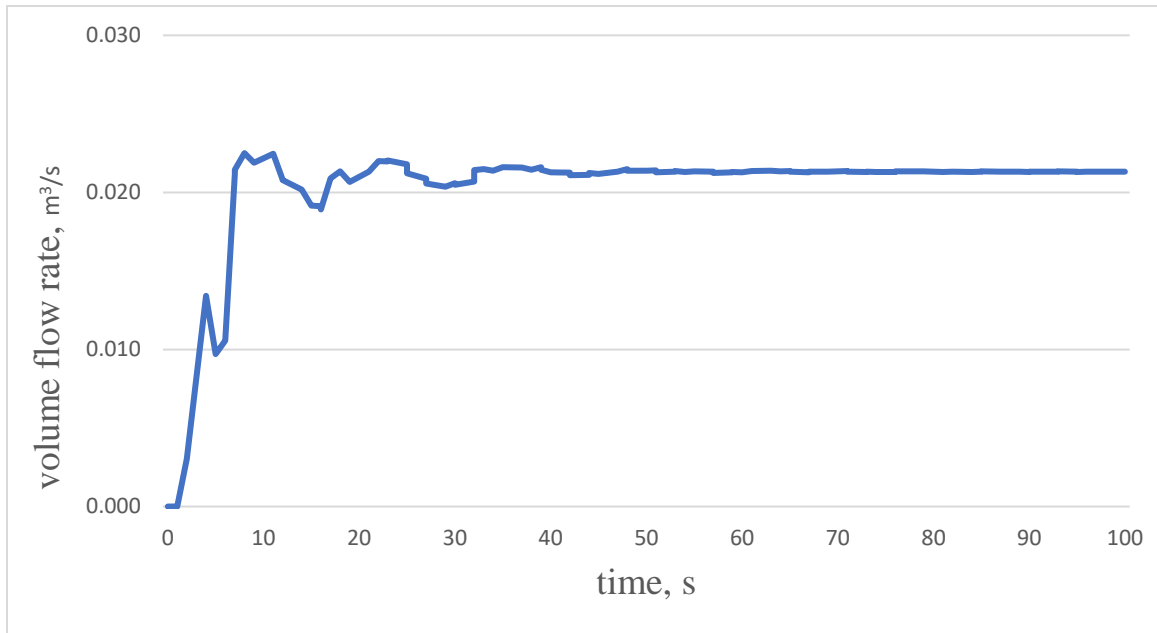
Appendix D . The discharge for the model with 50 cm wide

Figure D-1 Gate opening is 6 cm (Experiment 1)

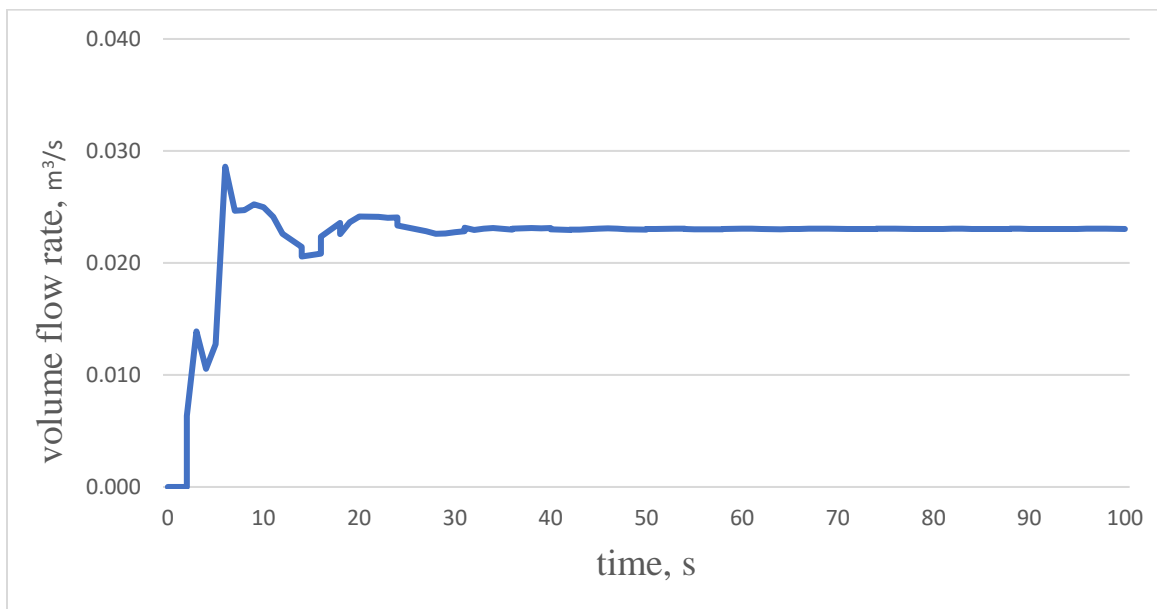


Figure D-2 Gate opening is 6 cm (Experiment 2)

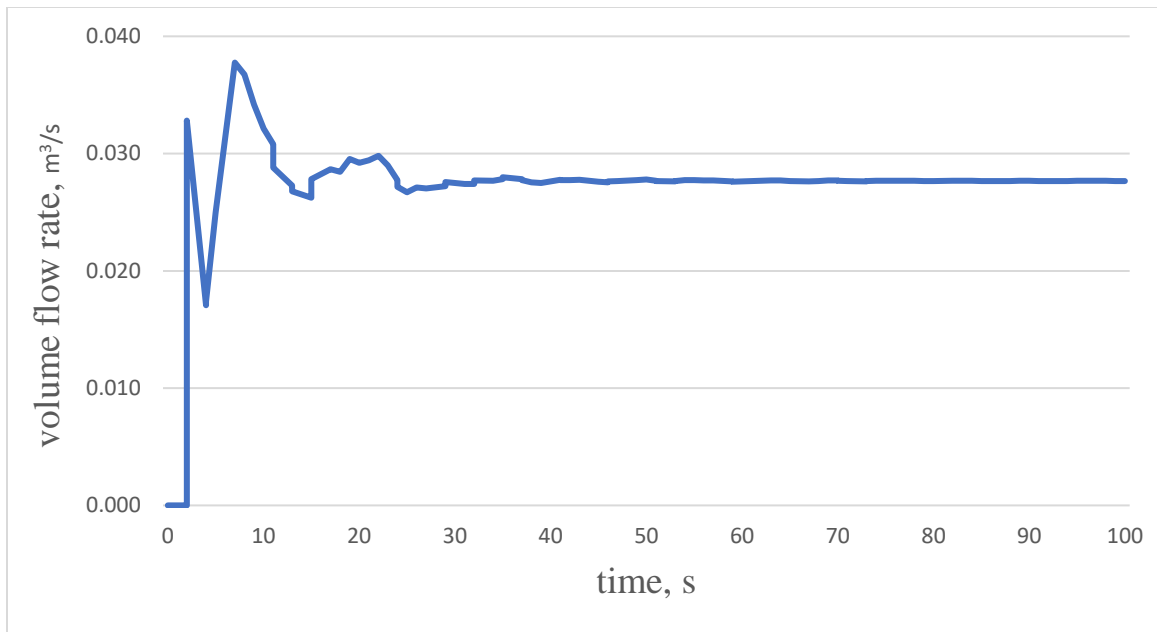


Figure D-3 Gate opening is 6 cm (Experiment 3)

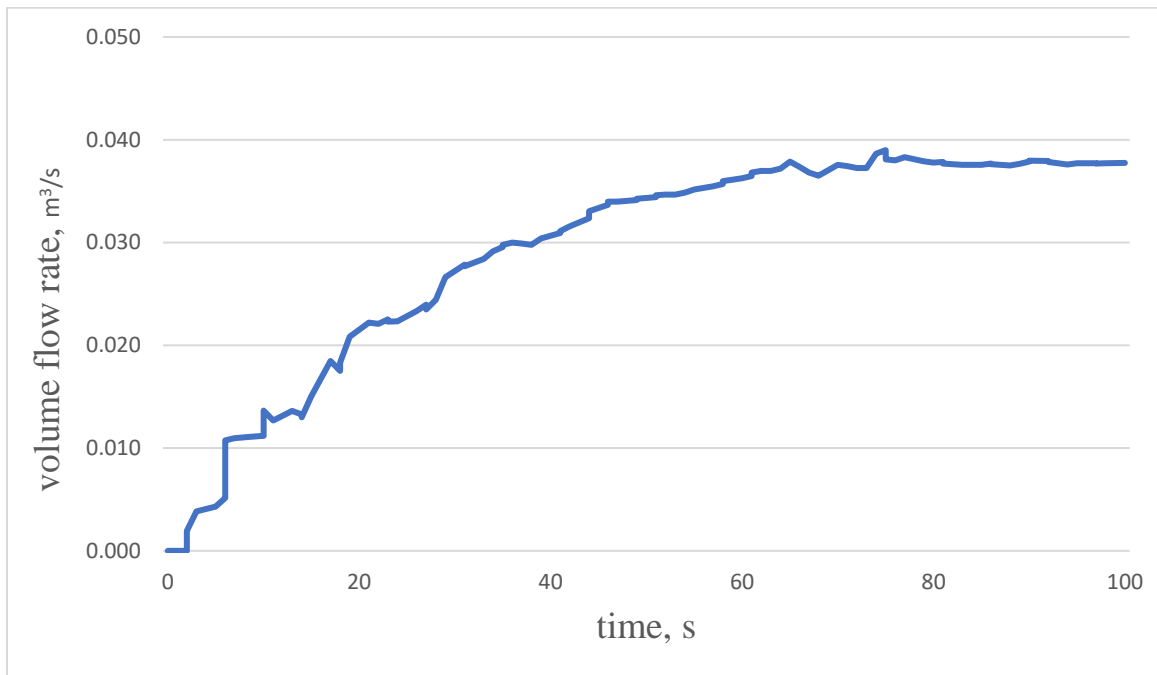


Figure D-4 Gate opening is 10 cm (Experiment 3)

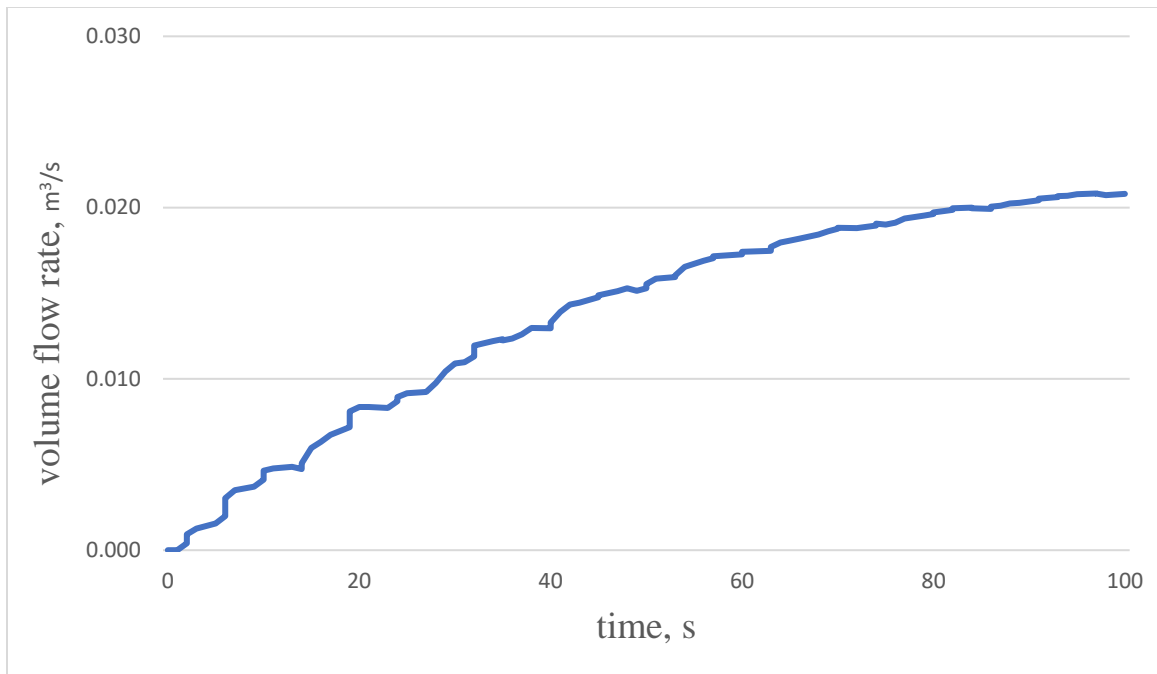


Figure D-5 Full opening of the gate (Experiment 4)

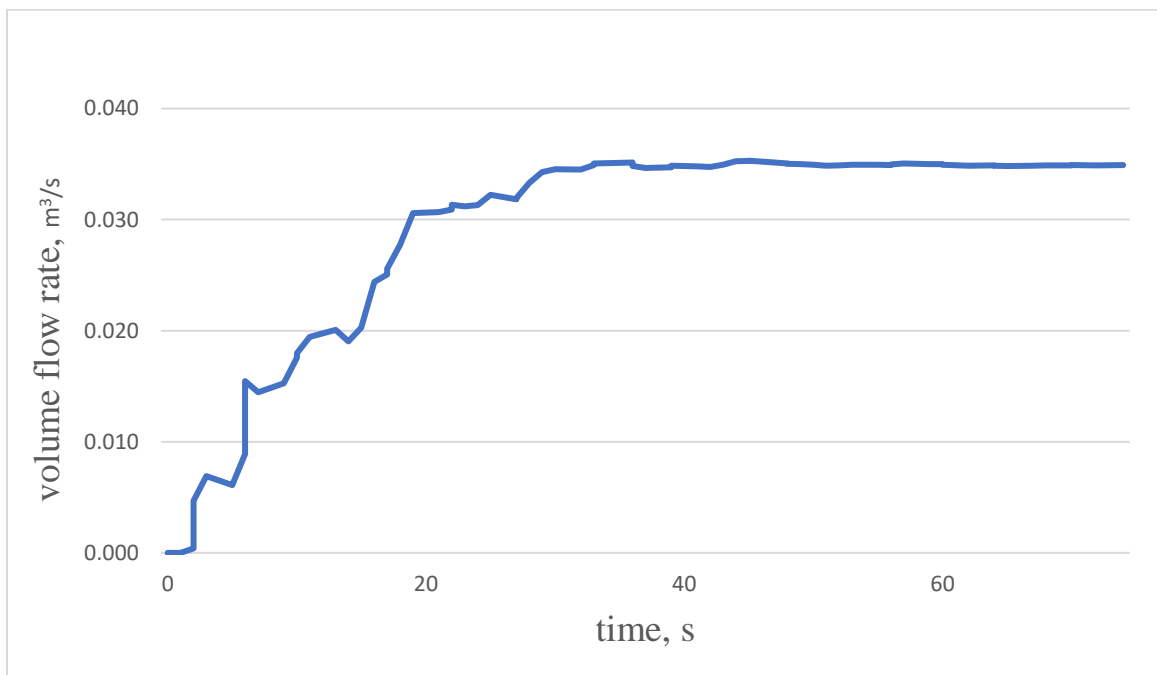


Figure D-6 Gate opening is 10 cm (Experiment 4)

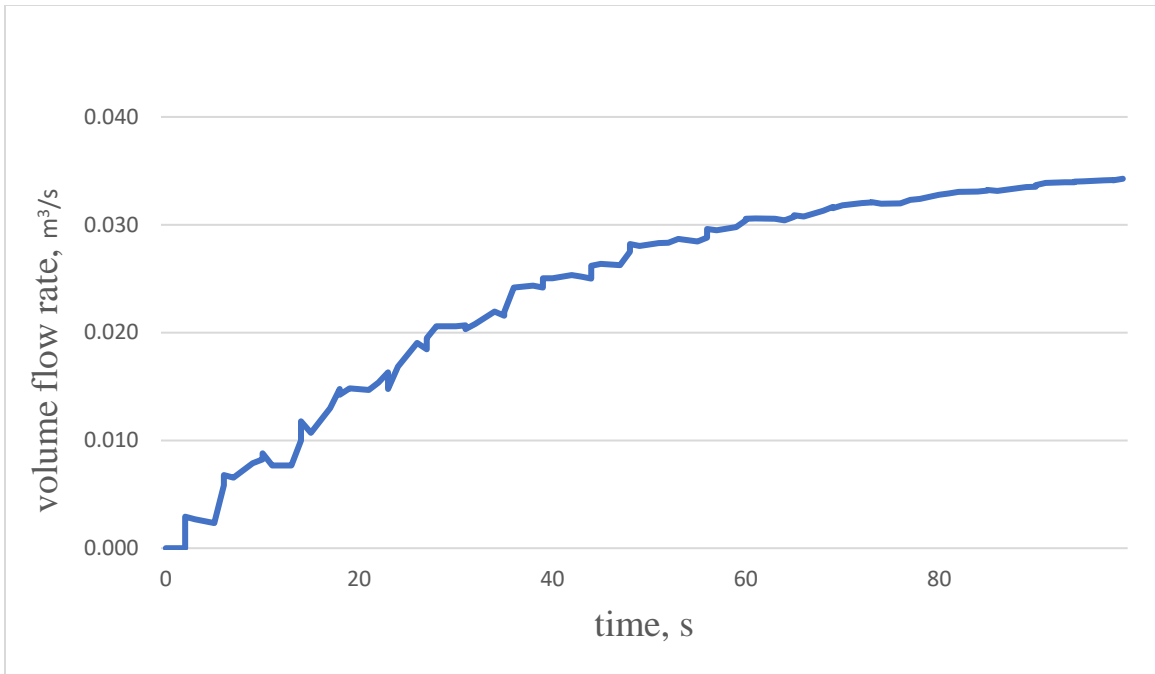


Figure D-7 Full opening of the gate (Experiment 8)

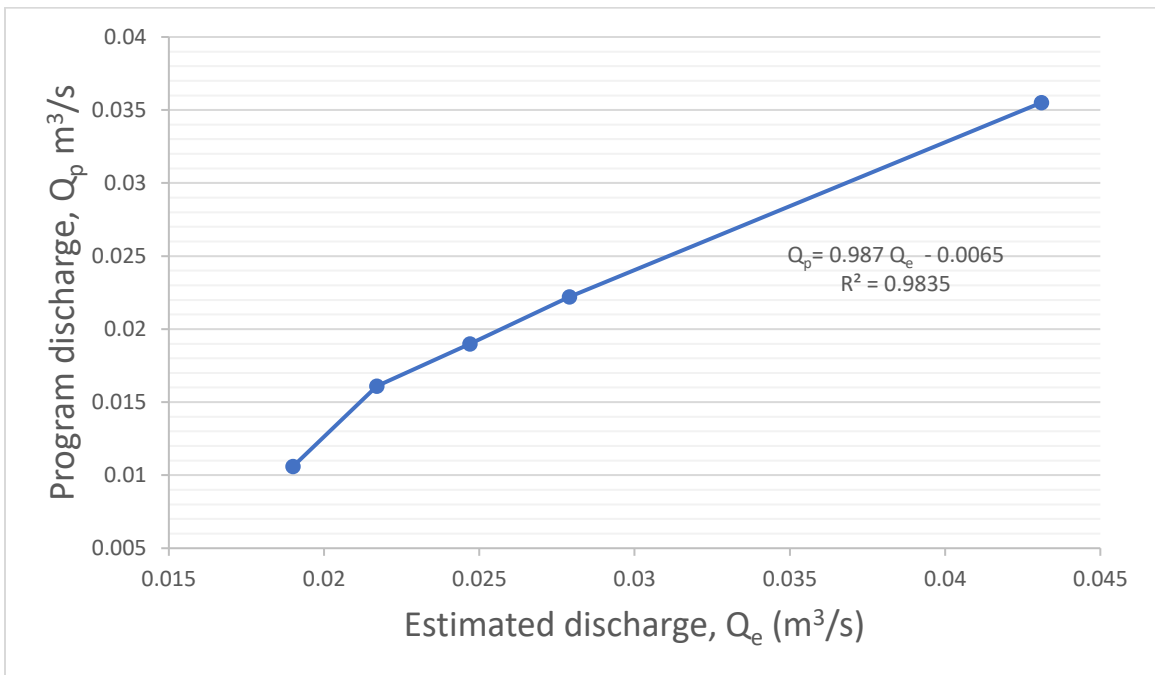


Figure D-8 Relationship between estimated discharge and software discharge in 50 cm wide and full opening

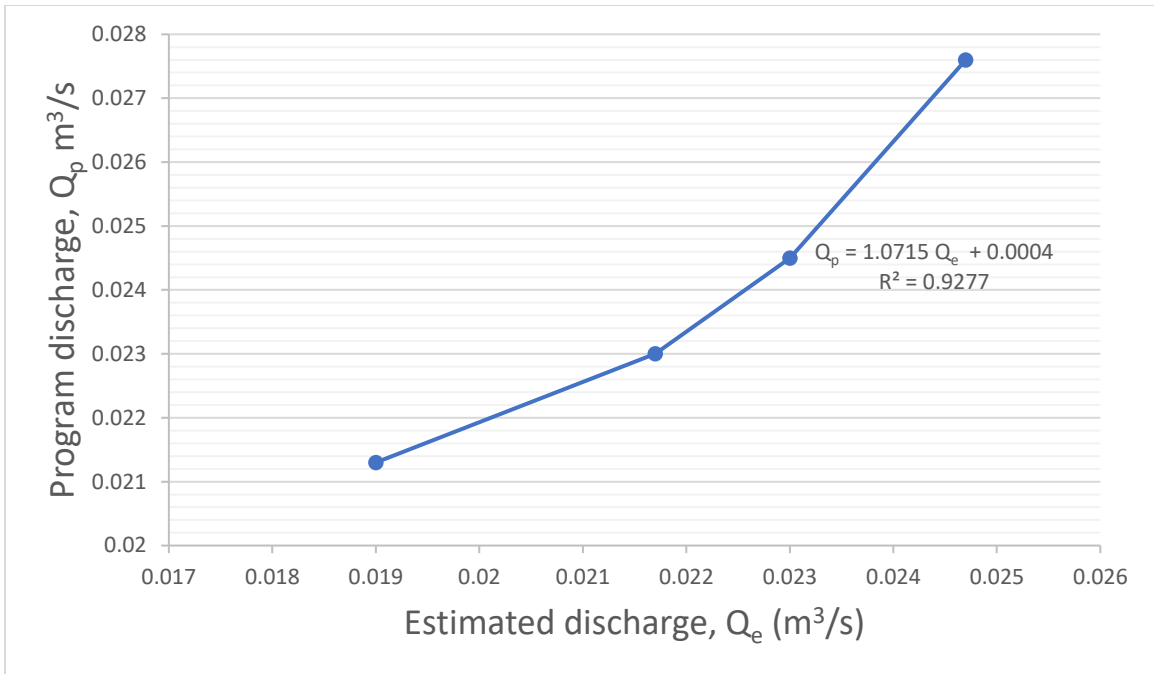


Figure D-9 Relationship between estimated discharge and software discharge in 50 cm wide and 6 cm opening

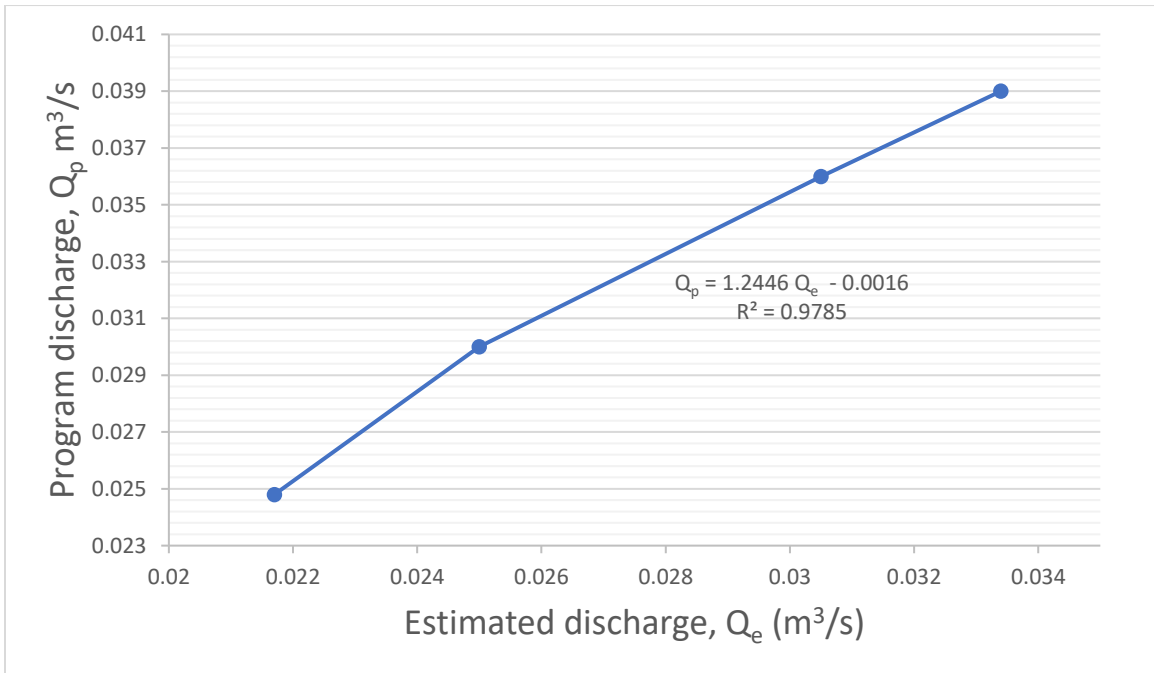


Figure D-10 Relationship between estimated discharge and software discharge in 50 cm wide and 10 cm opening

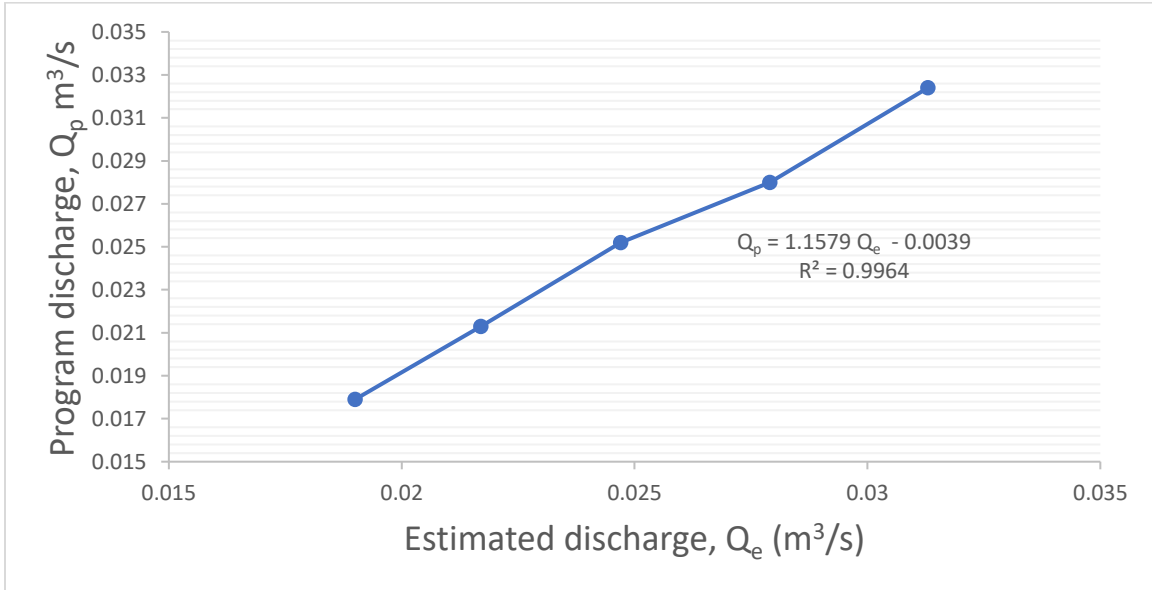
Appendix E. The discharge for the model with 3*10 cm wide

Figure E-1 Relationship between estimated discharge and software discharge in 3*10 cm wide full opening

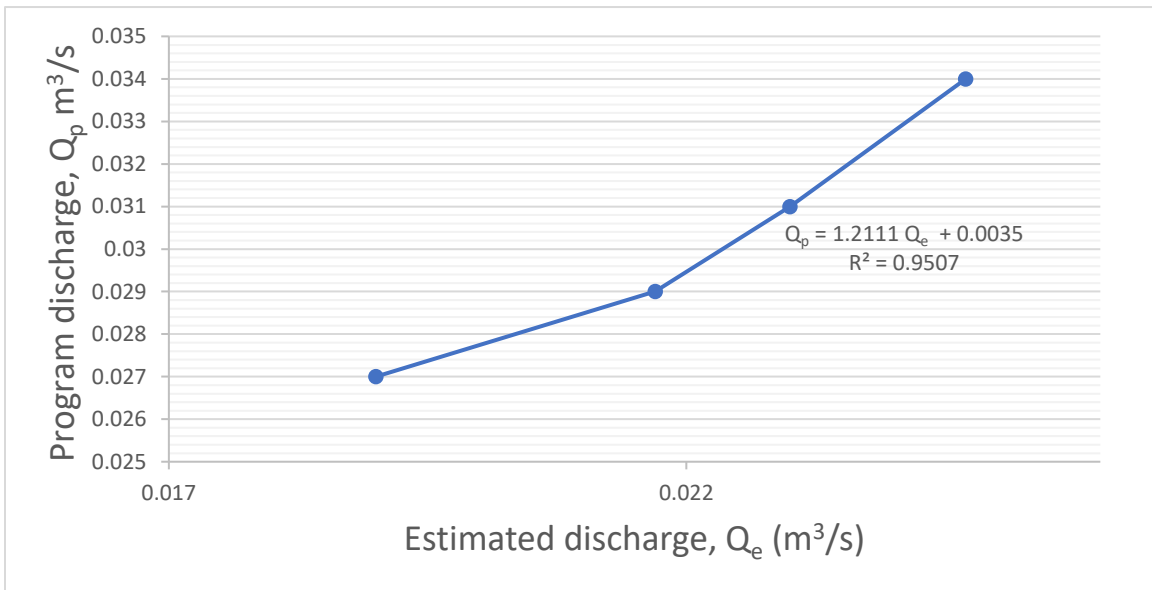


Figure E-2 Relationship between estimated discharge and software discharge in 3*10 cm wide and 7 cm opening

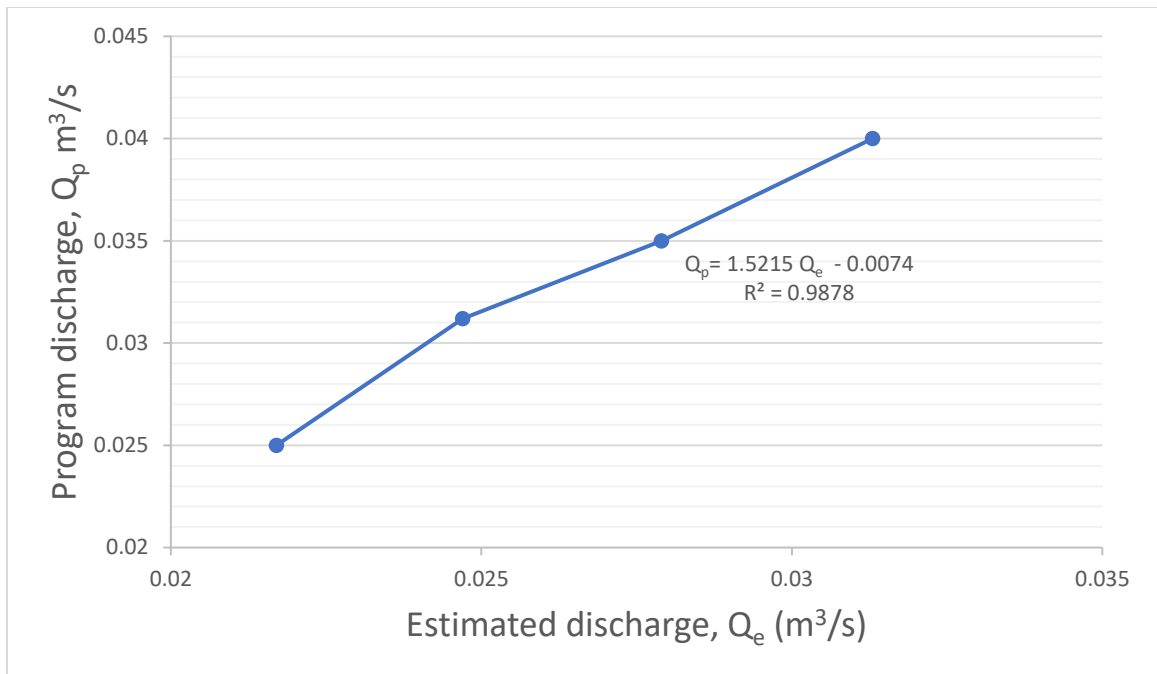


Figure E-3: Relationship between estimated discharge and software discharge in 3*10 cm wide and 10 cm opening

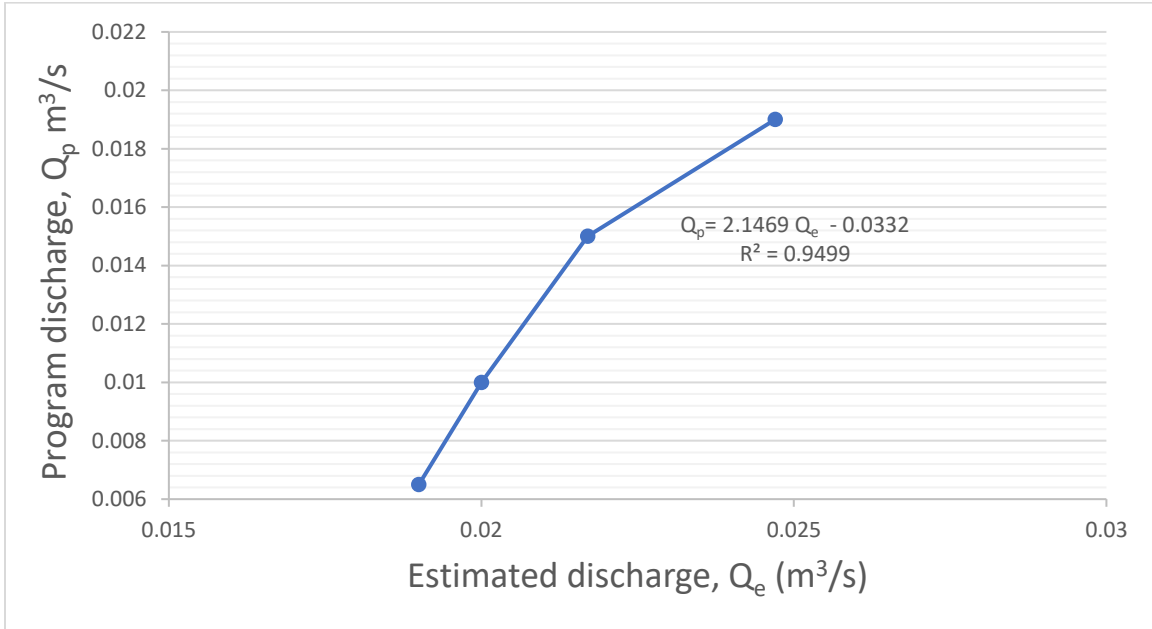
Appendix F. The discharge for the model with 3*20 cm wide

Figure F-1 Relationship between estimated discharge and software discharge in 3*20 cm wide and full opening

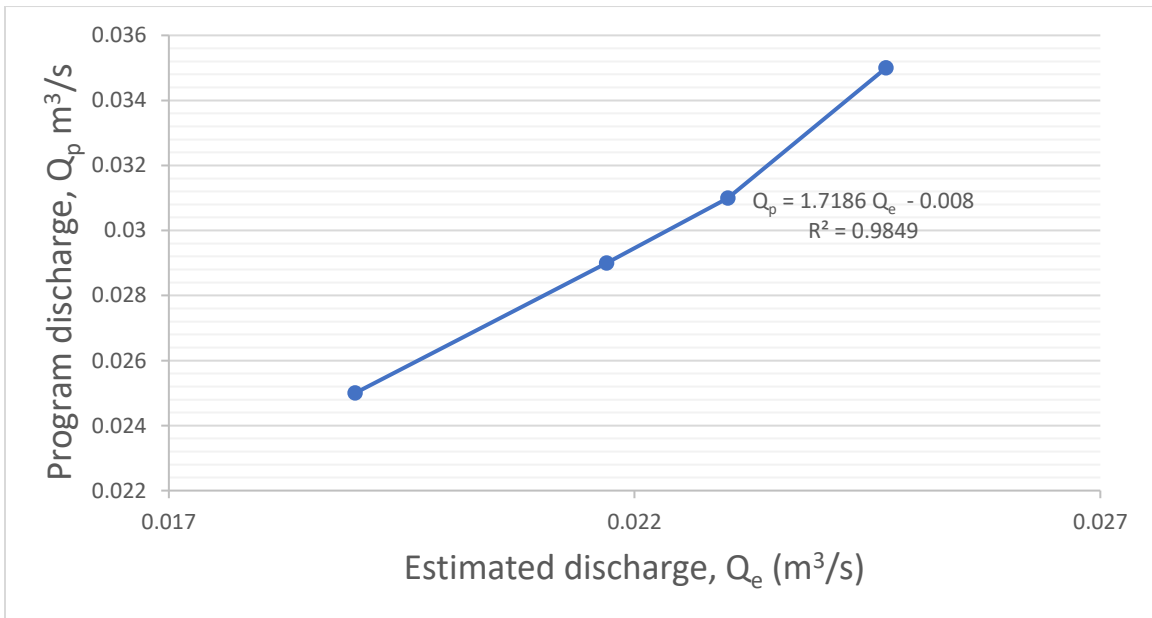


Figure F-2 Relationship between estimated discharge and software discharge in 3*20 cm wide and 5 cm opening

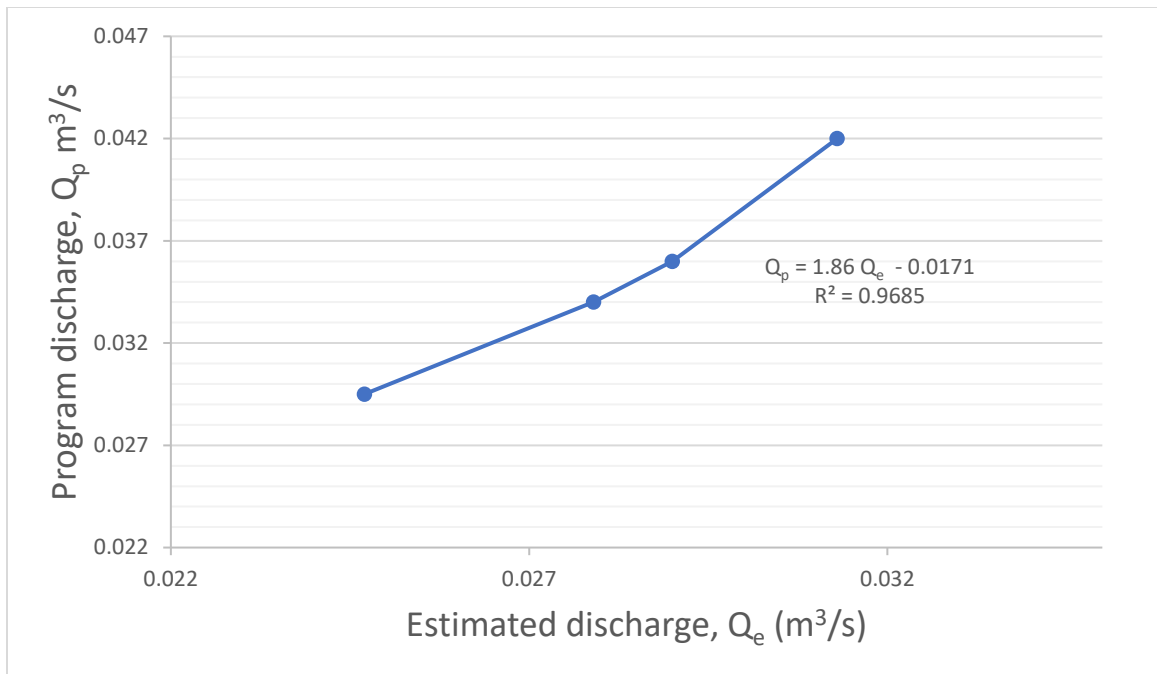


Figure F-3 Relationship between estimated discharge and software discharge in 3*20 cm wide and 10 cm opening

Appendix G . Laboratory data from (Labeed A. Jawad Al-Taher, 1987) and software discharge.

Table G-1 Laboratory data and calculated discharge for the 15 cm width of the gate.

Experiment	Gate opening H (cm)	Water at the inlet Y1 (cm)	Water at the outlet Y2 (cm)	Q estimated (m ³ /s)	Q software (m ³ /s)
1,1	OPEN	18.85	11.12	0.019	0.0195
1,2	15	19.7	11.12	0.019	0.0205
2,1	OPEN	20.6	12.11	0.0217	0.0221
2,2	16	22.12	12.11	0.0217	0.0232
2,3	15	22.94	12.11	0.0217	0.023
3,5	16	25.7	13.12	0.0247	0.0253
3,6	15	26.86	13.12	0.0247	0.0276
4,1	OPEN	24.4	14.17	0.0279	0.0293
4,2	20	25.4	14.17	0.0279	0.031
5,1	OPEN	23.5	13.64	0.0263	0.0275
5,6	16	27.74	13.64	0.0263	0.0298
6,1	OPEN	17.2	10.17	0.0164	0.0168
6,5	10	23.96	10.17	0.0164	0.02

Table G-2 Laboratory data and calculated discharge for the 25 cm width of the gate.

Experiment	Gate opening H (cm)	Water at the inlet Y1 (cm)	Water at the outlet Y2 (cm)	Q estimated (m ³ /s)	Q software (m ³ /s)
1,1	Open	13.26	11.12	0.019	0.0195
1,6	9	16.1	11.12	0.019	0.023
2,1	open	14.7	12.11	0.0217	0.0227
2,4	9	19.4	12.11	0.0217	0.0264
3,1	Open	15.9	13.12	0.0247	0.0255
3,2	12	27.2	13.12	0.0247	0.03
3,5	9	23.4	13.12	0.0247	0.0286
4,1	Open	16.93	14.17	0.0279	0.0287
4,3	12	20.20	14.17	0.0279	0.031
4,6	9	27.4	14.17	0.0279	0.0286
5,1	Open	18.5	15.24	0.0313	0.0323
5,2	15	19.4	15.24	0.0313	0.0292
5,5	12	23.4	15.24	0.0313	0.034

6,1	Open	19.9	16.34	0.035	0.0374
6,2	15	21.7	16.34	0.035	0.0303
6,6	12	26.75	16.34	0.035	0.0392
7,1	Open	21.42	17.47	0.0389	0.04
7,5	15	25.5	17.47	0.0389	0.0456
8,1	Open	22.75	18.63	0.0431	0.0441

Table G-3 Laboratory data and calculated discharge for the 35 cm width of the gate.

Experiment	Gate opening H (cm)	Water at the inlet Y1 (cm)	Water at the outlet Y2 (cm)	Q estimated (m ³ /s)	Q software (m ³ /s)
1,1	Open	10.5	9.98	0.016	0.0138
2,1	Open	12.41	11.87	0.021	0.0196
3,1	Open	14.44	13.72	0.0265	0.024
4,1	Open	16.3	15.46	0.032	0.0316
5,1	Open	18.28	17.47	0.0389	0.0348

6,1	Open	19.45	18.63	0.0431	0.0444
6,2	10	27.4	18.63	0.0431	0.052
7,4	10	21.5	16.34	0.035	0.036
8,3	10	16.45	14.17	0.0279	0.0283
8,6	6	27.6	14.17	0.0279	0.034
9,6	6	21	12.61	0.0232	0.0292
10,4	6	15.7	11.12	0.019	0.0235

Table G-4 Laboratory data and calculated discharge for the 50 cm width of the gate.

Experiment	Gate opening H (cm)	Water at the inlet Y1 (cm)	Water at the outlet Y2 (cm)	Q estimated (m ³ /s)	Q software (m ³ /s)
1,1	Open	11.23	11.12	0.019	0.0234
1,5	6	13.5	11.12	0.019	0.0213
2,1	Open	12.28	12.11	0.0217	0.0253
2,2	10	12.53	12.11	0.0217	0.0199

3,1	Open	13.35	13.12	0.0247	0.035
3,2	10	13.95	13.12	0.0305	0.0321
3,5	6	17.7	13.12	0.0247	0.0276
4,1	Open	14.44	14.17	0.0279	0.0363
4,3	10	15.32	14.17	0.0334	0.0285
8,1	Open	19.08	18.63	0.0431	0.0355
8,5	10	23.1	18.63	0.0431	0.0648

Table G-5 Laboratory data and calculated discharge for 3*10 cm width of the gate.

Experiment	Gate opening H (cm)	Water at the inlet Y1 (cm)	Water at the outlet Y2 (cm)	Q estimated (m ³ /s)	Q software (m ³ /s)
1,1	Open	12.15	11.12	0.019	0.0179
1,6	7	15.57	11.12	0.019	0.027
2,1	Open	13.25	12.11	0.0217	0.0213
2,2	10	14.23	12.11	0.0217	0.025
2,5	7	19.3	12.11	0.0217	0.029

3,1	Open	14.6	13.12	0.0247	0.0252
3,3	10	16.4	13.12	0.0247	0.0312
4,1	Open	15.86	14.17	0.0279	0.028
4,5	10	19.00	14.17	0.0279	0.035
5,1	Open	17.17	15.24	0.0313	0.0324
5,5	10	22.1	15.24	0.0313	0.04

Table G-6 Laboratory data and calculated discharge for 3*20 cm width of the gate.

Experiment	Gate opening H (cm)	Water at the inlet Y1 (cm)	Water at the outlet Y2 (cm)	Q estimated (m ³ /s)	Q software (m ³ /s)
1,1	Open	11.16	11.12	0.019	0.0065
1,5	5	14.00	11.12	0.019	0.025
2,1	Open	12.19	12.11	0.0217	0.015
2,5	5	16.5	12.11	0.0217	0.029

2,2	9	12.62	12.11	0.0217	
2,3	7	13.73	12.11	0.0217	
2,4	6	14.7	12.11	0.0217	
3,1	Open	13.2	13.12	0.0247	0.019
3,2	10	13.7	13.12	0.0247	0.0295
3,6	5	18.9	13.12	0.0247	0.035
4,2	10	15	14.17	0.0279	0.034
5,3	10	16.7	15.24	0.0313	0.042
7,1	Open	17.57	17.47	0.0389	0.394

Table G-7 Laboratory data and calculated discharge for 5*10 cm width of the gate.

Experiment	Gate opening H (cm)	Water at the inlet Y1 (cm)	Water at the outlet Y2 (cm)	Q estimated (m ³ /s)	Q software (m ³ /s)
1,1	Open	11.28	11.12	0.019	0.0123
2,3	6	16	12.11	0.0217	0.0245

3,1	Open	13.27	13.12	0.0247	0.031
4,2	10	15.55	14.17	0.0279	0.0297
5,1	Open	15.38	15.24	0.0313	0.0322
5,3	10	17.2	15.24	0.0313	0.0327
6,4	10	19.5	16.34	0.0350	0.365
7,1	Open	17.7	17.47	0.0389	0.397
8,5	10	24.5	18.63	0.0431	0.443

Appendix H . Equations between dimensional parameters and discharge

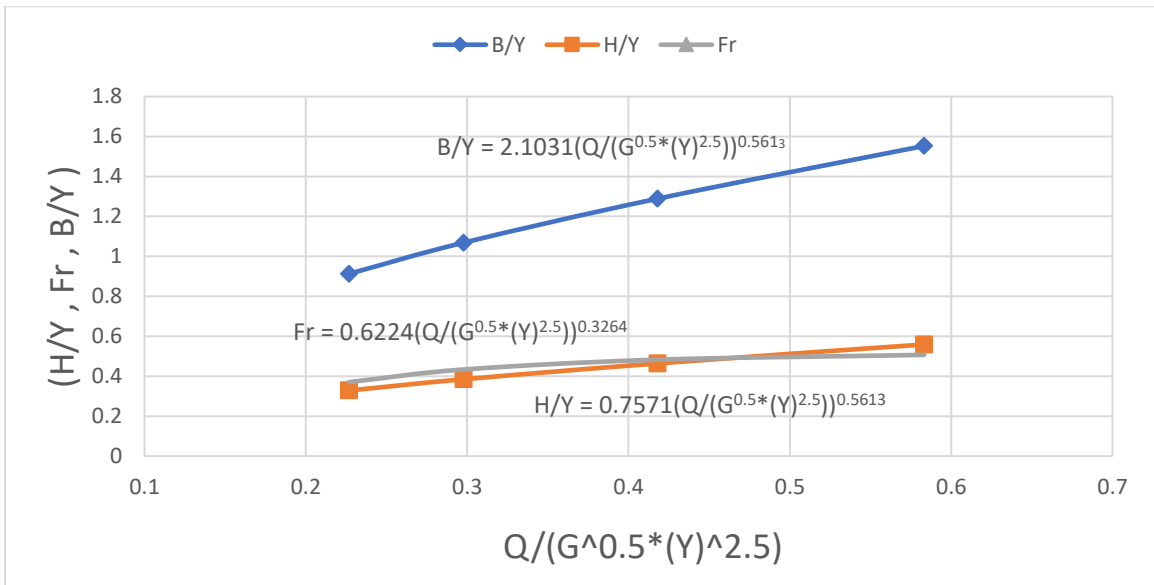


Figure H-1: Equations of 25 cm width and 9 cm open of the gate

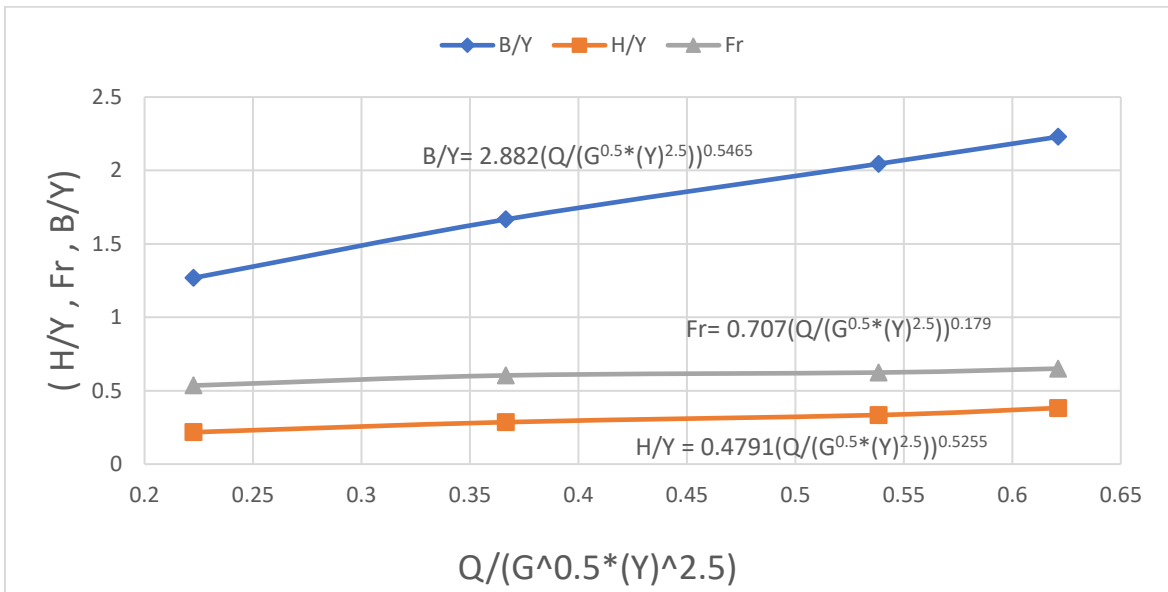


Figure H-2: Equations of 35 cm width and 6 cm open of the gate

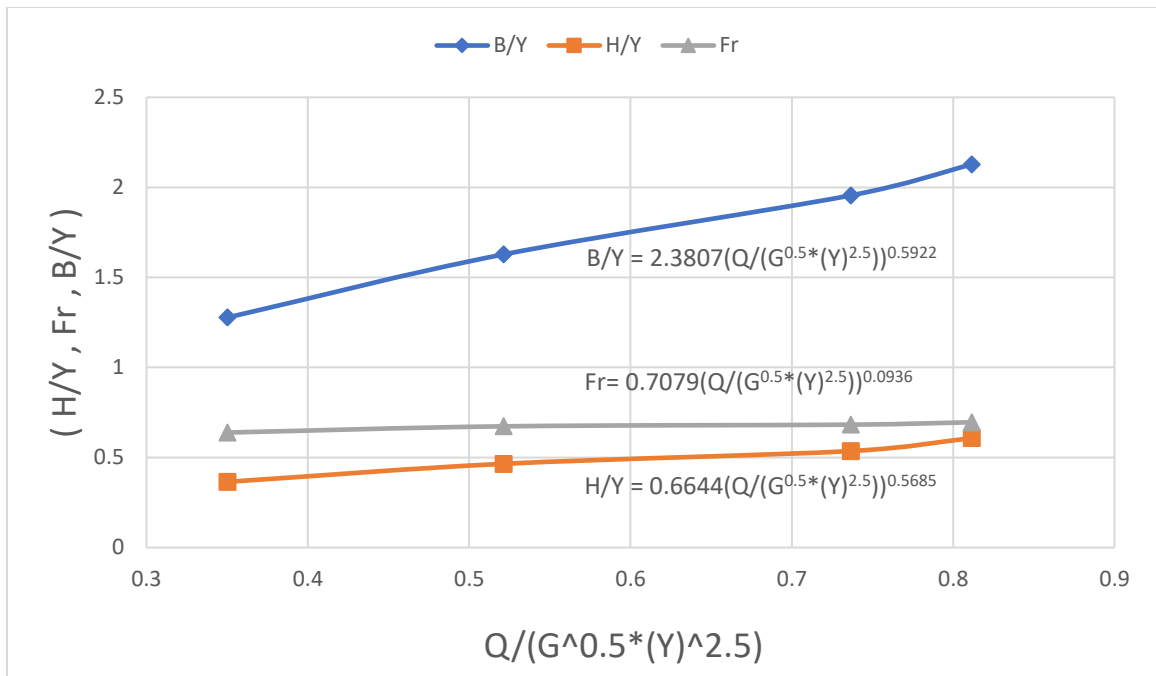


Figure H-3: Equations of 35 cm width and 10 cm open of the gate

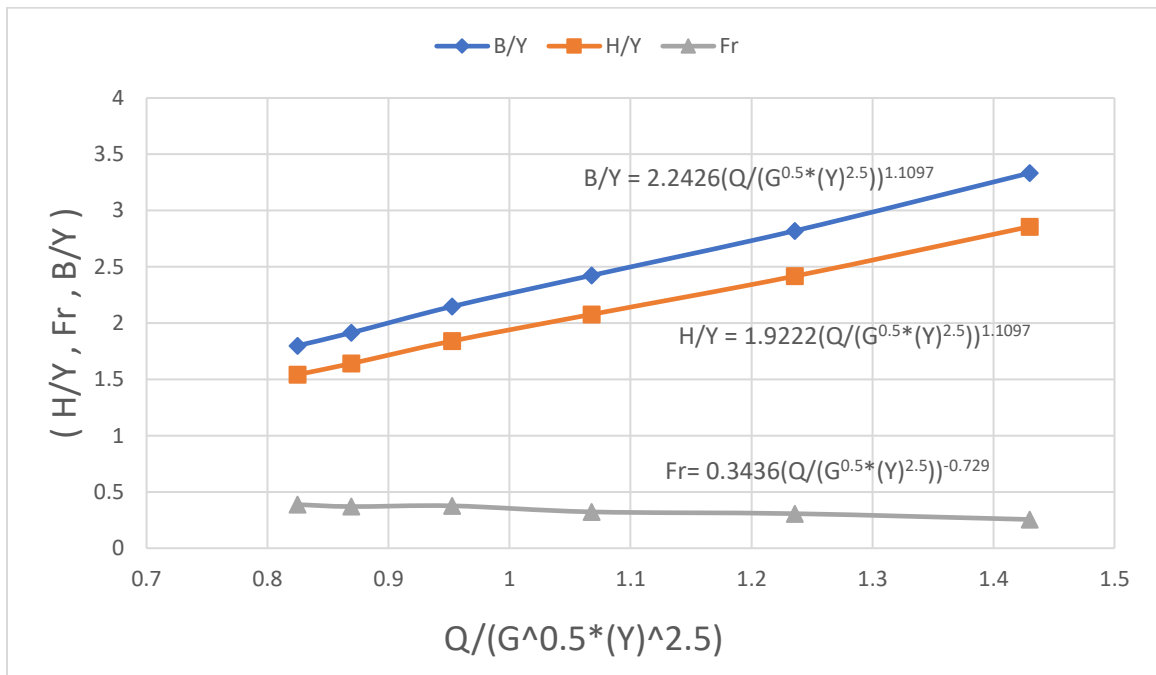


Figure H-4: Equations of 35 cm width and full opening of the gate

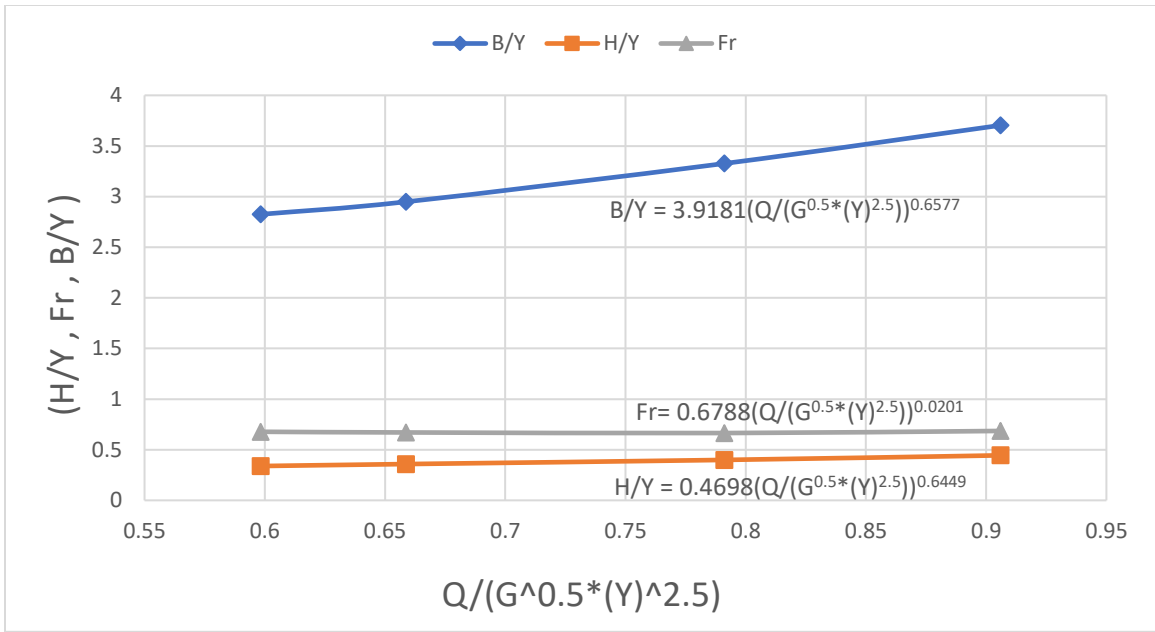


Figure H-5: Equations of 50 cm width and 6 cm open of the gate

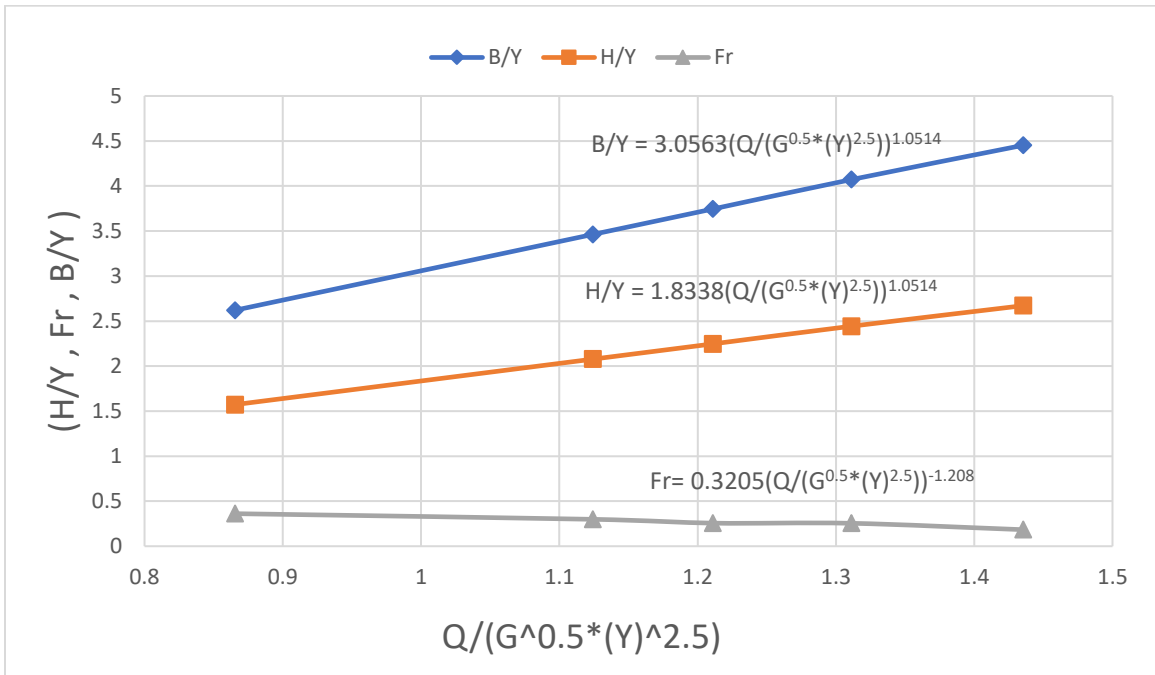


Figure H-6: Equations of 50 cm width and full opening of the gate

الخلاصة

في هذه الدراسة تم فحص حالي الجريان عند الفتح الكلي والفتح الجزئي لبوابة الناظم. تم إجراء المحاكاة باستخدام برنامج التدفق ثلاثي الأبعاد، وتمت مقارنة النتائج مع المعادلات العامة والتجريبية لحساب التصريف من خلال قنوة المياه التي تم تناولها في بحث لبيد عام 1987. من أهداف هذا البحث هي معرفة تأثير فتح البوابة وعرضها ورقم فرود على معدل التدفق، ودراسة العوامل البعدية وغير البعدية الأكثر تأثيراً على التفريغ، ومعايرة التصريف من التجارب العملية مع التصريف المستخرج من برنامج CFD في برنامج FLOW-3D واستخراج معادلة حساب التصريف بناء على البيانات المتوفرة بسهولة في أقسام الموارد المائية. استناداً إلى نتائج النمذجة من المعايرة، يمكن القول أن نهج CFD هو أداة مفيدة لنمذجة نمط التصريف في النواظم، وتم استخراج المعادلة الرئيسية، والتي أظهرت تقدير جيد بقيمة $R^2 = 0.756$ و $RMSE = 0.4872$ مع $MAE = 0.412$ التي يمكن استخدامها دون الحاجة إلى برامج أو أعمال ميدانية أو نماذج فيزيائية، فقط القياسات الأولية التي يمكن الحصول عليها من دوائر الموارد المائية وتم التوصل إلى أن (H/Y) له التأثير الأكبر على معدل التدفق بنسبة 45.8%، يليه (B/Y) بنسبة 29.4%، وأخيراً (Fr) بنسبة 24.8%. تم استخدام ستة نماذج من المنظمات ذات الفتحة الواحدة أو ذات الفتحات المتعددة في تجارب المياه المخبرية و تمت معايرة هذه النماذج باستخدام بيانات دكتور لبيد في عام 1987 عن طريق حساب التصريف بناء على نتائج القياسات المخبرية.



جمهورية العراق
وزارة التعليم العالي و البحث العلمي
جامعة كربلاء
كلية الهندسة
قسم الهندسة المدنية

التحقيق العددي لتقدير معدل الجريان خلال النواظم

رسالة مقدمة الى مجلس كلية الهندسة / جامعة كربلاء وهي جزء من متطلبات نيل
درجة الماجستير في علوم الهندسة المدنية
من قبل:

حامد احمد مهدي

(بكالوريوس علوم الهندسة المدنية جامعة كربلاء) 2019

باشراف :

اد.د حسام هادي علوان

